Streptococcus agalactiae infection of gestational tissues induces innate immune responses including the release of placental macrophage extracellular traps.

By

Ryan Steven Doster, M.D.

Dissertation

Submitted to the Faculty of the

Graduate School of Vanderbilt University

in partial fulfillment of the requirements

for the degree of

DOCTOR OF PHILOSOPHY

In

Microbe-Host Interactions

January 31, 2019

Nashville, Tennessee

Approved:

David M. Aronoff, M.D

Timothy L. Cover, M.D

Leslie J. Crofford, M.D.

Eric P. Skaar, Ph.D.

Steven D. Townsend, Ph.D.

ACKNOWLEDGEMENTS

Since I came to Vanderbilt University Medical Center in 2013 for Infectious Diseases Fellowship, many people have contributed to this work and my development as a physician-scientist. First, I thank my mentors, Dr. David Aronoff and Dr. Jennifer Gaddy, for their tireless commitment to mentoring and their efforts on behalf of me and my early career. I thank Dr. Roy Zent and the Physician Scientist Doctoral Program for providing the opportunity for physicians, like myself with goal of becoming physician-scientists, an avenue to pursue those aspirations. Additionally, I thank the Division of Infectious Diseases, including Dr. Patty Wright and Dr. Anna Person, for their tremendous support in this endeavor and allowing me to break with the traditional fellowship track to pursue additional research training. There are several people that contributed to this work through assistance with experimental design and execution, technical skills, data analysis and interpretation, manuscript preparation and editing, and friendship. Specifically, I thank Lisa Rogers, Jessica Sutton, Dr. Kate Haley, and Dr. Vishesh Kothary for their assistance in all these areas. Additionally, I thank members of the Aronoff, Gaddy, Osteen, and Serezani labs and my Dissertation Committee for feedback that has strengthened and advanced this work. Last and most important, I thank my wife, Kristen, for her support of me and my career through several years of training which have included long hours away from home, moving our family to seek new opportunities, and lots of pro bono editing work; your contributions are beyond measure.

TABLE OF CONTENTS

LIST OF TABLES

Page

LIST OF FIGURES

Page

CHAPTER I

Introduction

BACKGROUND:

Preterm birth: Preterm birth, or birth before 37 weeks gestation, is a worldwide health epidemic. 15 million babies are born prematurely each year, affecting one in ten of all births (1). Prematurity is the world's leading cause of newborn deaths and second leading cause of all child deaths, accounting for 40% of deaths among children under five years of age (1). Over 1 million children die annually due to complications of preterm birth, and those that survive are at risk for life-long health complications (1). Long term health consequences of preterm birth range from cognitive impairment including autism spectrum disorder and learning disabilities to chronic physical health conditions including chronic lung disease, metabolic disorders, and increased risk for cardiovascular and renal disease (2, 3). Additionally, preterm birth and low birth weight have societal consequences and are associated with lower educational qualifications and decreased rate of employment (4). Despite the focus on this issue by organizations including the World Health Organization, the March of Dimes, and the Bill and Melinda Gates Foundation, preterm birth rates are increasing in almost all countries (1). The United States' rate of preterm birth increased to 9.84% in 2016 (5). Focused research is needed to better understand the rising rates of preterm birth worldwide.

Perinatal infections lead to adverse pregnancy outcomes: Chorioamnionitis, or infection of the fetal membranes, is a major cause of preterm birth, preterm premature rupture of membranes, stillbirth, and neonatal sepsis (6-10). Over 40% of preterm births are related to infection, and this estimate has been increasing with the use of more sensitive diagnostic techniques (11, 12). Additionally, the percent of preterm births related to intra-uterine infection increases with earlier gestational age of delivery (11, 13, 14).

Intrauterine infection is thought to result most often from ascending infection from the vaginal canal. Alternative, and less common, mechanisms of chorioamnionitis pathogenesis include hematogenous dissemination to the placenta (such as with *Listeria*) or retrograde seeding from the peritoneal cavity (15, 16). Common intrauterine pathogens include *Ureaplasma urealyticum*, *Streptococcus agalactiae*, *Mycoplasma hominis*, *Fusobacterium nucleatum*, and *Escherichia coli,* but vaginal pathogens including *Gardnerella vaginalis* and pathogenic bacteria such as *Staphylococcus aureus* have also been implicated as causative organisms in cases of chorioamnionitis (11). As pathogens ascend, bacterial pathogen-associated molecular patterns (PAMPs) are recognized by

host cells, and proinflammatory pathways are triggered leading to production and release of cytokines, prostaglandins, and matrix metalloproteinases which lead to downstream effects including neutrophil infiltration from the maternal decidual, a hallmark of histologic chorioamnionitis, and weakening of the gestational membranes (16, 17). These changes culminate in clinical outcomes including premature rupture of membranes, preterm birth, and fetal inflammatory response syndrome (18). Despite the scope and impact of this problem, significant gaps remain in our knowledge of the pathogenesis of perinatal infections (1).

Group B *Streptococcus* perinatal infections result in significant morbidity and mortality: *Streptococcus agalactiae*, also known as Group B *Streptococcus* (GBS), is a Gram-positive bacteria that is a common part of the genitourinary and gastrointestinal microbiota of healthy women (19). In the 1970s, GBS emerged as a leading cause of neonatal infections, where maternal vaginal colonization can lead to transmission to the infant either *in utero* by ascending infection or during birth through neonatal aspiration during delivery (19-24). Today, GBS remains a leading cause of perinatal infections including neonatal sepsis and meningitis (3, 11, 25-30). 50% of pregnant women screen positive for rectovaginal GBS colonization at some point during gestation, and late pregnancy carriage ranges from 11-35% depending on the population surveyed (25, 31-34). Multivariate analyses of risk factors for GBS early-onset neonatal sepsis demonstrate that maternal GBS colonization is the overwhelming predictor of risk, with an odds ratio exceeding 200 (35, 36). Due to the prevalence and severity of GBS disease, the Centers for Disease Control and Prevention (CDC) recommends universal culture-based rectovaginal GBS screening during the third trimester followed by intrapartum antibiotic prophylaxis for women testing positive (24). While antibiotic treatment is effective at preventing early-onset sepsis, this approach has not eliminated invasive disease and is complicated by the facts that antimicrobial resistance is emerging in GBS and adverse effects of antibiotic use during pregnancy are concerning (24, 37, 38). Vaccine approaches will certainly help prevent invasive disease, but current anti-capsular vaccine approaches may be limited by emerging, virulent GBS strains with unique capsular serotypes (28, 39, 40).

GBS pathogenesis in chorioamnionitis: GBS is unique among perinatal pathogens in that vaginal colonization is recognized as a clear risk factor invasive infection, but many colonized women develop no overt disease (24, 35). GBS vaginal colonization is thought to be mediated by expression of adhesion proteins including surface serine-rich repeat (Srr) proteins, pili, and bacterial surface adhesins including BsaB and BibA, and expression of these virulence factors may be modulated by environmental factors including pH of the vaginal canal (41-45). GBS biofilm formation is thought to

promote persistence in the face of pressures from the vaginal microbiota and host immune responses (41). Bacterial adhesins and biofilm regulatory protein A (BrpA) are through to contribute to GBS biofilm responses, but *in vitro* studies evaluating environmental modulators of GBS biofilm have demonstrated mixed results (46-49). It remains unclear what environmental signals may trigger phenotypic changes in GBS that might promote invasion, but GBS sequence analyses suggest that GBS may have up to 20 two-component systems (50). The CovRS two-component system has been estimated to regulate up to 27% of the entire GBS genome including inhibitory effects on surface adhesins and toxin production including β-hemolysin (51-53). In the vaginal canal, GBS strains have shown variable ability to colonize and persist on epithelial cells, and GBS colonization stimulates inflammatory cytokine responses from vaginal tissues (54). Additionally, recent studies suggest that GBS interactions with vaginal epithelial cells may stimulate epithelial exfoliation as a mechanism to propel ascending infection in a mouse model, but it remains unclear if a similar pathway occurs in humans (55).

GBS is equipped with mechanisms to subvert host responses including a polysaccharide capsule with terminal sialic acid residues, which are similar to host cell epitopes (41). GBS sialic acid residues are recognized by sialic acid-binding immunoglobin-like lectins (Siglecs) on phagocytes, which dampen cellular responses including phagocytosis, oxidative burst, and bacterial killing (56, 57). It remains unclear how GBS ascends past the cervical mucus plug to reach the uterine cavity and the fetal membranes, but GBS is recognized by fetal membrane tissues and stimulates cytokine release and upregulation of antimicrobial host responses including β-defensin proteins within these tissues (58, 59). Similarly, in a rhesus model of GBS chorioamnionitis, intraamniotic inoculation with GBS resulted in increases in amniotic fluid cytokines including IL-6, IL-1β, and TNF-α as well as prostaglandin E_2; changes in these mediators were followed by increases in uterine contractility and cervical dilation (60). Additional non-human primate studies have shown similar cytokine changes that were associated with fetal lung injury (61).

Virulence factors contribute to further GBS invasion of gestational tissues. The ornithine pigment, β-hemolysin, induces host cell death by increasing membrane permeability and is important for invasion of maternal fetal-barriers and causing fetal infection (53, 62, 63). The relevance of this toxin has also been evaluated in nonhuman primate models, which demonstrated increased expression of β-hemolysin resulted in enhanced invasion of the amniotic cavity and the fetus (64). Even non-pigmented strains can still demonstrate virulence and GBS proteases including hyaluronidase may contribute to infection as hyaluronidase activity is associated with increased ascending GBS infection, preterm birth, and fetal demise (65, 66). Despite our increasing knowledge

of mediators of GBS pathogenesis during the perinatal period, these studies have not yet led to interventions to alleviate the burden of GBS infection.

Macrophages play important roles during pregnancy: Pregnancy represents a unique immunologic state in which the maternal immune system must dampen its responses against foreign antigens of the semiallogenic fetus while defending the gravid uterus from infection. Excessive inflammation can result in adverse pregnancy events including loss of pregnancy, preterm birth, intrauterine growth restriction, and preeclampsia (67). Multiple mechanisms exist to support maternal-fetal tolerance including production of anti-inflammatory cytokines that alter the number and function of immune cells at the maternal-fetal interface (68-70). Macrophages represent 20-30% of the leukocytes within gestational tissues (71). During gestation, fetally-derived macrophages, called Hofbauer cells or placental macrophages, play key roles in placental invasion, implantation, angiogenesis, tissue remodeling, and development (72, 73). Placental macrophage inflammatory states are carefully regulated throughout pregnancy. During implantation M1 or proinflammatory activation states predominate, but as the pregnancy progresses there is a shift to an M2, or anti-inflammatory, tolerogenic, and tissue remodeling phenotype to support fetal development (74-77). Macrophages contribute to immune tolerance by secretion of anti-inflammatory cytokines including IL-10, TGF-β, and prostaglandin E_2, which inhibit production of proinflammatory cytokines (78-81). Disruption of appropriate macrophage polarization is associated with abnormal pregnancies including spontaneous abortions, preterm labor, preeclampsia, fetal intrauterine growth restriction (74).

As placental macrophages are present within fetal membrane and placental tissues, these cells are likely the initial phagocytes to encounter invading bacteria, but our understanding of how placental macrophages contribute to host defense within gestational tissues is limited. Outside of gestational tissues, macrophages contribute to host defenses against bacteria, including GBS, by recognizing bacteria via pathogen recognition receptors such as Toll-like receptors (TLR). GBS cells and bacterial products are recognized by TLR2, TLR6 and TLR9 on macrophages and stimulate macrophage release of proinflammatory mediators including IL-1β and TNF-α, phagocytosis of bacterial cells, and production of bactericidal reactive oxygen species (82-89). To counter macrophage responses, GBS produces the pore forming toxin, β-hemolysin, which has been shown to alter macrophage cytoskeletal changes, induce apoptosis, and promote bacterial persistence within macrophages (90, 91). How bacterial-macrophage interactions contribute to adverse pregnancy outcomes remain poorly understood, but typical macrophage responses in the context of pregnancy including the release of proinflammatory cytokines could be detrimental to maternal-fetal tolerance and could precipitate cascades that result in preterm contractions and preterm rupture of membranes

(15). As studies describe the vital role of macrophages during progression of normal pregnancy, it becomes essential to study pathologic states, such as infection, that might disrupt the carefully orchestrated progression of inflammation during pregnancy.

RATIONAL FOR THESE STUDIES:

Despite interventions such as antepartum antibiotic prophylaxis and attempts at GBS vaccine development, GBS remains a leading cause of perinatal infections. These infections result in infant mortality as well as life-long health co-morbidities for survivors. Despite, awareness of GBS perinatal infections since the 1970's and continued high rates of pregnancies complicated by bacterial infection, there remains significant gaps in our knowledge of the mechanisms that govern bacterial colonization of the vagina and key host-microbial interactions that precipitate adverse pregnancy outcomes. These studies sought to better define interactions of GBS and other perinatal pathogens with gestational tissues and tissue resident placental macrophages at the host-pathogen interface to define responses that might contribute to adverse pregnancy outcomes.

CHAPTER II

Staphylococcus aureus infection of human gestational membranes induces bacterial biofilm formation and host production of cytokines

INTRODUCTION:

Bacterial infection–related preterm birth is a leading cause of infant morbidity and mortality (11). Despite medical advancements and targeted interventions, approximately 15 million cases of preterm birth occur annually, complicating 1 in 10 births and highlighting a need for prophylactic measures to prevent disease (92). Infections during pregnancy occur as pathogens ascend from the vagina through the cervix to the gestational membranes, but hematogenous spread to the placenta also occurs (15). Infection of fetal membranes results in a profound innate immune cell infiltrate, a process referred to as chorioamnionitis (11). Infection and the subsequent inflammatory response result in release of cytokines, prostaglandins, and matrix metalloproteases (MMPs). These mediators promote uterine contraction and metalloprotease-induced membrane damage, ultimately resulting in premature rupture of membranes and preterm birth (15). However, immunologic responses to specific pathogens during chorioamnionitis remain largely uncharacterized.

Numerous bacterial pathogens, including *Escherichia coli*, *Ureaplasma urealyticum*, *Mycoplasma hominis*, *Gardnerella vaginalis*, and *Streptococcus agalactiae* have been associated with preterm birth, chorioamnionitis, and early onset neonatal sepsis (11). *Staphylococcus aureus*, a common component of the human skin microbiota and a major nosocomial and community-acquired pathogen, is gaining attention as an emerging cause of chorioamnionitis and preterm birth, particularly in individuals with extensive healthcare exposure (93, 94). Understanding how *S. aureus* adheres to, persists on, and breaches gestational membranes to alter host pregnancy biology will aid in the understanding of pathogenesis. Furthermore, elucidating the host immunological changes that result from *S. aureus* infection of gestational membranes could provide novel chemotherapeutic targets and inform global cytokine responses that perturb fetal-maternal tolerance. We present a model of *S. aureus* co-culture with explanted human gestational membrane tissue as an important tool that revealed increased secretion of interleukin 1β (IL-1β), interleukin 2 (IL-2), interleukin 6 (IL-6), granulocyte-macrophage colony-stimulating factor (GM-CSF), interferon γ (IFN-γ), and tumor necrosis factor α (TNF-α) in response to S. aureus infection.

METHODS:

Bacterial strains: *S. aureus* strain USA300 (American Type Culture Collection, Manassas, Virginia) was cultured on tryptic soy agar plates supplemented with 5% sheep blood (blood agar plates) at 37°C in ambient air overnight. Bacteria were subcultured from blood agar plates into Todd-Hewitt broth and incubated under aerobic shaking conditions at 37°C in ambient air overnight. The following day, bacterial density was measured spectrophotometrically at OD_{600}.

Gestational membrane co-culture: Gestational membranes were excised from placental tissues from females who delivered healthy infants at full term by cesarean section without labor. Deidentified tissue samples were provided by the Cooperative Human Tissue Network, which is funded by the National Cancer Institute. All tissues were collected in accordance with Vanderbilt University Institutional Review Board (approval 131 607). Gestational membranes were processed into 12-mm punch biopsy sections, and sections were placed, with the amnion side down, in a 12-well dish containing Dulbecco's modified Eagle's medium (DMEM), high-glucose, HEPES, no-phenol-red cell culture medium (Gibco, Carlsbad, California) supplemented with 1% fetal bovine serum and PEN-STREP antibiotic/antimycotic mixture (Gibco). Sections were incubated overnight at 37°C in ambient air containing 5% CO_2; washed 3 times with prewarmed, sterile phosphate buffered saline (pH 7.4); and placed again in DMEM, high-glucose, HEPES, no-phenol-red cell culture medium (lacking the PEN-STREP antibiotic/antimycotic mixture). Bacterial cells were added to the choriodecidual surface of the gestational membranes at a multiplicity of infection of 1×10^7 cells per 12-mm diameter membrane, using a predetermined coefficient of bacterial density of 1 $OD_{600} = 1 \times 10^9$ cells. Concomitantly, uninfected gestational membrane samples were also maintained. Cocultures were incubated at 37°C in ambient air containing 5% CO_2 for 24 hours.

Histological examination: Human gestational membrane samples derived from at least 3 distinct subjects were used for cocultures described above. After 24 hours of coculture, samples were washed 3 times with phosphate-buffered saline and fixed in 10% neutral buffered formalin prior to embedment in paraffin. Samples were sectioned into 5-μm-thick sections and stained with hematoxylin and eosin. Two sections were taken from each tissue block, giving multiple fields for histological examination per sample. Micrographs were taken at magnifications of 100×, 200×, and 400×, and representative micrographs from 3 separate replicates are shown.

Scanning electron microscopy: We prepared human gestational membrane samples from the co-culture studies described above for scanning electron microscopy analyses by washing them 3 times

with 0.05 M sodium cacodylate buffer and fixing them in 2.0% paraformaldehyde and 2.5% glutaraldehyde in 0.05 M sodium cacodylate buffer for 4 hours prior to sequential dehydration with increasing concentrations of ethanol. Samples were dried at the critical point, using a CO_2 drier (Tousimis); mounted onto an aluminum stub; and sputter coated with 80/20 gold-palladium. A thin strip of colloidal silver was painted at the sample edge to dissipate sample charging. Samples were imaged with a FEI Quanta 250 field-emission gun scanning electron microscope. Images are representative of 3 replicates from 3 different subjects.

Analyses of secreted cytokines: After 24 hours of coculture, supernatant fractions were collected and centrifuged at 8000 × g to remove any cellular debris. Secreted cytokines (IL-1β, IL-2, IL-6, GM-CSF, IFN-γ, and TNF-α) were evaluated using the Quantikine enzyme-linked immunosorbent assay kit (R + D Systems, Minneapolis, Minnesota) per the manufacturer's instructions. *S. aureus*–infected samples were compared to uninfected samples for analysis. The assay was repeated with 3 replicates from 3 separate subjects.

Statistical analyses: Statistical analysis of cytokine secretion analyses was performed using the Student's *t* test (without multiple variable correction). All data analyzed in this work were derived from at least 3 separate biological replicates from separate subjects. Statistical analyses were performed using Prism (version 6.0 g; GraphPad Software, La Jolla, California) and Excel (version 14.6.3; Microsoft, Redmond, Washington).

RESULTS:

***S. aureus* infects the choriodecidual face of gestational membranes:** Histopathological examination of gestational membranes alone or cocultured with *S. aureus* revealed canonical tissue architecture, including well-defined decidua parietalis, chorion, and amnion (**Figure II.1 A&E**). Bacteria seeded onto the choriodecidual face of the membranes could clearly be visualized within the choriodecidua in large staphylococcal microcolonies (**Figure II.1 E&F**). Within 24 hours of infection, these bacteria penetrated the chorion but did not appear to have traversed to the amnion.

***S. aureus* forms biofilms on gestational membranes:** To better characterize the structure of *S. aureus* microcolonies within the tissue coculture system, we used high-resolution field-emission gun scanning electron microscopy (**Figure II.1 C&D, G&H**). Field-emission gun scanning electron microscopy revealed that *S. aureus* grows and forms biofilms on the choriodecidual surface of gestational membranes (**Figure II.1 G &H**), structures that were absent from control uninfected

membranes (**Figure II.1 C&D**). These microcolony biofilms measured approximately 150 μm × 125 μm, and within these structures typical nutrient channel architecture was seen (**Figure II.1H**).

***S. aureus* induces cytokine production in gestational membranes:** Gestational membranes are thought to participate in immune surveillance via expression of pathogen-recognition receptors such as Toll-like receptors (95). The interaction of *S. aureus* with gestational membranes led us to hypothesize that alterations in host cytokine responses could be a consequence. Cytokine secretion in supernatant fractions isolated from gestational membranes cultured in medium alone (uninfected) or co-cultured with *S. aureus* were evaluated by sandwich ELISA. Our results (**Figure II.2**) indicated that *S. aureus* infection induces significant increases in secretion of IL-1β ($P = 0.0202$), IL-2 ($P = 0.0200$), IL-6 ($P = 0.0216$), GM-CSF ($P < 0.001$), IFN-γ ($P = 0.00629$), and TNF-α ($P = 0.00579$). These results suggest this explanted tissue model is capable of responding to bacterial infection.

DISCUSSION:

Intrauterine inflammation is a key factor that contributes to preterm parturition. Often this inflammation is a response to bacterial infection. Intrauterine infections typically occur as pathogens that colonize cervical or vaginal epithelium ascend to infect the choriodecidua, penetrate to the amnion, and translocate into the amniotic cavity, resulting in neonatal sepsis (11, 15, 95). Thus, ascending infection during pregnancy can ultimately result in disease outcomes for both mother and child.

In addition to its increasing prevalence as a cause of soft-tissue infections, recent evidence suggests that *S. aureus* is emerging as a causative agent of chorioamnionitis and preterm birth (93, 94). *S. aureus* vaginal colonization rates are estimated to be around 15% and are associated with Group B *Streptococcus* colonization (96). A prospective cross-sectional study of 105 women without preterm premature rupture of membranes (PPROM) and 105 with PPROM indicated that *Streptococcus* species, *S. aureus*, and *E. coli* were significantly more prevalent in women with PPROM, compared with women without PPROM (97). Additionally, methicillin-resistant *S. aureus*–associated chorioamnionitis has also been documented (94). Thus, emerging antibiotic-resistant *S. aureus* is a growing concern for maternal-fetal health, and a better understanding of the pathogenesis may reveal novel biomarkers for maternal-fetal inflammatory diseases and potential targets that could be exploited to perturb the interaction between *S. aureus* and gestational tissue.

S. aureus infects soft tissues and forms tenacious biofilms on these surfaces (98). The biofilm community provides a selective advantage for bacteria, aiding in the resistance to antimicrobials and

host immunity (99, 100). *S. aureus* exploits the proinflammatory activity of α-hemolysin to promote disruption of vaginal tissue and enhance biofilm formation (101).

Gestational membranes represent the final barrier between ascending pathogens and the amniotic cavity. These tissues provide dynamic immune surveillance through the expression of pathogen-recognition receptors (95). Our findings establish that *S. aureus* infection of gestational membranes induces release of proinflammatory cytokines, including IL-1β, IL-2, IL-6, GM-CSF, TNF-α, and IFN-γ, results that were congruent with previous models of *S. aureus* soft-tissue infection (102). In synovial tissues, *S. aureus* infection resulting in proinflammatory cytokine release induces activation in MMPs and subsequent tissue damage (103). Previous studies of gestational tissues have shown that interactions between GM-CSF and TNF-α result in membrane weakening (104). Furthermore, during pregnancy, increases in IL-1β, TNF-α, IL-6, and IFN-γ levels promote neutrophil release of MMPs that directly degrade membrane components, contributing to preterm premature ruptures of membranes and preterm birth (15). Taken together, these results reveal that *S. aureus* infection results in biofilm formation on the choriodecidual surface of gestational membranes and potentiates a cytokine storm within these tissues that is similar to that seen in patients with chorioamnionitis (15). Furthermore, the gestational co-culture tissue model provides an excellent tool to study host-pathogen interactions at the final barrier of maternal-fetal host defenses. This model could be used to identify novel virulence factors that could be exploited as potential vaccine or drug targets.

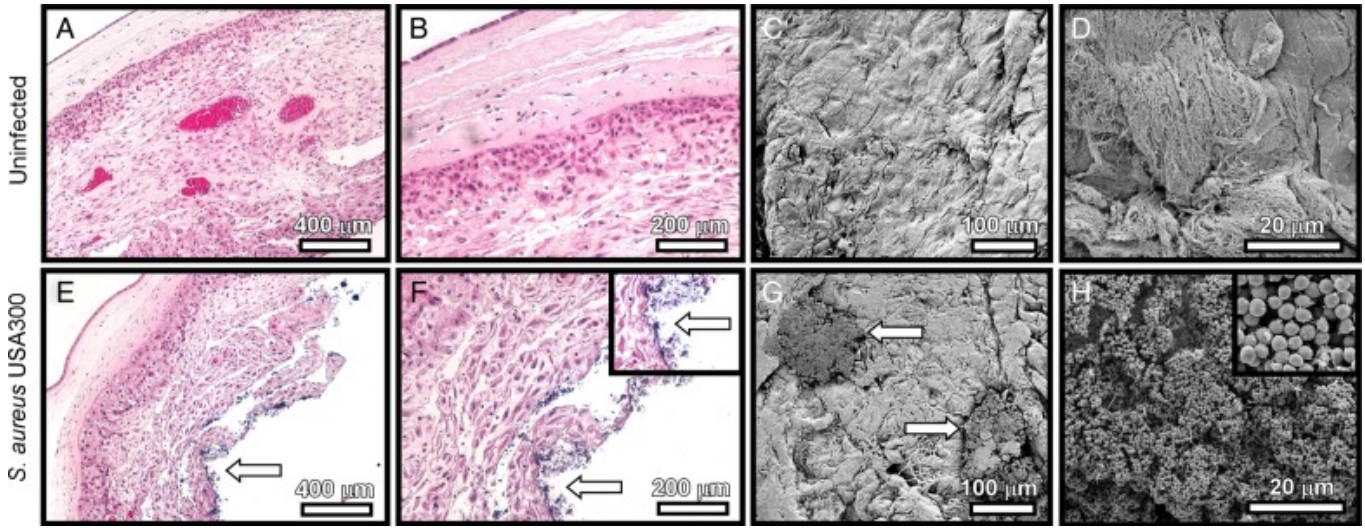

Figure II.1: Analysis of *Staphylococcus aureus* interaction with gestational membranes. A, B, E, and F: Micrographs of hematoxylin-eosin–stained sections of gestational membranes alone (A&B) or cocultured with *S. aureus* (E&F) at 100× (A&E), 200× (B&F), and 400× (F, insert) original magnification. Representative micrographs show preserved tissue architecture within the gestational membranes (A&E). Micrographs (B&F) show similar tissue architecture between membranes alone (B) and membranes cocultured with *S. aureus* (F); white arrows indicate bacterial microcolony formation. C, D, G, and H: Scanning electron micrographs of gestational membranes alone (C&D) or *S. aureus*–infected gestational membranes (G&H) at 250× (C&G), 2,000× (D&H), and 20,000× (H, insert) original magnification.

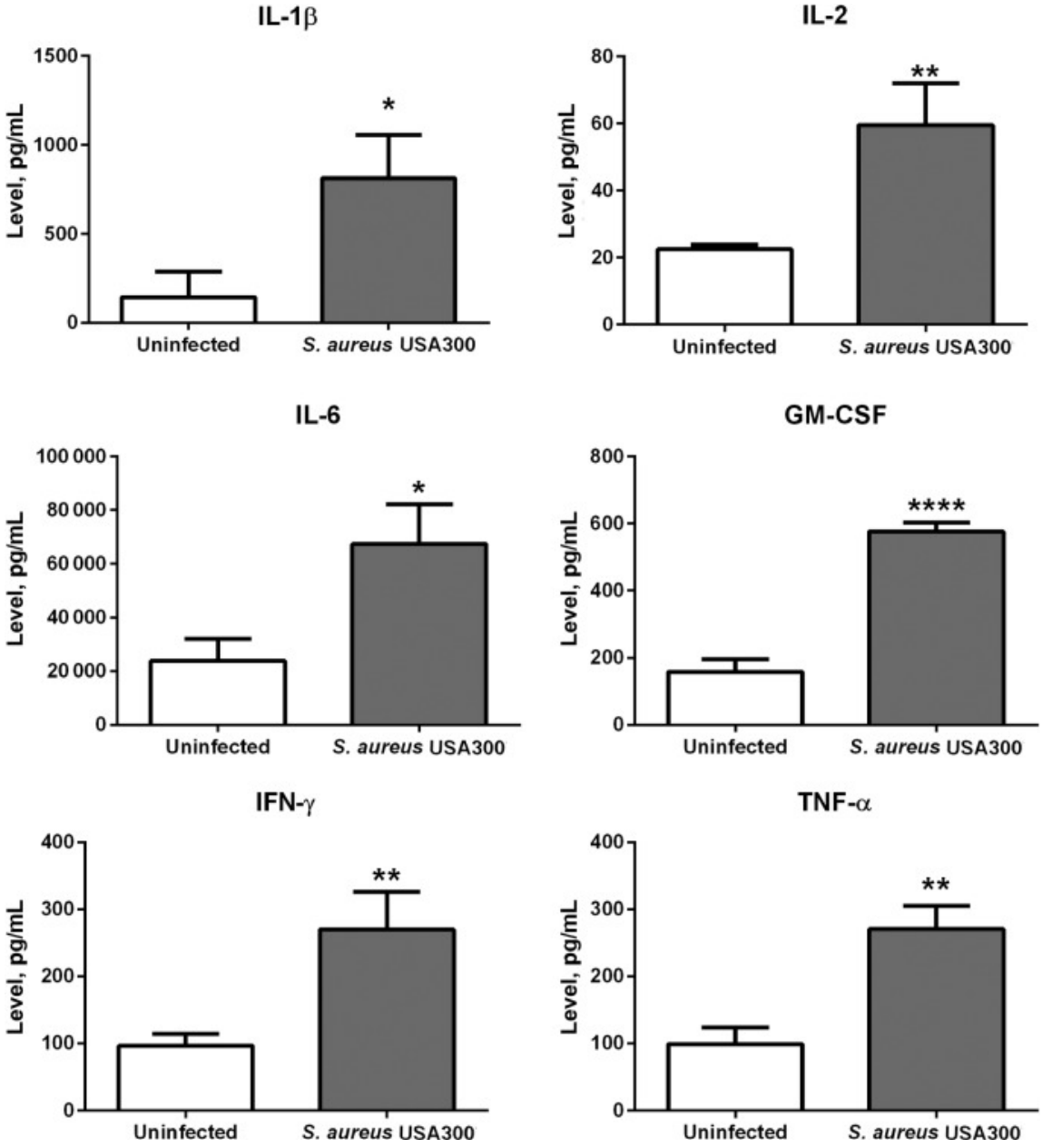

Figure II.2: Analysis of cytokine secretion in response to *Staphylococcus aureus* infection. Interleukin 1β (IL-1β), interleukin 2 (IL-2), interleukin 6 (IL-6), granulocyte-macrophage colony-stimulating factor (GM-CSF), interferon γ (IFN-γ), and tumor necrosis factor α (TNF-α) production was assessed in secreted fractions derived from gestational membranes alone or infected with *S. aureus*. Significant increases in IL-1β, IL-2, IL-6, GM-CSF, IFN-γ, and TNF-α levels were detected in *S. aureus*–infected gestational membranes as compared to uninfected tissues. Bars indicate means ± standard errors of the mean levels of cytokines secreted from samples derived from 4–7 individuals. **P* < .05, ***P* < .01, and *****P* < .0001, by the Student's *t* test with the Welch correction.

CHAPTER III

Streptococcus agalactiae infects human fetal membranes tissues by forming biofilms and invading membrane tissues.

INTRODUCTION:

Streptococcus agalactiae, also known as Group B *Streptococcus* (GBS), is an encapsulated Gram-positive coccus that colonizes 10-35% of pregnant women in late pregnancy, but the prevalence and serotype distribution vary worldwide (34). GBS serotypes I-V account for 98% of colonizing isolates worldwide (34). GBS vaginal colonization is an important risk factor for invasive GBS infections that include chorioamnionitis, or infection of the fetal membranes, and neonatal sepsis. To date, the dynamics of GBS colonization remain poorly understood as do the factors that allow progression from asymptomatic colonization to invasive disease.

It has been hypothesized that biofilm may be an important virulence strategy for GBS to colonize the vaginal mucosa and subsequently invade, but to date this has not been definitively established (19). Other *Streptococcus* species including *S. pneumoniae* and *S. pyogenes* utilize biofilms to colonize mucosal surfaces (nasopharynx) prior to causing invasive disease (105-107). Biofilms are also a common form of microbial growth within the vagina as *Gardenerella* and *Candida* biofilms are known to contribute to vaginitis (108). Biofilms offer advantages during pathogenesis by aiding in surface adhesion, niche establishment, and modulation of and protection against host immune responses (107, 109-113). Though many women test positive for GBS during routine, late pregnancy screening, most women do not maintain colonization throughout pregnancy (114). Longitudinal human studies of GBS carriage during pregnancy highlight interesting aspects of vaginal immune responses. Women who produced GBS-serotype-specific antibodies demonstrated lower rates of rectovaginal acquisition of that specific serotype, but not other serotypes, during pregnancy (115). This serotype-specific antibody response was inadequate to increase clearance rates of those women already colonized, suggesting that something, possibly biofilms, may hinder this immune response. Many have evaluated GBS biofilms *in vitro* and controversy remains regarding optimal biofilm growth conditions and relevance of *in vitro* models (usually on abiotic surfaces) compared with defining biofilms in living tissues, which represents technical challenges (47, 49, 116-118).

We sought to understand GBS interactions with gestational tissues, in particular human fetal membranes, which represent a key barrier between the infant and invading microbes. We previously demonstrated an *ex vivo* human fetal membrane model of chorioamnionitis that was deployed to

evaluate interactions and subsequent immune responses at this important barrier (119). Here we demonstrate that GBS forms biofilms on the choriodecidual surface of human fetal membranes, invades membrane tissues, and stimulates release of inflammatory cytokines. GBS biofilm formation is modulated by environmental signals including glucose and zinc availability.

METHODS:

Bacterial strains and growth conditions: Several clinical isolates of GBS were provided by Dr. Shannon Manning from Michigan State University. The multi-locus sequence type and capsular type of these strains are show in **Table III.1**. GBS cells were cultured on tryptic soy agar plates supplemented with 5% sheep blood (blood agar plates) at 37ºC in ambient air overnight. Bacteria were sub-cultured from blood agar plates into Todd-Hewitt broth (THB) and incubated (aerobically, shaking at 200 RPM) at 37ºC in ambient air overnight. The following day, bacterial density was measured spectrophotometrically at an optical density of 600 nm (OD_{600}), and bacterial numbers were determined with a coefficient of 1 OD_{600}= 10^9 CFU/mL.

Biofilm assays: GBS cells were inoculated into THB or THB supplemented with glucose, zinc chloride, or the synthetic zinc chelator, N,N,N',N'-tetrakis (2-pyridylmethyl) ethylenediamine (TPEN) in polystyrene dishes at a MOI of 10^6 CFU/mL of media. Plates were incubated at 37°C in ambient air for 24 hours. At 24 hours, measurements were taken at OD_{600} as a measure of bacterial growth (biomass). Wells were washed and stained with 10% crystal violet solution for 10-15 minutes prior to washing three times with PBS and drying. Residual crystal violet stain was solubilized with 80% ethanol/20% acetone, and the resulting color change was measured at OD_{540}, representing biofilm production. Results are expressed as the ratio of biofilm:biomass to control for any changes in bacterial proliferation

Mouse chorioamnionitis model: GBS infection of pregnant mice and subsequent analyses were performed as previously described with some modifications (62). Briefly, C57BL6/J mice were purchased from Jackson Laboratories and mated in harem breeding strategies overnight. Pregnancy was confirmed the following day by the presence of a mucus plug to establish the embryonic date (E0.5). On embryonic day 13 (E13.5) dams were anesthetized using isoflurane chambers and 50 µL of inoculum containing 10^3 colony forming units (CFU) in THB medium plus 10% gelatin was introduced into the vagina. Sham controls were inoculated with 50 µL of THB medium containing 10% gelatin. Animals were housed singly until embryonic day 15 (E15.5) at which time they were sacrificed by carbon dioxide euthanasia procedures and necropsy was performed to isolate fetal-placental units.

Mouse tissue immunohistochemistry: Pregnant animals were sacrificed on day E15.5 and fetal-placental units were fixed in 10% neutral buffered formalin prior to embedment in paraffin. Tissues were cut into 5 μm sections and multiple sections were placed on each slide for analysis. Immunohistochemistry staining was performed by the Vanderbilt Translational Pathology Shared Resource using the Leica Bond Max IHC stainer (Leica Biosystems, Buffalo Grove IL). Enzymatic induced antigen retrieval was performed using Proteinase K (Dako, Agilent, Santa Clara, CA) for 5 minutes. Slides were incubated with anti-F4/80 (NB600-404, Novus Biologicals LLC, Littleton, CO) for 1 hour at a 1:900 dilution and then incubated in a rabbit anti-rat secondary (BA-4001, Vector Laboratories, Inc., Burlingame, CA) for 15 minutes at a 1:2000 dilution. Slides were the dehydrated, cleared and cover slipped. Images were captured using a high throughput Leica SCN400 Slide Scanner automated digital image system from Leica Microsystems. Whole slides were imaged at 20X magnification to a resolution of 0.5 μm/pixel.

Human fetal membrane culture: Human fetal membranes were excised from placental tissues from women who delivered healthy, full-term infants by cesarean section without labor. Deidentified tissue samples were provided by the Cooperative Human Tissue Network, which is funded by the National Cancer Institute. All tissues were collected in accordance with Vanderbilt University Institutional Review Board (approval #131607) and Declaration of Helsinki. Fetal membranes were processed into 12-mm punch biopsies (119) or mounted on transwell devices (58, 59). For immunohistochemistry, slides were processed as above using a rabbit polyclonal anti-GBS antibody (abcam, ab78846) or anti-CD68 (PA0191, Leica, Buffalo Grove, IL) for 1 h. Slides were then dehydrated, cleared and cover slipped. Images were captured using a high throughput Leica SCN400 Slide Scanner automated digital image system from Leica Microsystems. Whole slides were imaged at 20X magnification to a resolution of 0.5 μm/pixel.

Statistical analyses: Statistical analyses of fetal membrane cytokine and biofilm quantification were performed using Student's *t* test and One-Way ANOVA, respectively. Student's *t* test. *P* values < 0.05 were considered significant. All data analyzed in this work were derived from at least three separate biological replicates. Statistical analyses were performed using GraphPad Prism Software (Version 6.0g, GraphPad Software Inc., La Jolla CA).

RESULTS:

GBS infection of human fetal membrane tissues results in biofilm formation, tissue invasion, and stimulation of cytokine release: We had previously shown that perinatal pathogens including *Staphylococcus aureus* and *Escherichia coli* form biofilms on human fetal membrane tissues (119). To test the hypothesis that GBS could form biofilms on fetal membrane tissues, full thickness, fetal membrane tissues from non-laboring C-sections were arranged in transwell structures to create two chambers separated by the membrane tissues. GBS cells were added to the choriodecidual surface for 48 hours. At 48 hour of infection GBS formed biofilm structures on the choriodecidual surface (**Figure III.1**). Immunohistochemistry analysis using anti-GBS cell lysate antibodies demonstrated GBS microcolonies on the choriodecidual surface. Additionally, GBS was also found to have invaded into the membrane tissues toward the amniotic epithelium (**Figure III.1B**). As GBS infected and invaded membrane tissues, it was hypothesized that GBS infection would result in release of cytokines. Supernatants from fetal membrane co-cultures were investigated to understand the subsequent immune response to infection. GBS infection resulted in significant increases in IL-1β and IL-6 with a trend toward significance in GM-CSF release. No significant differences in INF-γ, TNF-α or IL-2 were identified in at 48 hours of infection (**Figure III.2**).

Macrophages traffic to the area of GBS infection in fetal membrane and mouse placental tissues: As IL-6 signaling results in macrophage recruitment to sites of infection and human chorioamnionitis is associated with proinflammatory cytokine changes and influx of immune cells into membrane tissues, we evaluated GBS infected human fetal membranes for the presence of macrophages (16). Immunohistochemistry analysis identified $CD68^+$ macrophages co-localizing to areas of GBS infection within the choriodecidua (**Figure III.3**). In addition to the *ex vivo* human tissue model, a mouse model of ascending perinatal GBS infection was also interrogated (120). Within both, mouse fetal membranes and placental tissues, $F4/80^+$ macrophages were found at the tissue location of GBS infection (**Figure III.4**).

Environmental availability of glucose and zinc modify GBS biofilm formation: As GBS formed biofilms on fetal membrane tissues, environmental factors that might module the GBS biofilm response were investigated. In order to cause perinatal infections, it is thought that GBS cells from the gastrointestinal tract are transferred to the vaginal canal, where there are differences in nutrient availability that may alter bacterial virulence strategies (41, 121, 122). Previous reports have suggested that diverse bacterial species are stimulated to form biofilm in response to glucose and changes in zinc availability (47, 123-125). Several clinical isolates' *in vitro* biofilm formation was

evaluated using a crystal violet plate assay (126). Compared to GBS biofilms grown in standard media, biofilms grown in media supplemented with 1% glucose (10 mM) resulted in an increase in biofilm formation in all but one of the GBS strains tested (**Figure III.5**). Next, GB00037 was evaluated for biofilm formation in the presence of the synthetic zinc chelator, N,N,N',N'-tetrakis (2-pyridylmethyl) ethylenediamine (TPEN). Under conditions of zinc restriction, GB00037 produced significantly more biofilm (**Figure III.6**), a result that was reversed by the addition of an exogenous source of nutrient zinc, zinc chloride. To further investigate the role of environmental zinc availability on biofilm formation, human fetal membrane tissues were infected with GBS in media supplemented with TPEN or TPEN and exogenous zinc chloride. As with *in vitro* biofilms, conditions of zinc restriction imposed by the presence of TPEN stimulated biofilm production, whereas the addition of exogenous zinc chloride, abrogated this response (**Figure III.7**).

DISCUSSION:

Despite that GBS is a leading cause of perinatal and neonatal infections, knowledge gaps remain concerning how GBS infection results in adverse pregnancy outcomes including preterm birth, stillbirth, and neonatal sepsis. Here, we employed an *ex vivo* model of chorioamnionitis using human fetal membrane tissues and a mouse model of ascending infection to investigate interactions between GBS cells and gestational tissues with the goal of understanding how these interactions may contribute to adverse pregnancy outcomes.

GBS infection of human fetal membrane tissues resulted in biofilm formation on the choriodecidual surface. We have previously shown that other perinatal pathogens including *E. coli* and *S. aureus* are also capable of forming biofilms on these tissues (119). Biofilms offer advantages during pathogenesis by aiding in surface adhesion, niche establishment, and modulation of and protection against host immune responses (107, 109-113). In addition to forming biofilms, at 48 hours of infection, GBS was also found to invade fetal membrane tissues toward the amniotic epithelium. These results contradict prior studies using human fetal membrane tissues that did not see GBS tissue invasion, but these studies only allowed infection to proceed for 24 hours (58, 59). Additionally, one study noted that recovery of GBS from human fetal membrane tissue homogenates and supernatants decreased after 4 hours of time; based on our data, we speculate that this finding may represent bacterial clumping in biofilms rather than a decrease in bacterial proliferation or viability (59). Other groups have identified GBS invasion of gestational tissues and have suggested that the hemolytic pigment β-hemolysin may be important in this process (53, 63). GB00037, the strain used in this study, produces minimal β-hemolysin, but other virulence factors including GBS hyaluronidase (HylB) may contribute to its virulence in the absence of pigment (65).

In response to GBS infection, we found that human fetal membrane tissues released significantly more IL-1β, IL-6, and a trend toward more GM-CSF than uninfected controls. Our results mirror prior studies that have demonstrated GBS infection of fetal membrane tissues lead to the production of these inflammatory cytokines (59). We did not identify a significant increase in TNF-α in our system as has been seen in shorter infection time courses (59). Previous studies have shown that IL-1β is important to mounting anti-microbial responses within fetal membrane tissues through stimulating production of antimicrobial peptides such as human beta defensins (59, 127). Our results also reinforce findings from non-human primate models of GBS perinatal infection where amniotic fluid concentrations of proinflammatory cytokines including IL-1β, IL-6, and TNF-α increased prior to delivery (60). IL-6 and IL-1β play important roles in the cascades that result in premature rupture of membranes and preterm birth as these cytokines influence granulocyte trafficking to the site of infection, deposition of matrix degrading enzymes, and prostaglandin synthesis (8, 16, 128)

As the cytokines described above attract granulocytes and macrophages represent 20-30% of the leukocytes within gestational tissues (71), we investigated if tissue resident macrophages were found in areas of GBS infection. We found that in both, an *ex vivo* model of chorioamnionitis and an *in vivo* mouse model of ascending GBS infection, macrophages could be seen by immunohistochemistry analysis localized to the area of infection (129). Fetally-derived macrophages, called Hofbauer cells or placental macrophages (PMs), are thought to play key roles in placental implantation and development (72, 73). Components of gestational tissues including decidual stromal cells communicate to placental macrophages via chemical mediators such as prostaglandins to influence macrophage functions such as TNF-α release and phagocytosis, but the functions of resident macrophages within gestational tissues during infection are less clear (129).

As GBS was found to form biofilms on the choriodecidual surface during fetal membrane infection, we investigated environmental factors that may contribute to GBS biofilm responses. Our results indicate that higher concentrations of glucose and lower concentrations of zinc stimulate GBS biofilm production. As in our study, prior investigations into clinical GBS isolates' *in vitro* biofilm formation has demonstrated variable results (47). Previous studies have reported that capsular type III, ST-17 strains, which are considered to be hypervirulent, may produce more biofilm, but others have shown that colonizing and not invasive strains produce more robust biofilms (49, 130). Our results that higher glucose concentrations lead to enhanced biofilm formation mirrors prior studies, but there are conflicting reports whether the glucose content itself drives biofilm formation or if changes in environmental pH due to glucose metabolism by GBS may be more important for changes in biofilm phenotypes (49, 131). Additionally, other carbohydrates may have different effects on GBS biofilm formation as some human breast milk oligosaccharides have been found to alter GBS biofilm

formation and growth kinetics (132, 133). Conditions of limited zinc availability stimulated GBS biofilm production, and supplementation with exogenous zinc chloride diminished GBS biofilm responses. Zinc has previously been shown to alter biofilm response of diverse bacterial pathogens, and zinc is important for pathogenesis in other streptococcal species (123, 134). Glucose and zinc may represent important environmental factors in GBS colonization, as GBS is thought to move from the gastrointestinal tract, an environment of low glucose availability, to the vaginal canal, where available glucose concentrations are relatively higher and free zinc concentrations are low (121, 122, 135). These shifts in glucose and zinc availability may drive biofilm production, supporting colonization. Interestingly, maternal zinc deficiency and gestational diabetes are associated with increased risk of infection (136-138).

In summary, GBS infection of human fetal membrane tissue results in biofilm formation on the choriodecidual surface and invasion of GBS cells into the membrane tissues. In response to infection, proinflammatory cytokines including IL-1β and IL-6 are released and membrane resident macrophages traffic to the site of GBS infection. GBS biofilm responses are modulated by environmental signals including glucose and zinc availability, which may represent environmental cues to support GBS vaginal colonization.

Table III.1: Characteristics of GBS strains evaluated for biofilm formation.

GBS Strain	Molecular Serotype	Multi-Locus Sequence Type	Setting of Isolation	Source
GB00590	III	ST-19	Vaginal colonization	(139)
GB00079	III	ST-19	Early onset sepsis	(139)
GB00241	V	ST-23	Vaginal Colonization	(139)
GB00037	V	ST-1	Invasive infection	(140)
GB01454	V	ST-1	Stillbirth	(139)
GB01084 (CNCTC 10/84)	V	ST-26	Invasive infection	ATCC #49447(141)
GB2603 V/R	V	Unknown	Unknown	ATCC #BAA-611 (51)

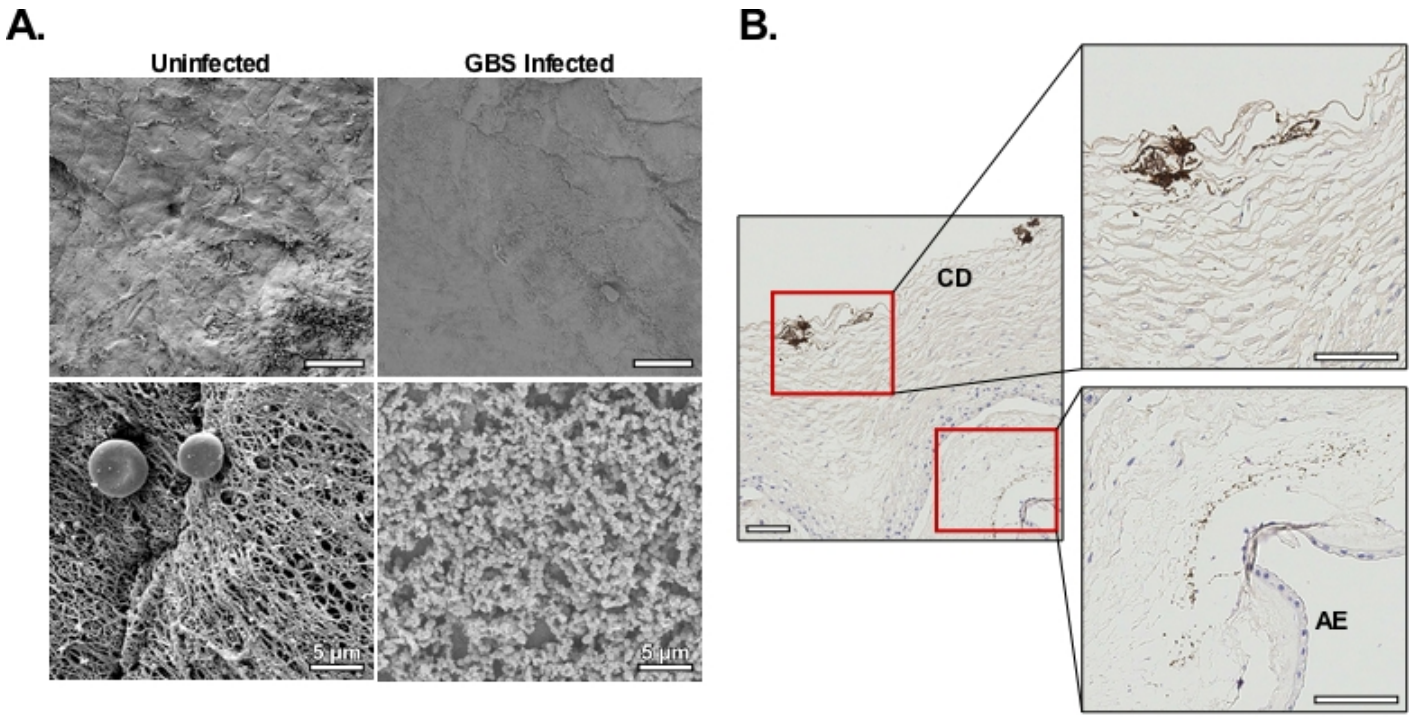

Figure III.1: GBS infection results in biofilm formation on the surface of human fetal membrane tissues and tissue invasion. Human fetal membrane tissues were excised from healthy, non-laboring C-sections, organized into transwell structures, and infected with GBS cells. (A) GBS infection of fetal membrane tissues results in biofilm structures on the choriodecidual face of fetal membrane tissues that were not seen in uninfected tissues (left). (B) Immunohistochemistry analysis using an anti-GBS lysate antibody demonstrates GBS microcolonies within the choriodecidua (CD) and tissue invasion toward the amniotic epithelium (AE). Unless noted, scale bars represent 100 μm.

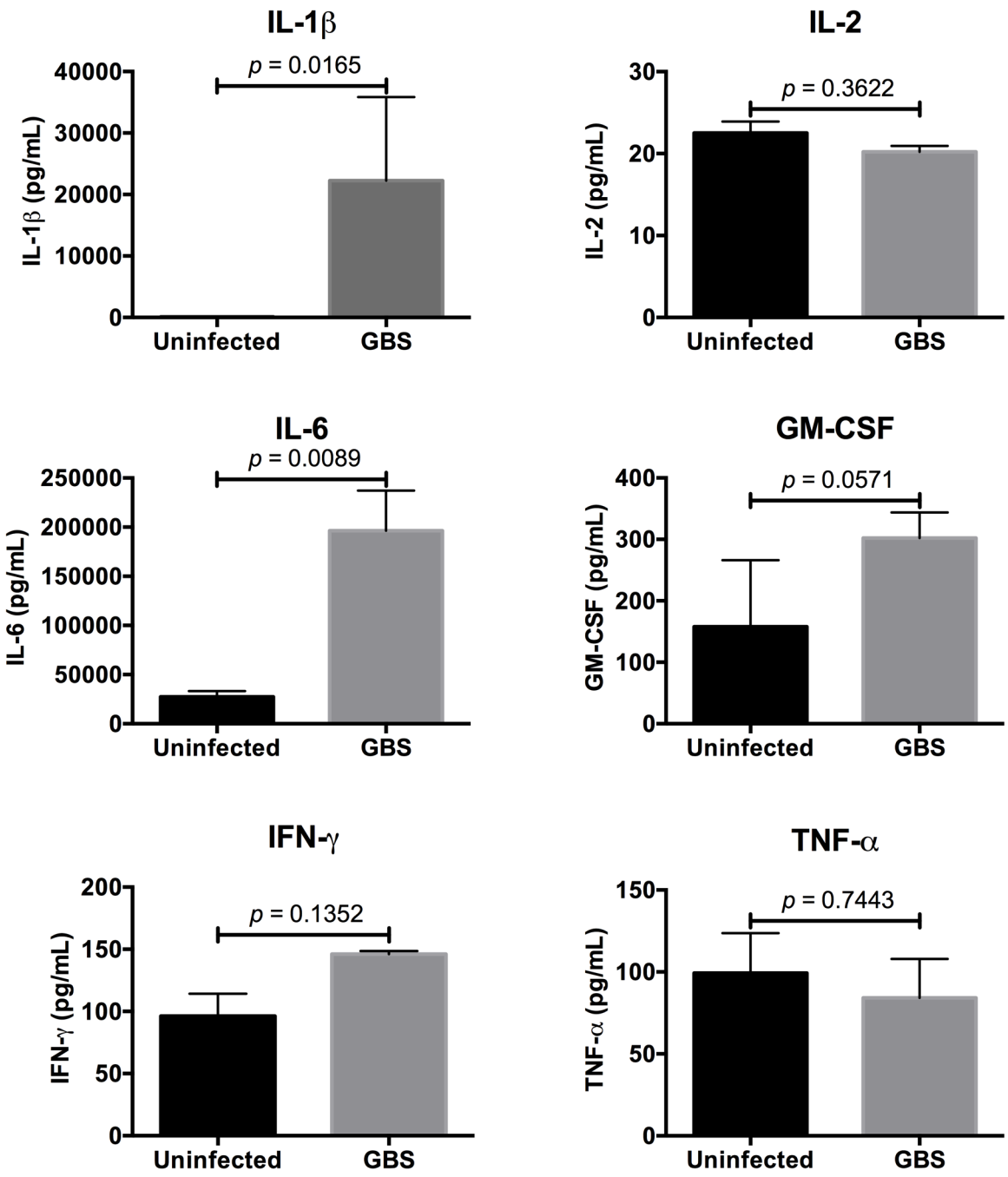

Figure III.2: GBS infection of fetal membrane tissues leads to cytokine release. Fetal membrane tissues were infected with GB00037 cells for 48 hours and co-culture supernatants were evaluated for cytokine release by ELISA. Data represent mean ± SE of 3-8 samples from different placenta tissues. *P* values are as listed above, 2-tailed Student's *t* test.

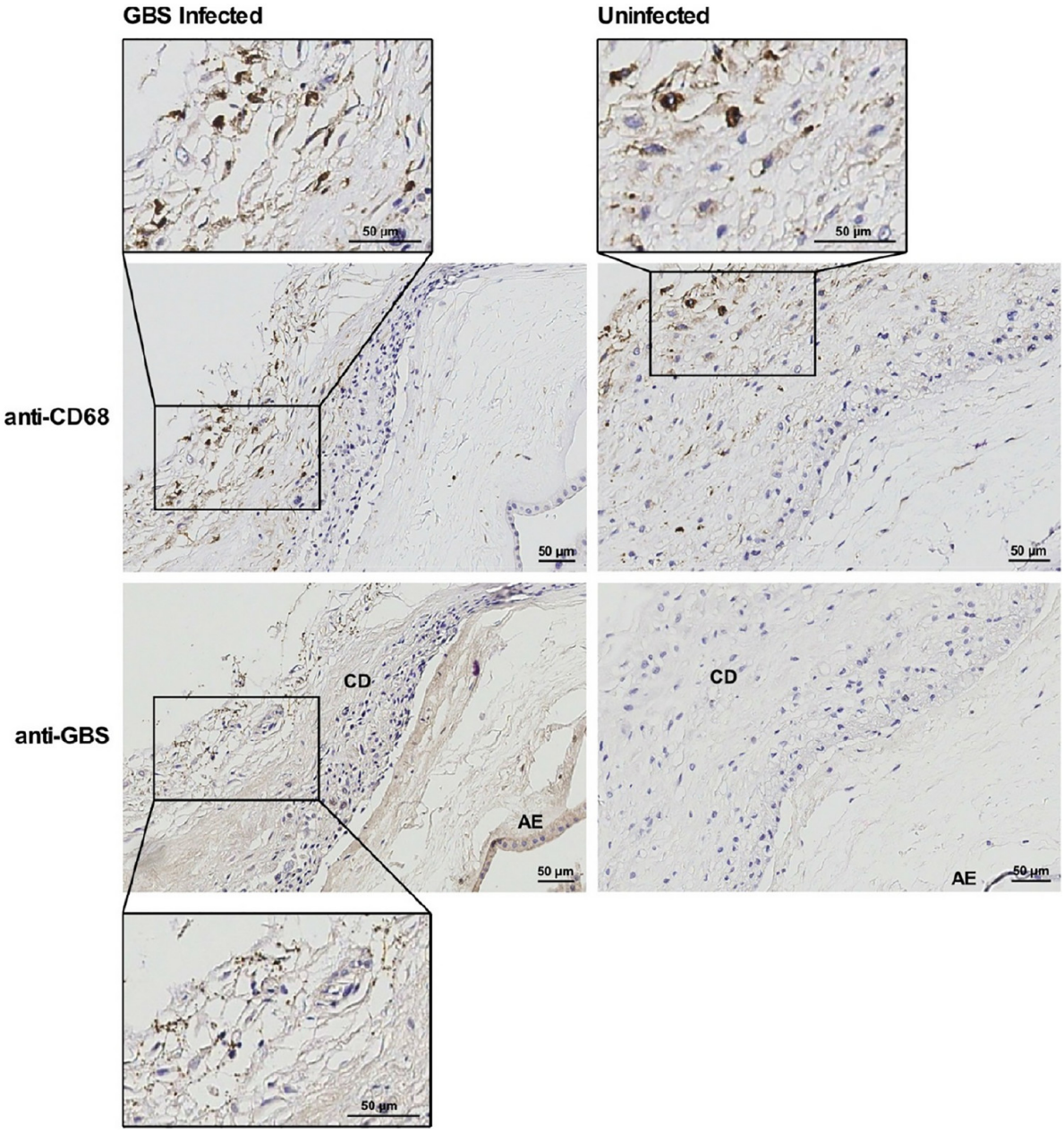

Figure III.3: Macrophages traffic to the site of GBS infection in an *ex vivo* chorioamnionitis model utilizing human fetal membrane tissues. Human gestational membranes were organized into transwell constructs and infected with GBS (10^6 CFU GB00037) on the choriodecidual surface for 48 hours before tissue processing and immunohistochemistry analysis. Tissues were stained with anti-CD68 for macrophages (top panels) or anti-GBS (bottom panels). Tissue analysis shows invasion of human membrane tissues *in vitro* by GBS and the presence of macrophages within the choriodecidua (CD) at the site of infection. AE = amniotic epithelium.

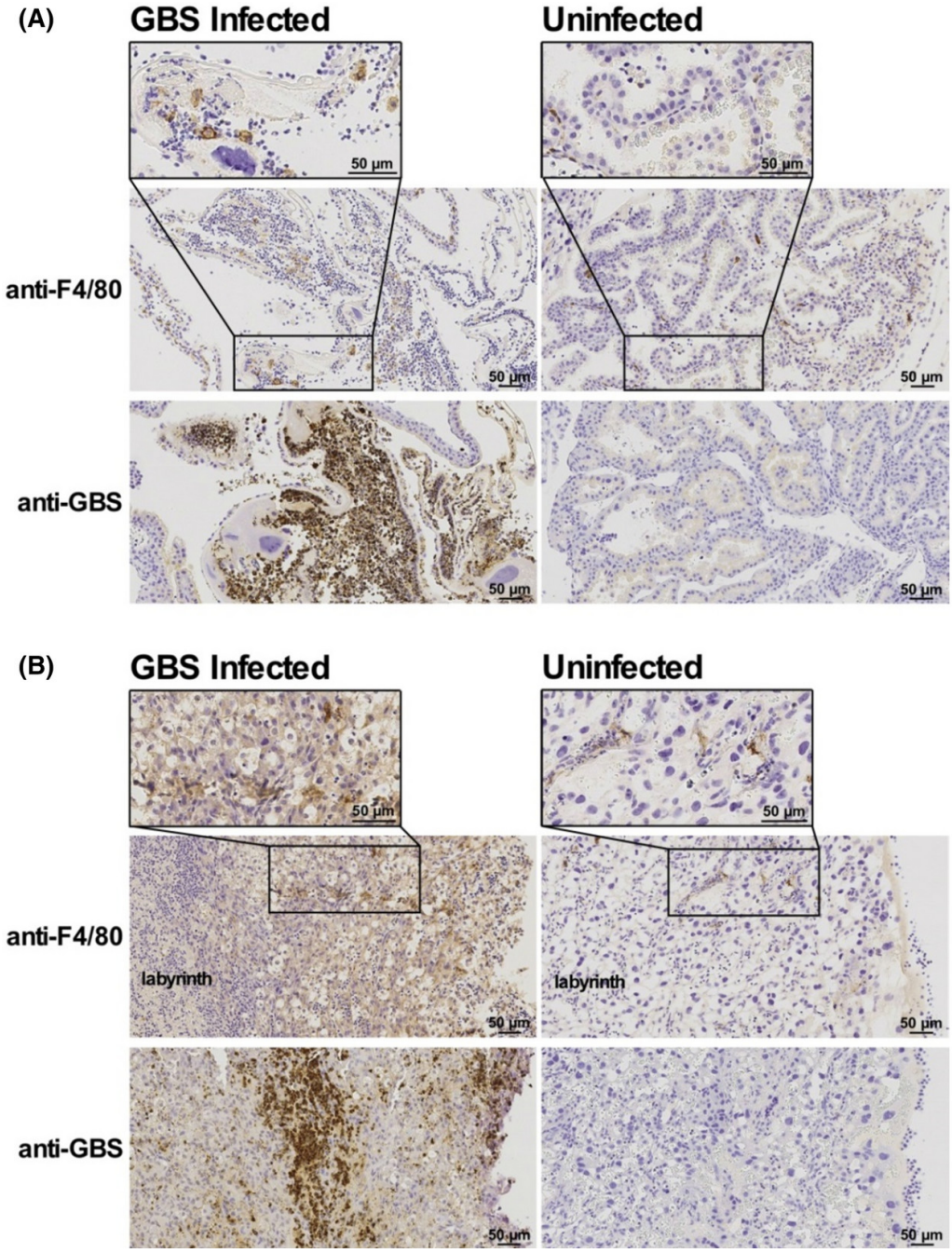

Figure III.4: Mouse model of ascending chorioamnionitis results in GBS gestational tissue invasion and macrophage recruitment. Pregnant mice at day E13.5 were intravaginally inoculated with 1×10^3 CFU GBS strain GB00037 and sacrificed on E15.5 (48 h after infection). Placental tissues were dissected and evaluated by immunohistochemistry for GBS invasion and the presence of F4/80$^+$ macrophages. Tissue analysis demonstrates that, after 48 h of ascending infection, GBS invades into (A) gestational membrane (B) and placental tissues (bottom panels). F4/80$^+$ macrophages traffic to the site of tissue infections (top panels of A and B).

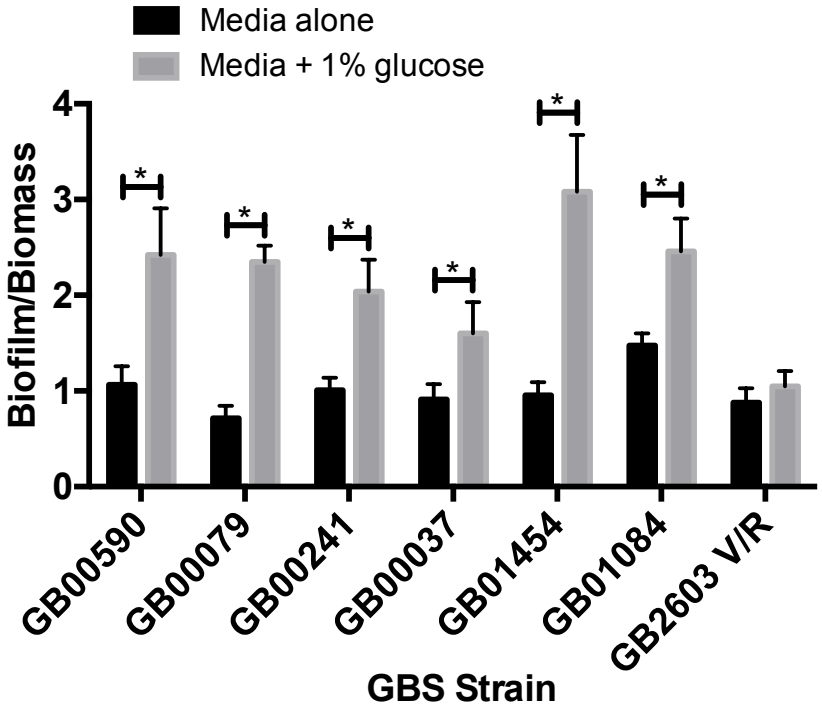

Figure III.5: Glucose availability alters biofilm production of GBS clinical isolates. GBS cells were grown in media alone or media supplemented with glucose and analyzed for biofilm production. * represents *P* <0.05, two-tailed Student's *t* test.

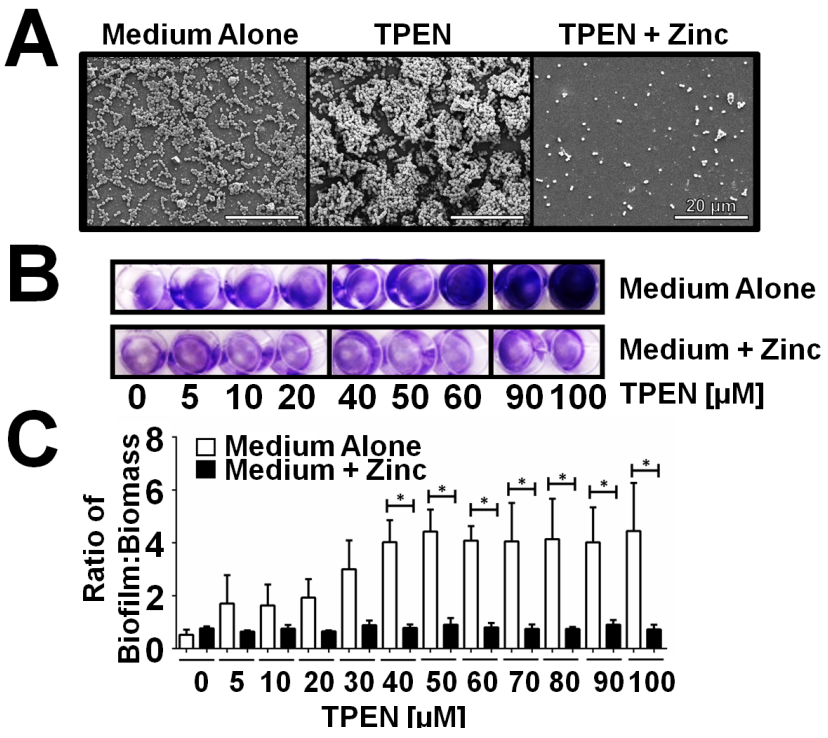

Figure III.6: Zinc sequestration enhances GBS biofilm formation. A) Scanning electron micrographs of GBS grown in media alone, media supplemented with a zinc chelator (TPEN), or in the presence of TPEN and excess exogenous zinc chloride (TPEN + Zinc). B) Increasing concentration of TPEN enhances macroscopic biofilm formation as evidenced by crystal violet staining. This phenotype is reversed by the addition of exogenous zinc. C) Quantification of biofilm formation compared to total biomass. **P* <0.05, two-tailed Student's *t*-test.

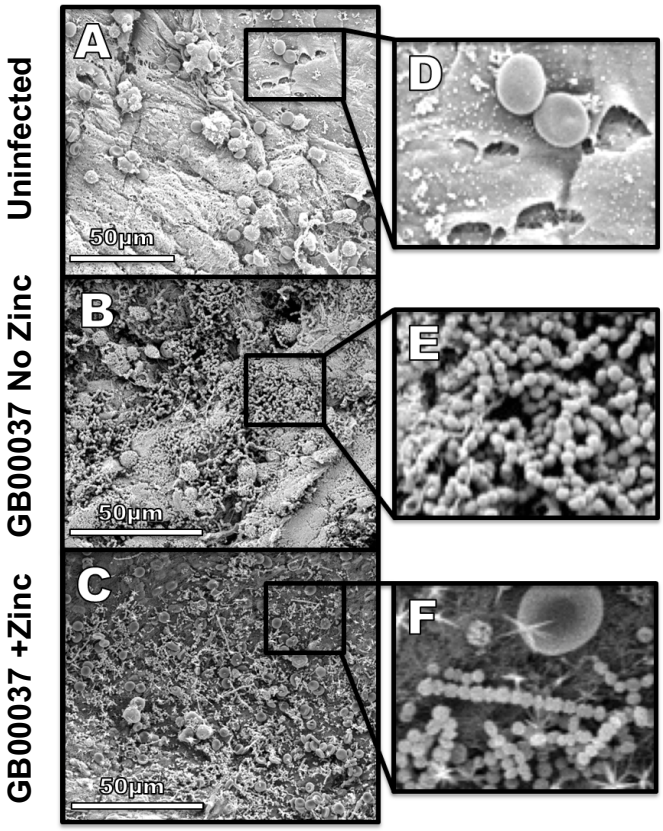

Figure III.7: Zinc availability alters GBS biofilm formation on human fetal membrane tissues. High-resolution scanning electron microscopy images of human fetal membrane tissues A & D) Uninfected, B & E) GB00037-infected membranes without zinc supplementation, C & F) GBS-infected membranes with zinc supplementation. Inset panels in D-F show high magnification. Zinc supplementation abrogates biofilm formation on human fetal membrane tissues.

CHAPTER IV

Raman microspectroscopy identifies *Streptococcus agalactiae* on *ex vivo* human fetal membrane tissues

INTRODUCTION:

Streptococcus agalactiae, also known as Group B *Streptococcus* (GBS), colonizes 10-40% of women during pregnancy, and GBS vaginal colonization is an important risk factor for chorioamnionitis, or infection of the fetal membranes, and neonatal sepsis (142). The Centers for Disease Control and Prevention recommends culture-based rectovaginal GBS screening during the third trimester followed by intrapartum antibiotic prophylaxis for women testing positive (24). Although this strategy has reduced the incidence of early-onset sepsis by 80%, 15% of full-term and 50% of preterm births do not receive screening prior to delivery (143). Additionally, prior studies of women delivering neonates with early-onset GBS sepsis found that in 75-82% of the cases the mothers had been appropriately screened for GBS carriage but had (falsely) tested negative (144, 145), indicating the need for a more sensitive detection method. Traditional culture-based screening requires 24-72 hours to provide results; PCR testing could reduce this time to a few hours, but this technology is not available in all settings (146). A rapid GBS diagnostic test could provide opportunities to identify GBS colonized women at the time of labor and focus the use of antibiotic therapy.

Raman spectroscopy (RS) is an inelastic light scattering technique that provides a biochemical “fingerprint” with sensitivity to features such as nucleic acids, carbohydrates, lipids, and proteins. Raman microspectroscopy (RμS), which provides higher spectral resolution, has been used to characterize bacteria and provide discrimination at the genus and species levels in vitro (147, 148). This technique could provide opportunities to identify GBS or other bacteria as a rapid diagnostic test, minimizing sample preparation and streamlining diagnostic information.

Due to the pressing need to accurately and rapidly determine the intrapartum GBS status of women, the ability of RμS to identify bacteria cultured on agar and in an *ex vivo* human tissue model of chorioamnionitis was investigated, comparing GBS with other pathogens implicated in perinatal infections and chorioamnionitis (119). Here, we demonstrate that GBS has unique Raman spectral features that can be observed whether RμS is used to interrogate bacterial colonies on agar or ex vivo infected fetal membrane tissues. Detecting characteristic GBS spectral patterns suggests that this technology might inform new lab-based or point-of-care diagnostic tests to identify GBS colonization or infection.

METHODS:

Bacterial culture: For RμS colony measurements, diverse capsular serotype isolates of *Streptococcus agalactiae* (**Table IV.1**), an invasive clinical isolate of *Escherichia coli* (149), and methicillin-resistant *Staphylococcus aureus* (MRSA) strain USA300, (ATCC #BAA-1717, Manassas, VA) were cultured on Mueller-Hinton (MH) agar (BD, Franklin Lakes, NJ) to minimize signal contribution from media.

For human fetal membrane infection, three GBS strains, *E. coli*, and MRSA were cultured on tryptic soy agar supplemented with 5% sheep blood at 37ºC in ambient air overnight. Bacteria were sub-cultured from blood agar plates into Todd-Hewitt broth (BD) and incubated (shaking at 200 RPM) at 37ºC in ambient air overnight. Cells were then washed, suspended in phosphate buffered saline (pH 7.4), and bacterial density was measured spectrophotometrically at an optical density of 600 nm (OD_{600}).

Human fetal membrane co-culture: The Vanderbilt Institutional Review Board approved (approval 131607) isolation of de-identified human fetal membrane tissues was conducted as previously described (119). Bacteria were added to the fetal membrane choriodecidual surface at a multiplicity of infection of $1x10^6$ cells per 12 mm diameter membrane, using a predetermined coefficient of bacterial density of 1 OD_{600}= $1x10^9$ cells. Uninfected membrane samples were also maintained. Co-cultures were incubated at 37ºC in ambient air containing 5% CO_2 for 48-72 hours prior to RμS evaluation.

Raman microspectroscopy: A Raman microscope (inVia Raman Microscope, Renishaw plc, Gloucestershire, UK) with an 830 nm laser diode was used for spectral measurements (150). For bacterial colonies, a 100X objective (N PLAN EPI, NA=0.85, Leica, Weltzlar, Germany) was used to focus the laser at ~12 mW. Fetal membrane tissue spectra were measured using a 50X objective (N PLAN EPI, NA=0.75, Leica) to focus a 40 μm laser line on the sample at ~23 mW. Raman scattered light was detected as previously described with a spectral resolution of ~1 cm^{-1} (150).

Spectral measurements for bacterial colonies included one spot per colony and three colonies per bacteria using a 15-second exposure with 9 accumulations from 800-1700 cm^{-1}. Raman measurements from three different locations were performed on each punch biopsy tissue (total of 34). These included control (uninfected, n=5), GB00037 (n=6), GB00590 (n=5), GB01084 (n=6), *E. coli* (n=5), and MRSA (n=7) representing at least 3 separate placental samples with 1-3 technical replicates. Acquisition parameters for fetal membrane tissues included a 15-second exposure with 3 accumulations.

Raman data processing & spectral analysis: Spectral data processing prior to analysis including fluorescence background subtraction and noise smoothing was performed as previously described (150). A 9th degree modified polynomial fit was used for spectral measurements from GBS colonies and tissue model. Post-processed, non-normalized Raman spectra were z-scored for subsequent analysis. Principal component analysis (PCA), a non-supervised data reduction statistical approach, was performed on z-scored bacterial colony spectra using singular value decomposition (SVD). The scores output from PCA-SVD were then used to calculate the distance between each data point in orthogonal vector space using the Euclidean distance measure. A hierarchical cluster analysis (HCA) was designed based on the PCA-SVD score distances calculated and an agglomerative clustering approach with single linkage.

A machine learning algorithm, sparse multinomial logistic regression (SMLR) (151), was utilized to discriminate across the different tissues (150). Briefly, training data was compiled based on RμS measurements of the fetal membrane tissues. For this analysis, a value called SMLR feature importance (SMLR-FI), a linear combination of importance (weight) and frequency of features, was used to determine biomarkers critical for successful classification of infected biofilm tissues (152). A posterior probability of class membership was plotted for infected membrane tissues. Evaluation of this algorithm was performed using a *k*-fold cross validation (leave-one-tissue-out).

Scanning electron microscopy: Following RμS analysis, human fetal membrane samples were prepared for scanning electron microscopy as previously described (119). Samples were imaged with a FEI Quanta 250 field-emission gun scanning electron microscope (FEG-SEM). Images are representative of three replicates from three different subjects.

RESULTS:

Raman microspectroscopy (RμS) differentiates bacterial species and strains on agar: A diverse set of GBS strains were selected based on capsular type, multilocus sequence types (MLST), and β-hemolysin pigment production (**Table IV.1**). Visual differences in colony pigmentation are evident across strains (**Figure IV.1A**). Corresponding Raman spectra of GBS, MRSA, and *E. coli* bacterial colonies are shown in **Figure IV.1B**. Major strain biochemical variations are highlighted in the gray bands of Raman spectra. For example, GB01084 contains two Raman peaks at 1121 cm^{-1} and 1506 cm^{-1} that are higher in intensity compared to other GBS, *E. coli*, and MRSA strains. Similarly, MRSA contains unique Raman peaks at 1159 cm^{-1} and 1525 cm^{-1} that are not present in any other strain evaluated. The HCA dendrogram presents clusters of MRSA, GB01084, *E. coli*, and the remaining

GBS strains studied based on the dissimilarity of the pairwise distances of observations (PCA-SVD scores from principal components 1 and 2) from their respective Raman spectra (**Figure IV.1C**).

RμS distinguishes bacterial infection in explanted fetal membrane tissues: Given similarities of the spectra collected from GBS on agar, human fetal membrane tissues were investigated as a biologically relevant model to determine if RμS was sensitive enough to identify GBS spectral features within infected tissues. As a first step, mean-normalized Raman spectra of uninfected and infected tissues were compared (**Figure IV.2**). Vertical gray bands represent important biochemical features for classification of infected tissues based on a SMLR-FI of at least 25%. A probability of class membership plot highlights correctly classified spectral measurements compared to incorrectly classified measurements with respect to control and infected tissues (**Figure IV.2B**). A sensitivity of 97.7% and specificity of 66.7% for detection of infection on fetal membrane tissues was determined from the output confusion matrix (**Figure IV.2C**). The ability of RμS to differentiate GBS strains from *E. coli* and MRSA was further evaluated in these tissues. Mean-normalized Raman spectra of GBS, *E. coli*, and MRSA infected tissues are shown along with vertical gray bands indicating SMLR-FI features of at least 25% (**Figure IV.3A**). A probability of class membership plot shows correctly identified measurements compared to those incorrectly classified of GBS versus *E. coli* or MRSA (**Figure IV.3B**). Membrane tissues infected with GBS were detected with 100.0% sensitivity and 88.9% specificity (**Figure IV.3C**). Scanning electron microscopy imaging identifies bacterial cells present in biofilm structures at the area of Raman measurements (denoted by a small cut into membrane tissues seen at low magnification) as demonstrated by the multilayered bacterial cells embedded in extracellular polymeric substances (**Figure IV.3D**).

DISCUSSION:

GBS remains an important perinatal pathogen despite recommendations to screen and prophylactically treat colonized women during pregnancy. Here, RμS was investigated as a means to identify GBS on agar plates and human fetal membrane tissues infected ex vivo. Using RμS, GBS was found to have unique spectral features compared to another Gram-positive bacteria, *S. aureus*, and the Gram-negative perinatal pathogen, *E. coli*. Additionally, spectral patterns of GBS strains varied, suggesting that each strain has a unique spectral signature, while maintaining GBS-common identifiable markers. Qualitative analysis of Raman spectra from bacterial colonies presents differences in the 1121 cm^{-1} (C-C stretching), 1159 cm^{-1} (C-C stretching), 1506 cm^{-1} (C=C stretching), and 1525 cm^{-1} (C=C stretching) Raman bands, which correspond to pigmentation caused by a carotenoid (153). This pigmentation of GBS cells results from production of beta-hemolysin, a

carotenoid pigment and virulence factor. Nonetheless, non-pigmented strains are also capable of causing clinical disease, thus using RμS to screen for pigment alone would be insufficient (65). Given that RμS can differentiate colonies on agar plates, it could be used to expedite bacterial identification in microbiology labs once adequate spectral libraries of bacterial Raman spectra are constructed.

More importantly, RμS is able to identify fetal membrane tissues infected with GBS and distinguish these from uninfected tissues or those infected with *E. coli* or MRSA. Spectra from infected and uninfected membrane tissue specimens highlight major differences in peak intensity and width for the two groups in Raman bands 880-955 cm^{-1}, 1110-1128 cm^{-1}, 1492-1515 cm^{-1}, and 1645-1672 cm^{-1} (Supp. Fig. 1A). In addition, higher standard deviation is present in Raman spectra of GBS-infected tissues at 1121 cm^{-1} (C-C stretching) and 1506 cm^{-1} (C=C stretching) since these features are more intense in GB01084 compared to GB00037 and GB00590. To identify more subtle spectral differences, SMLR-FI was implemented across tissue types. Features important for characterizing uninfected fetal membrane tissue include 889 cm^{-1} (SMLR-FI=0.56) related to biological protein structures in tissue, 910 cm^{-1} (SMLR-FI=0.87) related to fatty acids, and 1661 cm^{-1} (SMLR-FI=0.56) as part of amide I (C=O stretch). Twelve features above a 25% SMLR-FI were found to be important for distinguishing GBS-infected tissue, including 853 cm^{-1} (SMLR-FI=0.50) as part of tyrosine and 1406 cm^{-1} (SMLR-FI=0.76) related to lipids. Tissues infected with *E. coli* presented ten features above the SMLR-FI threshold and include 858 cm^{-1} (C-C stretch, SMLR-FI=0.58) and 1157 cm^{-1} (C-C related to carotenoid, SMLR-FI=0.53). The Raman peak at 1157 cm^{-1} (C-C related to carotenoid, SMLR-FI=1.0) was most important for identification of MRSA-infected tissue relative to nine other features above 25% SMLR-FI. When compared against *E. coli* or MRSA infected tissue, RμS is able to identify GBS infected tissues with 100.0% sensitivity and 88.9% specificity using SEM imaging to confirm bacterial presence at the site of Raman measurements.

In conclusion, Raman spectroscopy has the ability to detect bacterial infection of human fetal membrane tissue and distinguish between GBS versus MRSA or *E. coli*. As this technology progresses it holds promise to identify GBS and other bacteria on different tissues, thereby providing more rapid assessment than traditional diagnostic microbiology. More work is needed to reach this goal including construction of bacterial spectral libraries to compare biochemical features between strains, further engineering to allow *in vivo* spectral measurements on various tissues, and evaluating polymicrobial infections to determine if spectral signatures of pathogenic bacteria can be isolated in the presence of normal bacterial communities or microbiota. This study takes the first step to expand research in this area.

Table IV.1: GBS strains evaluated by Raman spectroscopy.

GBS Strain	Molecular Serotype	Multi-Locus Sequence Type	Setting of Isolation	Source
GB00037	V	ST-1	Neonatal sepsis	(140)
GB00590	III	ST-19	Vaginal/rectal Colonization	(139)
GB00002	Ia	ST-23	Vaginal/rectal Colonization	(139)
GB01084 (CNCTC 10/84)	V	ST-26	Unknown	ATCC #49447 (141)
GB2603 V/R	V	Unknown	Unknown	ATCC #BAA-611 (51)

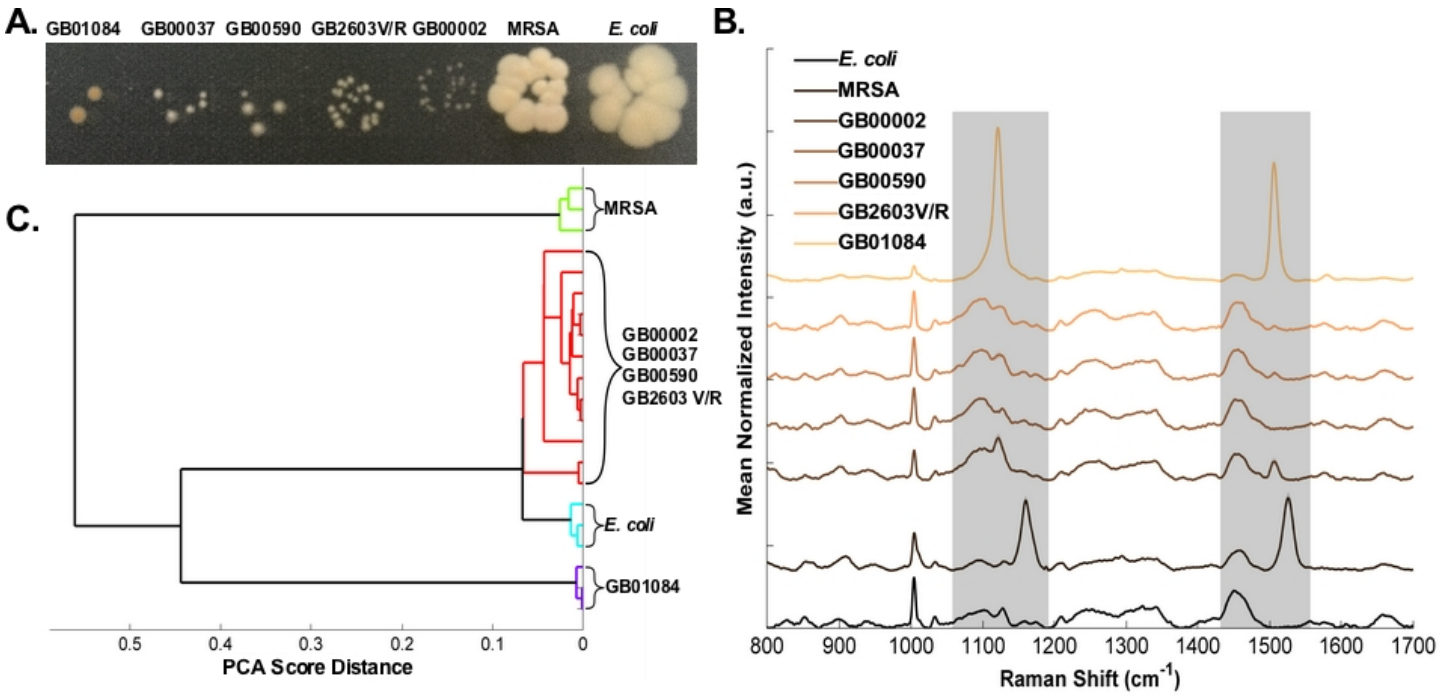

Figure IV.1: Raman spectra of GBS, MRSA, and *E. coli* bacterial colonies present distinct biochemical features. A: Bacterial cells from five Group B *Streptococcus* (GBS) strains, *S. aureus* strain USA300 (MRSA), and *E. coli* serotype O75:H5:K1 were grown on Mueller-Hinton (MH) agar to demonstrate pigmentation differences of the strains. B: Mean ± standard deviation Raman spectra of bacterial colonies. C: Hierarchical cluster analysis (HCA) of bacterial colony measurements based on principal component analysis scores.

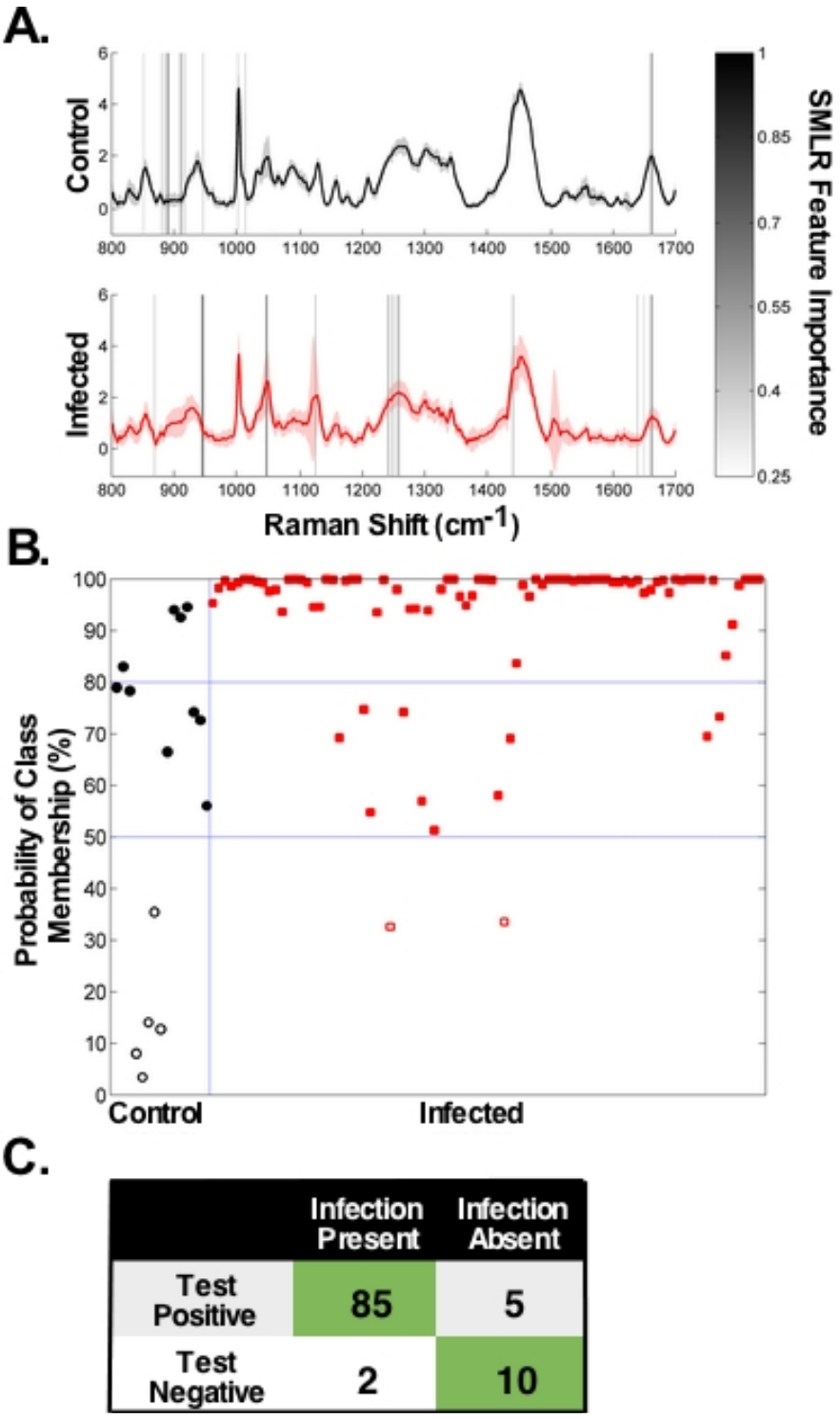

Figure IV.2: Raman microspectroscopy distinguishes infected versus uninfected fetal membrane tissues. A: Mean ± standard deviation Raman spectra of infected tissues compared to control (uninfected) specimens. Gray vertical bands represent biochemical features important for classification based on sparse multinomial logistic regression (SMLR). B: Posterior probability of class membership plot of Raman spectra with respect to infected and uninfected tissues. Filled markers represent correctly classified Raman spectra and unfilled markers represent incorrectly classified spectra. C: Confusion matrix showing the performance of the SMLR classifier.

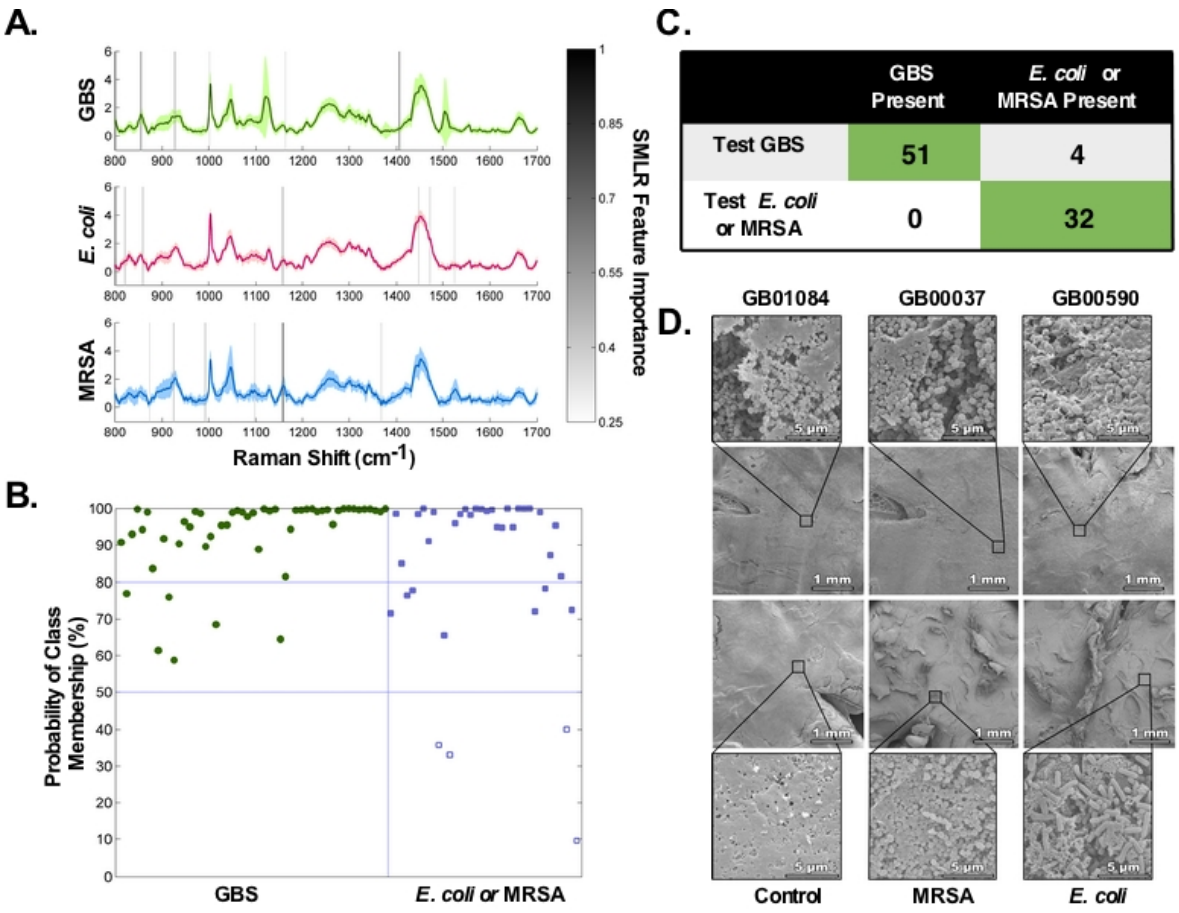

Figure IV.3: Raman microspectroscopy of *ex vivo* infected fetal membrane tissues identifies and differentiates bacterial cells within tissues. A: Mean ± standard deviation Raman spectra for Group B *Streptococcus* strains (GB01084, GB00037, and GB00590), *E. coli*, and *S. aureus* strain USA300 (MRSA) infected tissues. Gray vertical bands represent biochemical features important for classification based on sparse multinomial logistic regression (SMLR). B: Posterior probability of class membership plot for each tissue type. Filled markers represent correctly classified Raman spectra and unfilled markers represented incorrectly classified spectra. C: Confusion matrix representing the performance of the SMLR classifier for each tissue type. D: Scanning electron microscopy images of fetal membrane tissues used for Raman analysis to verify the presence of bacteria at the location of Raman measurements. A small cut was made into the membrane tissues to denote the relative location of Raman evaluation. Inserts demonstrate bacterial cells and extracellular polymeric substances, suggestive of biofilms, seen in these locations.

CHAPTER V

Group B *Streptococcus* induces neutrophil recruitment to gestational tissues and elaboration of extracellular traps and nutritional immunity

INTRODUCTION:

GBS and pregnancy: *Streptococcus agalactiae* (Group B *Streptococcus*, GBS) is a leading cause of adverse pregnancy and neonatal outcomes including stillbirth, chorioamnionitis, preterm birth, and neonatal sepsis and meningitis (16, 24, 33, 154). While up to 50% of pregnant women screen positive for GBS rectovaginal colonization at some point during pregnancy, most women maintain asymptomatic colonization (33). However, in some neonates, invasive GBS disease occurs via vertical transmission either from ascending vaginal infection during pregnancy or from exposure during vaginal delivery, resulting in lifelong health impairments for affected children(16, 24, 33, 154, 155). Consequently, the CDC recommends routine GBS screening during late pregnancy and antibiotic prophylaxis for those testing positive (154). Despite this intervention, GBS remains the leading infectious cause of morbidity and mortality among neonates in the United States (24).

Chorioamnionitis and neutrophils: Ascending bacterial infection from the lower genital tract to the uterine cavity is the most common cause of intra-amniotic infection, which leads to profound inflammation of the extraplacental membranes surrounding the fetus; a process that is termed chorioamnionitis (16, 155). Ascending microorganisms are first localized in the supracervical decidua; subsequent propagation and chorioamniotic passage leads to microbial infection of the amniotic cavity and even the fetus (16). Microbial invasion of the amniotic cavity has been shown to induce a robust inflammatory response including an increase in pro-inflammatory cytokines such as IL-1, TNF-alpha, IL-6, and IL-8, as well as a dramatic increase in neutrophil count (16). Histopathologically, the characteristic morphologic feature of acute chorioamnionitis is diffuse infiltration of neutrophils of maternal origin into the extraplacental membranes (16, 155, 156).

Neutrophils and extracellular traps: Colonization of the female genital tract by potential pathogens is a complex process influenced by the host innate immune response and the pathogenic potential of the invading microbe. GBS is distinctive in its ability to cause both invasive disease and asymptomatic colonization of the female genital tract (157). GBS is an important pathogen that causes invasive disease in pregnant hosts. In an effort to study how GBS colonizes the reproductive tract and causes ascending invasion of gestational tissues, we employed a mouse model of

ascending GBS vaginal infection during pregnancy which was pioneered by Randis *et al.* (62). Studies in this model have shown that the GBS toxin beta-hemolysin/cytolysin directly induced disruption of maternal-fetal barriers, causing chorioamnionitis, preterm birth, and stillbirth (62). Furthermore, studies of a murine model of chronic GBS genital tract colonization showed significant neutrophil infiltrates in the vaginal mucosa and the formation of DNA neutrophil extracellular traps (NETs) in response to GBS infection (158). Human neutrophils have also been shown to form NETs in vitro in response to GBS (158). NETs are a recently discovered antimicrobial mechanism composed of nuclear chromatin, histones, and other antimicrobial proteins that serve to immobilize and kill or inhibit the growth of invading microbes (159).

Neutrophils and nutritional immunity: High resolution imaging studies have revealed that the DNA which comprises NETs is studded with antimicrobial proteins such as myeloperoxidase, elastin, calprotectin (S100A8/S100A9 heterodimer) and lactoferrin (159). The latter two of these host proteins bind transition metals such as manganese, zinc, and/or iron at high affinity to effectively sequester these important nutrients away from invading pathogens in a process referred to as "nutritional immunity" (160). Proteomic analyses of amniotic fluid from cases of intra-amniotic infection have revealed dramatic changes in protein composition and increased presence of neutrophil-associated antimicrobial proteins, such as lactoferrin (16, 156). Previous work indicates that GBS has a strict requirement for iron to initiate bacterial growth in a chemically defined medium (161, 162). This, coupled with the observation that lactoferrin is elevated in GBS-infected tissues where neutrophils are abundant (16, 156), led us to hypothesize that neutrophilic infiltrates, which are characteristically present in chorioamnionitis, could potentially be controlling GBS growth and proliferation in the host by elaborating NETs studded with lactoferrin to chelate nutrient iron and starve invading GBS of essential iron. Our work demonstrates that neutrophils are recruited to the site of GBS infection in a murine model of ascending infection during pregnancy. Furthermore, we demonstrate that GBS-neutrophil interaction results in the elaboration of NETs decorated with the antimicrobial protein lactoferrin. In its apo- (unbound to iron) form, lactoferrin inhibits GBS growth and proliferation in a dose-dependent manner that can be abrogated by the presence of an exogenous source of nutrient metal.

METHODS:

Bacterial strains and culture conditions: The capsular type V *S. agalactiae* strain GB00037, obtained from a human case of neonatal sepsis (163), was cultured on tryptic soy agar plates supplemented with 5% sheep blood (blood agar plates) at 37ºC in ambient air overnight. Bacteria

were sub-cultured from blood agar plates into Todd-Hewitt broth (THB) and incubated (aerobically, shaking at 200 RPM) at 37ºC in ambient air overnight. The following day, bacterial density was measured spectrophotometrically at an optical density of 600 nm (OD_{600}), and bacterial numbers were determined with a coefficient of 1 OD_{600}= 10^9 CFU/mL.

Ethics statement: All animal experiments were performed in accordance with the Animal Welfare Act, U.S. federal law, and NIH guidelines. All experiments were carried out under a protocol approved by Vanderbilt University Institutional Animal Care and Use Committee (IACUC; M/14/034), a body that has been accredited by the Association of Assessment and Accreditation of Laboratory Animal Care (AAALAC).

Mouse model of GBS infection during pregnancy: GBS infection of pregnant mice and subsequent analyses were performed as previously described with some modifications (62). Experimental design is outlined in **Figure V.1**. Briefly, C57BL6/J mice were purchased from Jackson Laboratories and mated in harem breeding strategies overnight. Pregnancy was confirmed the following day by the presence of a mucus plug to establish the embryonic (E) day (E0.5). On embryonic day 13 (E13.5) dams were anesthetized using isoflurane chambers and 50 µL of inoculate containing 10^3 colony forming units (CFU) in THB medium plus 10% gelatin was introduced into the vagina. Sham controls were inoculated with 50 µL of THB medium containing 10% gelatin. Animals were housed singly until embryonic day 15 (E15.5) at which time they were sacrificed by carbon dioxide euthanasia procedures and necropsy was performed to isolate reproductive tissues including vagina, uterus, placenta, decidua, and fetus. For burden studies, a single tissue sample was derived from each separate dam. Four to six animals were utilized for each experimental group derived from three separate experiments (sham treated uninfected animals or GBS-infected animals). Tissues were analyzed for bacterial burden by enumerating CFU per mg of tissue by homogenizing tissues, performing serial dilution and quantitative culture on blood agar plates.

Immunohistochemistry and histopathological examination: Murine tissues (1 tissue sample per dam) from the GBS ascending vaginal infection during pregnancy model were fixed in 10% neutral buffered formalin prior to embedment in paraffin. Tissues were cut into 5 µm sections and multiple sections were placed on each slide for analysis. For histopathological examination, sections were stained with hematoxylin and eosin and evaluated by microscopical techniques. Additional sections of fetal-placental tissue were evaluated by immunohistochemical (IHC) techniques to determine the presence and spatial localization of GBS or lactoferrin. After quenching with 0.03% hydrogen

peroxide for 20 min at RT, tissues were treated with a heat-induced epitope retrieval solution (Universal decloacker, Biocare Medical, Concord, CA) using a pressure cooker at 121°C for 20 min and allowed to cool at RT prior to blocking with 10% normal goat serum in PBS pH 7.4 0.1M. Primary antibody, either a rabbit polyclonal antibody to GBS (Abcam, ab78846) or a mouse monoclonal antibody to lactoferrin (Abcam, ab166803), was applied for one hour. Detection of primary antibody was performed using the HRP-Polymer system for 30 min and developed with 3, 3'-diaminobenzidine tetrahydrochloride (DAB) (Dako, Carpinteria, CA). The sections were counterstained with hematoxylin, rinsed, dehydrated and mounted with Cytoseal XYL before light microscopy analysis was performed. Micrograph images were analyzed by ImageJ IHC toolbox plugin to quantify H-DAB staining by color detection, converted to 8-bit format and densitometry quantification as previously described (164).

Flow cytometry evaluation of neutrophils: Flow cytometry analyses were performed as previously described with some modifications (165). Four to seven placenta and decidua were collected from each animal (4-6 animals total) and pooled, weighed, minced with sterile scissors and digested in a solution containing 1 mg/mL collagenase, 1 mg/mL hyaluronidase and 150 µg/mL DNase I with agitation for 1 hour at 37ºC. A total of 40 mL of digestion solution was used per sample (each sample consisted of a single animal's pooled placenta or decidua, totaling 2-6 per animal) and samples were washed using RPMI +/+ medium (containing 1% antibiotic and 10% fetal bovine serum), centrifuged at 1500 RPM at 4°C for 10 min followed by 100 µm nylon mesh filtration to eliminate remaining particulates. Cells were then washed, as previously described, and the filtrate was resuspended in 25% Percoll in RPMI +/+, overlaid onto 50% Percoll, with 2 mL PBS layered above the 25% Percoll. Percoll gradient was centrifuged for 35 min at 1500 RPM without the brake and cells were washed as before, followed by 10 min at room temperature in RBC lysis buffer (eBiosciences). After two more washes with RPMI +/+, cells were counted, and one million cells were aliquoted into flow cytometry tubes. Cells were surface stained for 20 min at 4°C with anti-mouse CD45, anti-mouse CD11b, anti-mouse Neu7/4 (Ly-6B.2), anti-mouse GR1 (Ly6g) and FcR blocking reagent. Isotype controls were included in separate tubes. After surface staining, all cells were washed with PBS and stained with a live/dead viability dye (Life Technologies) for 30 minutes at 4°C. Cells were then washed with 4 mL PBS containing 1% BSA (FACS buffer), fixed for 15 min at 4°C with 1% paraformaldehyde in PBS, and washed again with FACS buffer. Cells were resuspended in FACS buffer and immediately acquired on a BD LSR2 Flow Cytometer (BD Biosciences). Analysis was performed with BD FACS Diva software (BD Biosciences).

Elicitation and isolation of murine neutrophils: Murine neutrophils were prepared by peritoneal casein elicitation protocol as previously described (166). Briefly, C57BL6/J mice (both male and female) aged 6-10 weeks old were purchased from Jackson Laboratories for these experiments. Mice were anesthetized with isoflurane and 1 mL of sterile casein solution (9% w/v in 1X PBS pH 7.2 containing 0.9 mM $CaCl_2$ and 0.5 mM $MgCl_2$) was injected into the peritoneal cavity of each mouse (2-4 mice per experiment). The following day, a second casein injection was performed and four hours after the second injection, mice were sacrificed, and neutrophils were isolated from the peritoneal cavity in 3-5 mL of sterile PBS. Cells were collected and washed in 1X red blood cell lysis buffer (RBC Lysis Buffer, Sigma Aldrich) before placing in RPMI 1640 medium supplemented with 10% fetal bovine serum, L-glutamine and HEPES buffer. Validation of cell purity by flow cytometry techniques described above reveals this protocol routinely yields >95% pure neutrophil populations.

Confocal laser scanning microscopy: Neutrophils isolated as described above were placed onto 12mm poly-L-lysine coated coverslips (ThermoFisher) and allowed to adhere to the surface for 1 hour before inoculation with bacterial cells. Bacteria were added to neutrophils at a multiplicity of infection of 50:1 and co-cultured for 24 hours in the presence or absence of 1 µg/mL of DNase. Concomitantly, uninfected samples were maintained as negative controls. Cells were stained with 1 µM Sytox green (green, Life Technologies) to target extracellular DNA, 30 nM 4',6-diamidino-2-phenylindole (DAPI, blue, Life Technologies) to target nuclear DNA, and mouse monoclonal antibody to lactoferrin (Abcam, ab166803) plus secondary goat-anti-mouse antibody conjugated to Alexa Fluor 647 (red) were applied to cells, agitating for one hour. Cells were washed with phosphate buffered saline (pH 7.4) three times before mounting onto slides and visualizing with a Zeiss LSM 710. Sytox green is an impermeable dye which is used to stain extracellular traps and is also used to differentiate between live and dead cells (167). DAPI stains condensed chromatin bright blue with increased intensity proportional to chromatin condensation, making it an efficient nuclear stain (168). When used in combination, Sytox green will stain extracellular DNA bright green, while DAPI stains nuclear chromatin blue. However, in the case of samples evaluated for NETosis where neutrophils frequently undergo cell death during the process, Sytox green enters dying cells staining both the nucleus, and the extracellular fibers green (resulting in co-staining of the nucleus both blue and green). NETs were identified by Sytox green staining of fibers extending outside of the cell nucleus containing condensed chromatin (DAPI-positive, blue regions). Images were analyzed in both widefield and confocal modalities at 630X magnification and micrographs were collected with Zen 2010 software. Micrographs shown are representative of three biological replicates. Images were analyzed, and

statistical analyses were performed with ImageJ and GraphPad Prism software. A total of 151-192 cells were quantified for each condition derived from more than 12 fields.

Field-emission gun scanning electron microscopy: Murine neutrophils isolated from the co-culture procedure described above were prepared for scanning electron microscopy analyses as previously described (167). Samples were subjected to washing three times with 0.05 M sodium cacodylate buffer and fixing in 2.0% paraformaldehyde, 2.5% glutaraldehyde in 0.05 M sodium cacodylate buffer for 4 hours. Secondary fixation with 0.1% osmium tetroxide was performed for 15 minutes prior to sequential dehydration with increasing concentrations of ethanol. Samples were dried at the critical point using a CO_2 drier (Tousimis), mounted onto an aluminum stub, and sputter-coated with 80/20 gold-palladium. A thin strip of colloidal silver was painted at the sample edge to dissipate sample charging. Samples were imaged with a FEI Quanta 250 field-emission gun scanning electron microscope (FEG-SEM). Images are representative of three replicates from three different experiments.

Preparation of holo- or apo-lactoferrin: Iron-bound (holo-) or unbound (apo-) lactoferrin was prepared as previously described (169). Briefly, 10 mM stock of lactoferrin (Sigma Aldrich) was dialyzed against either 0.1 M sodium citrate-bicarbonate buffer pH 8.2 alone to generate apo-lactoferrin, or buffer containing 70 mM ferric chloride to generate holo-lactoferrin. Both apo- and holo-lactoferrin were dialyzed against 1X phosphate buffered saline (PBS) containing Chelex Resin (Sigma Aldrich) to remove any unbound iron content.

Bacterial growth and viability analyses: For growth and viability analyses, bacteria were cultured overnight in THB (to an OD_{600} of ~0.8), then sub-cultured by performing a 1:100 dilution (roughly $8x10^6$ CFU/mL) in 60% THB plus 40% calprotectin buffer (100 mM NaCl, 3 mM $CaCl_2$, 20 mM Tris pH 7.5) (164, 169) referred to as “medium alone” or medium supplemented with increasing concentrations (100, 250, 500, 750, 1000 µg/mL) of purified apo- or holo-lactoferrin protein alone or supplemented with 100 µM ferric chloride. These concentrations span the physiological range at which lactoferrin would be present in inflamed tissues and neutrophil granules (170-172). Additionally, bacteria were grown in increasing concentrations of the synthetic chelator 2, 2’-dipyridyl (25, 50, 100, 150, 200, 250, 300, 350, 400 µM) in medium alone or medium supplemented with 250 µM ferric chloride. Bacterial growth was evaluated at 24 hours post-inoculation by spectrophotometric reading of OD_{600} or bacterial viability was evaluated at 24 hours by serial dilution and plating onto blood agar plates and quantifying viable colony forming units per mL of culture (CFU/mL).

Statistical analyses: Statistical analysis of flow cytometry and neutrophil NET quantifications was performed using Student's *t* test and One-Way ANOVA, respectively. Bacterial growth assays were analyzed by One-Way ANOVA with either Tukey's or Dunnet's post hoc multiple correction tests and Student's *t* test. *P* values < 0.05 were considered significant. All data analyzed in this work were derived from at least three separate biological replicates. Statistical analyses were performed using GraphPad Prism Software (Version 6.0, GraphPad Software Inc., La Jolla CA) and Microsoft Excel (Version 14.6.3, Microsoft Corporation, Redmond WA).

RESULTS:

GBS invades gestational tissues to cause invasive ascending infection during pregnancy: To evaluate GBS ascending infection during pregnancy, we utilized the mouse model of ascending GBS vaginal infection as previously described (62) and developed new outputs from this model by employing bacteriological culturing and IHC microscopy assays to evaluate bacterial burden in discrete tissue compartments within the gestational tissue. Our results reveal that GBS colonizes surface of the vagina (**Figure V.2**, **Figure V.3**) at an average burden of $3.6x10^6$ CFU/mg of tissue, and the bacterial colonization is spatially oriented at the lumen of the tissue within the vaginal mucosa as determined by IHC microscopic examination (**Figure V.2**). Furthermore, IHC microscopic analyses reveal GBS ascends in this model and colonizes at the lumen of the endometrium within the uterus, averaging $2.2x10^9$ CFU/mg (**Figure V.4**). IHC analyses also reveal that GBS invades the decidua and the placenta, and quantitative culture demonstrates bacterial burden averages $8.5x10^8$ CFU/mg in the decidua, $2.1x10^9$ CFU/mg in the placenta, and $3.3x10^8$ CFU/mg in the fetus.

GBS infection results in profound inflammation including recruitment of neutrophils to the placenta and the choriodecidua: Previous work indicates the murine model of ascending GBS infection during pregnancy mirrors the human histopathological changes associated with chorioamnionitis (155). In an effort to better characterize the inflammation present within this model, we employed the immunological tools readily available for utilization with this mouse model and performed both histopathological examination and correlative flow cytometry analyses using antibodies to CD45, Neu7/4, and GR1 which are specific for murine neutrophils (**Figure V.5**) and $CD45^+/Neu7/4^+/GR1^+$ gating strategies. Histopathological examination reveals profound infiltration of polymorphonuclear cells within GBS-infected decidua and placenta, a result that was not seen in uninfected samples (**Figure V.6**). This result was recapitulated using flow cytometry to analyze the placenta and decidua compartments, demonstrating 54% of viable CD45+ cells were $Neu7/4^+/GR1^+$ neutrophils in GBS-infected placenta vs. 19% of uninfected placenta, a significant increase in

neutrophils infiltrating the placenta in response to GBS infection (P <0.05). Similarly, 61% of viable $CD45^+$ cells were $Neu7/4^+/GR1^+$ neutrophils in GBS-infected decidua vs. 16% of uninfected decidua, a significant increase in neutrophils in the decidual compartment in response to GBS infection (**Figure V.7**, *P* <0.05). Furthermore, the preponderance of PMNs discovered in the decidual and placental compartment is associated with GBS staining, indicating neutrophils were recruited to the site of GBS infection within each tissue compartment.

Lactoferrin is associated with neutrophils in the decidua and placenta in response to GBS infection: Neutrophils play an important role in innate immunity against bacterial pathogens. One way they accomplish this is by secreting molecules with antimicrobial activity. Previous work has shown that lactoferrin is elevated in patients with intra-amniotic infections during pregnancy, disease states that are often associated with high proportions of neutrophilic infiltration of both the decidua and the placenta (16, 155, 156). We hypothesized that neutrophils recruited to the site of GBS infection could produce lactoferrin as an antimicrobial strategy. To test this, IHC analyses were employed to determine the spatial localization of lactoferrin within GBS-infected or uninfected gestational tissues (**Figure V.8**). Lactoferrin was highly abundant within the decidua and placenta of GBS-infected pregnant mice, a result that was not observed in uninfected control animals. Interestingly, lactoferrin staining was largely associated with areas of tissue exhibiting profound neutrophilic infiltrates (**Figure V.8 G&H**), and tissue compartments that stain positive by IHC for GBS in, indicating this protein is could be associated with neutrophils which are found at the site of GBS infection.

Neutrophils encountering GBS produce extracellular traps comprised of DNA: Due to the observation that GBS staining frequently co-localized with PMN infiltrates, we hypothesized that GBS-neutrophil interactions could influence the outcome of disease progression. Specifically, it was hypothesized that neutrophils exert an antimicrobial activity against GBS by secreting antimicrobial molecules, such as lactoferrin. To further evaluate this activity, *ex vivo* isolation of murine neutrophils was performed, and these cells were co-cultured with GBS at a MOI of 50:1 bacterial to host cells. Co-cultures were evaluated by high resolution microscopical techniques including high resolution field-emission gun scanning electron microscopy (FEG-SEM) and confocal laser scanning microscopy (CLSM). FEG-SEM results in **Figure V.9** indicate that neutrophil exposure to GBS results in enhanced neutrophil extracellular trap formation. Similarly, confocal analyses reveal GBS-treated samples have 24.5-fold enhanced neutrophil extracellular trap (NET) formation compared to uninfected controls (**Figure V.10**, *P* <0.05). These extracellular traps were ablated by treatment of

co-cultures with DNase I, confirming that DNA is a major component of these structures (**Figures V.9 and V.10**). Furthermore, CLSM analyses in **Figure V.10** in which co-cultures were stained with Sytox Green (an extracellular DNA stain, green) as well as DAPI (an intracellular DNA stain, blue) indicated extracellular traps, which appear to have GBS caught within their margins, are staining Sytox Green positive, confirming these are comprised of extracellular DNA. Conversely, uninfected controls and DNase I-treated GBS-neutrophil co-cultures have fewer apparent extracellular traps staining with Sytox Green (P <0.05).

Neutrophil extracellular traps comprised of DNA are studded with the antimicrobial glycoprotein lactoferrin: Previously published work indicates that lactoferrin secretion is enhanced in gestational tissues in response to GBS infection (156), and that lactoferrin is a putative antimicrobial protein which decorates the NET (159). We hypothesized that NET formation in response to GBS exposure could result in secretion of lactoferrin into the NET. To test this, we employed CLSM and immunofluorescence approaches to analyze subcellular spatial localization of lactoferrin (**Figure V.10**, anti-lactoferrin and Alexa Fluor 647 conjugated secondary antibody, red) with respect to the extracellular trap (Sytox Green, green). Our results indicate lactoferrin secretion into the extracellular trap was induced by GBS co-culture with PMNs. The lactoferrin associated with extracellular DNA that comprised the NET and was found spatially localized near structures consistent in size and arrangement with GBS cells, indicating lactoferrin may interact with GBS within the NET. DNase I treatment of the co-culture resulted in diminished NETs observed by CLSM, and this treatment also resulted in decreased extracellular lactoferrin and GBS-associated with PMNs, indicating lactoferrin was associated with the DNA which structurally comprises the extracellular trap, and that the NETs potentially served to immobilize GBS and expose them to antimicrobial insults including lactoferrin.

Lactoferrin exerts antimicrobial activity against GBS via iron sequestration: Because lactoferrin is an antimicrobial glycoprotein that binds and sequesters iron in a strategy to chelate nutrient iron away from invading microorganisms, we hypothesized that the deposition of lactoferrin within neutrophil extracellular traps could potentially inhibit GBS growth and viability. To test this, bacterial growth and viability assays were performed. Results in **Figure V.11** indicate that at concentrations of 100, 250, 500, 750, and 1000 μg/mL, apo-lactoferrin represses GBS growth 46%, 50%, 95%, 91%, and 94%, respectively, compared to cells cultured in medium alone. This result was recapitulated using the synthetic iron chelator 2, 2’ dipyridyl which has antimicrobial activity against GBS (**Figure V.12**). Interestingly, supplementation with 100 μM ferric chloride as an exogenous source of nutrient

iron restored bacterial cell density to levels that were comparable or higher than those grown in medium alone (**Figures V.11 and V.12**). Results in **Figure V.11** indicated that even at concentrations as high as 1000 μg/mL, holo-lactoferrin did not repress bacterial growth significantly compared to medium alone, a result that could be attributed to the fact that the iron-loaded form of this protein did not exert iron chelation activity on the bacteria within this particular growth medium. Taken together, these results indicate that the iron-sequestration activity of apo-lactoferrin has detrimental effects on GBS; diminishing both bacterial growth and viability through micronutrient starvation.

DISCUSSION:

GBS invades reproductive tissues, crosses the placenta and disseminates to the fetus: Colonization of the vaginal mucosa is a critical primary step in GBS pathogenesis during pregnancy. Once colonized, bacteria ascend into the intrauterine cavity, transverse the fetal membranes and cause severe neonatal disease outcomes including preterm birth, neonatal sepsis and neonatal demise. The advent of a model of ascending GBS infection in a pregnant mouse provides numerous genetic and immunological tools to study the complex dialogue between host and pathogen during pregnancy (62). We have further refined this model by dissecting the gestational tissue compartments and analyzing both enumeration of GBS burden and spatial distribution of bacteria by quantitative culture and immunohistochemical techniques. These experiments reveal that bacterial invasion could be observed in the vagina, uterus, decidua, placenta, and fetus with the highest burden being present in the uterus and the burden titrating as the bacteria penetrate the gravid host, as is expected in a model of invasion.

The murine model of ascending vaginal infection by GBS results in chorioamnionitis which is characterized by a profound infiltration of PMNs to the choriodecidua and placenta: In response to GBS infection, pro-inflammatory signaling cascades are promoted which ultimately lead to the recruitment of innate immune cells to the site of infection (62). Concordant with this, our work demonstrates that GBS infection elicits significant PMN recruitment to the placenta (2.5-fold increase compared to uninfected controls) and the decidua (3.3-fold increase compared to uninfected controls), a result that is in agreement with experiments performed in previous studies using this model indicating inflammation-related pathology scores are elevated in GBS-infected animals compared to sham-treated controls (62). It is interesting to note that the neutrophilic infiltrate within the gestational tissues mirrors the clinical presentation of chorioamnionitis in human subjects (155-157). This neutrophil response likely initiates an antimicrobial response, through phagocytosis and bacterial killing, as well as through the deposition of antimicrobial molecules at the site of infection.

Furthermore, it is likely that neutrophil presence results in the stimulation of pro-inflammatory signaling cascades which initiates further inflammation pathways leading to perturbed maternal-fetal tolerance and tissue destruction (172-175).

Murine PMNs form NETs in response to GBS: Neutrophils play a critical role in controlling invading pathogens (176). Emerging evidence indicates that one pathway neutrophils employ to combat pathogenic microbes is elaboration of NETs(159). NETs function as a structural component of the innate immune response which serves to immobilize microorganisms (159). NETs are largely comprised of DNA and associated histones which are decorated with antimicrobial molecules (159, 177). Because NETs can immobilize bacteria, bringing them into intimate contact with these antimicrobial proteins and glycoproteins, it is purported that NETs are an important arm of the antimicrobial defense strategies employed by the host (159, 177).

Our work indicates murine neutrophils deploy extracellular traps in response to encountering GBS. Previous work has shown that GBS-infected human tissues have abundant neutrophilic infiltrates and GBS induces NETosis in human neutrophils as determined by immunohistochemical and microscopical analyses using neutrophil elastase and histones, markers which are commonly associated with NETs (57, 178-182). Interestingly, work by Carey *et al.* shows that induction of NETosis is hemolysin-, indicating that GBS virulence factors participate in this process (158). Derre-Bobillot *et al.*, report that GBS encodes a DNase which is critical for liberating the bacterial cell from the murine NET, indicating GBS has mechanisms to evade this immunological response (178). It is worthy to note that in this report, the authors utilized murine PMNs which were elicited by thioglycolate treatment and subsequently stimulated with PMA (Phorbol-12-Myristate-13-Acetate) to induce murine NET formation. Murine NETs induced during co-culture with GBS are comprised of extracellular DNA, a result which agrees with previously published reports (158, 159). Our approach to studying GBS-dependent induction of NET formation has been employed by other groups utilizing extracellular DNA stains such as Sytox Green, or the biochemical approach of DNase-dependent degradation of NETs to determine the association of extracellular DNA with NET structures (57, 179).

NETs induced by GBS contain lactoferrin: It is increasingly appreciated that NETs are reservoirs of antimicrobial molecules (159, 183). A wide repertoire of antimicrobial molecules including calprotectin, lactoferrin, and cathelicidin has been associated with NETs (184). Many of these have been identified by unbiased proteomics techniques, targeted immunohistochemical techniques, and microbiological killing assays. These antimicrobial molecules are important mediators of innate immunity. Interestingly, both calprotectin and lactoferrin participate in chelation of nutrient metals, a

process that effectively sequesters transition metals away from pathogenic microbes (160, 185). Nutritional immunity is progressively recognized as a critical way to combat microbial infection (160, 164, 185). Lactoferrin is of particular interest as GBS induces elevated lactoferrin levels during infection of placental membranes, however the cellular contribution for this was obscure (59). Furthermore, elevated lactoferrin levels have been associated with GBS infection in neonates such as septicemia (186, 187). We report that GBS-induced NETs are a source of lactoferrin, however the role of these structures and antimicrobial molecules in the context of infection during pregnancy remains unknown.

Lactoferrin has antimicrobial activities against GBS: Lactoferrin is a neutrophil-associated glycoprotein with immunomodulatory properties which has been recognized as a broad-spectrum antimicrobial agent against numerous microorganisms (188-197). This activity is associated with lactoferrin's iron-binding properties which participate in nutritional immunity via iron sequestration (198-201). Iron is a strict nutritional requirement for numerous bacteria including GBS, thus chelation of this molecule could alter bacterial cell biology (161, 162). Our results indicate that apo-lactoferrin at 100, 250, 500, 750, 1000 μg/mL resulted in 1.8, 2.0, 19.6, 10.9, 16.7-fold, decreased bacterial viability, respectively. Work by other groups indicates bovine lactoferrin has been demonstrated to have bacteriostatic activity against GBS, and human lactoferrin has been observed to bind to lipoteichoic acids in *Streptococcus* spp., inhibit biofilm formation, and activate the complement pathway, indicating it has immunomodulatory and pleotropic effects (202-205). Interestingly, lactoferrin administration as a prebiotic is under consideration for women with preterm delivery and lactoferrin supplementation to formula has been shown to limit GBS growth >50% (206, 207).

Conclusion: We report that a pregnant mouse model of ascending GBS vaginal infection results in bacterial colonization of the reproductive tract and invasion of the placenta, decidua and fetus. As a consequence of GBS invasion, neutrophils are recruited to the placental and decidual compartments; likely as a host strategy to contain the infection. In response to GBS infection, lactoferrin is elevated within the placental and decidual tissue (**Figure V.13**). Furthermore, ex vivo results indicate neutrophils elaborate extracellular traps decorated with lactoferrin upon encountering GBS. Lactoferrin can subsequently exert an antimicrobial activity in vitro against GBS via chelation of nutrient iron, which is required for GBS growth and viability. Thus, a better understanding of lactoferrin deposition by neutrophils in NETs and the interplay of this important host molecule with GBS could lead to novel chemotherapeutic strategies as the utility of antibiotics wanes.

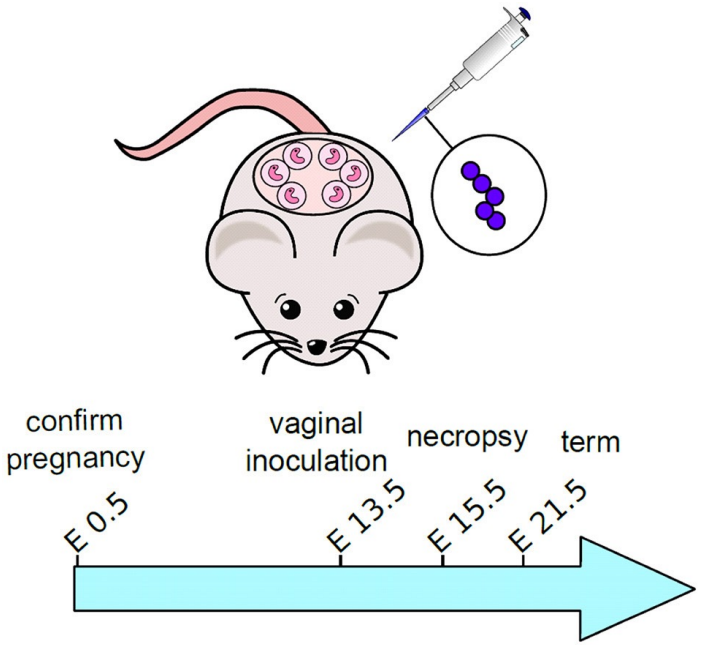

Figure V.1: Schematic representation of experimental design for mouse model of ascending GBS infection during pregnancy. Pregnant dams were vaginally inoculated with 10^3 CFU GBS on embryonic day 13.5. Animals were sacrificed, and tissues were analyzed 48-hours post-infection, on embryonic day 15.5.

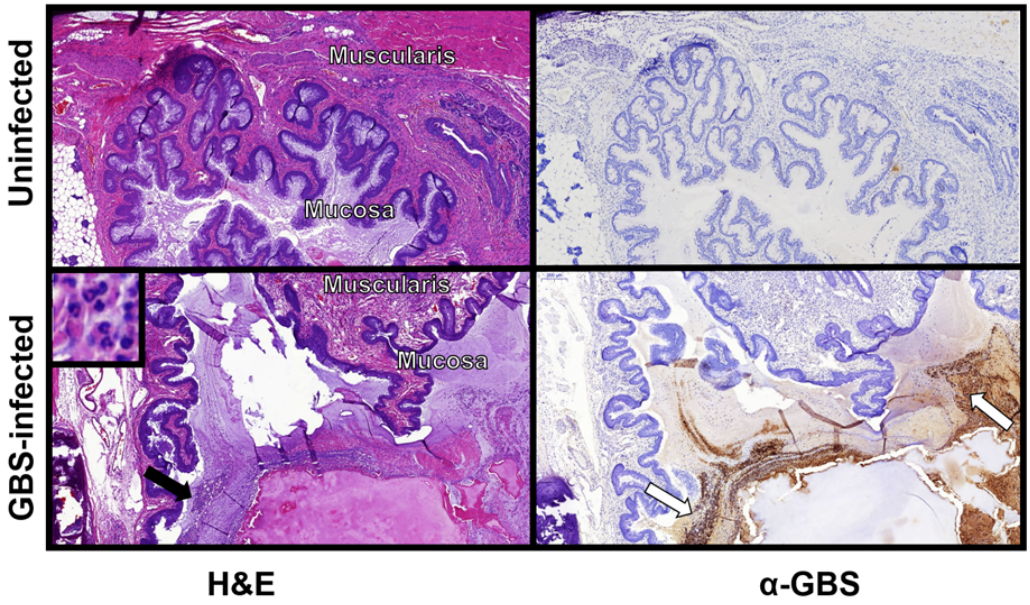

Figure V.2: Immunohistochemical and immunopathological analyses of uninfected or GBS-infected vaginal muscularis and mucosal tissue. Immunopathological examination by hematoxylin and eosin staining (H&E) reveal neutrophils at the surface of the mucosa (black arrows, inset panel of GBS-infected tissue micrograph), which corresponds to an area within the mucosa that is colonized by GBS as determined by immunohistochemical staining with a polyclonal rabbit antibody to GBS (white arrows, inset panel of GBS-infected tissue micrograph), a result that was not observed in uninfected tissue (Uninfected).

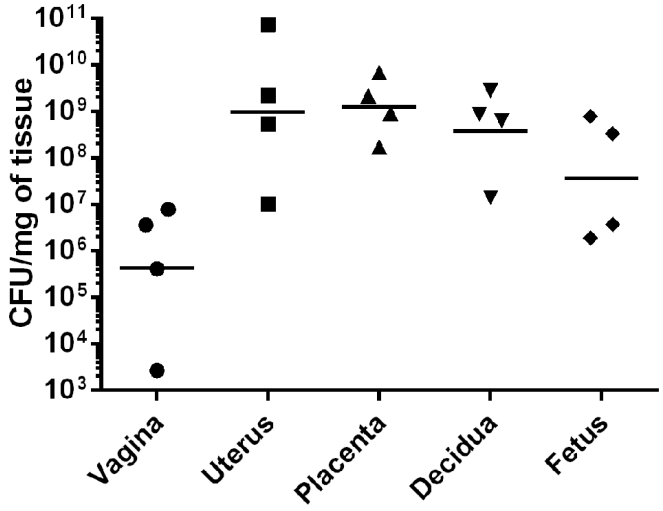

Figure V.3. GBS invades reproductive tissues and disseminates in the gravid host. Quantitative culture from tissues harvested from pregnant mice infected with GBS reveals bacterial presence in numerous gestational tissues. GBS bacteria ascend from the vagina to the uterus and invade the decidua, placenta and fetus (N=4). Points represent burden value from 1 tissue derived from 1 dam. Horizontal lines represent the geometric mean of bacterial burden.

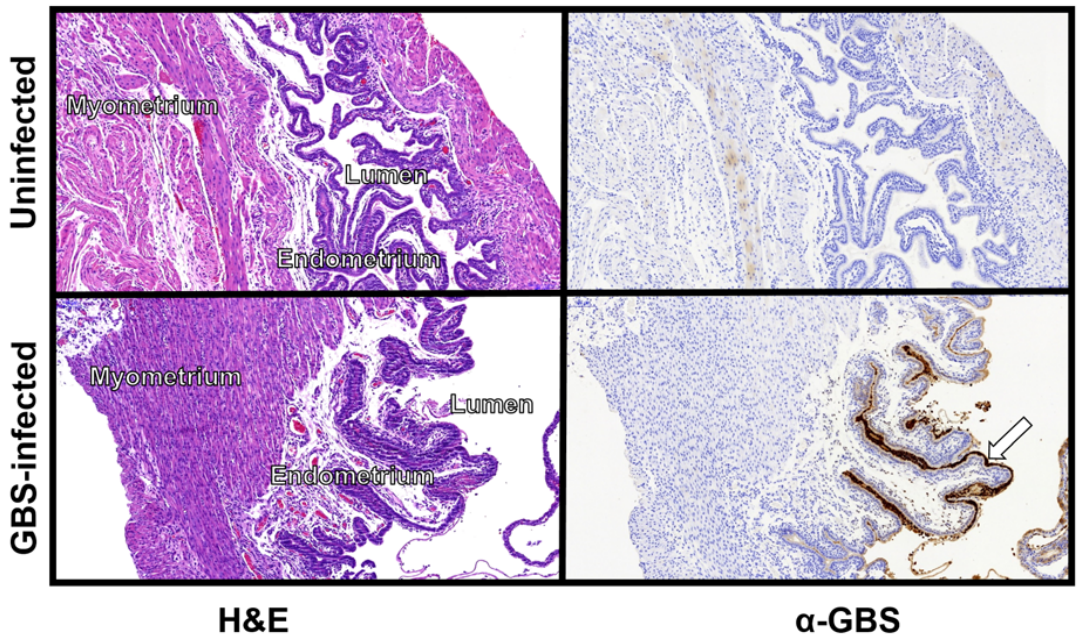

Figure V.4. Immunohistochemical and immunopathological analyses of uninfected or GBS-infected uterine tissue (myometrium, endometrium, and lumen). Immunopathological examination by hematoxylin and eosin staining (H&E) reveal preserved tissue architecture in both uninfected and GBS-infected animals. However, immunohistochemical staining indicates GBS colonizes the lumen and the surface of the endometrium as determined by staining with a polyclonal rabbit antibody to GBS (white arrows, inset panel of GBS-infected tissue micrograph), a result that was not observed in uninfected tissue (Uninfected).

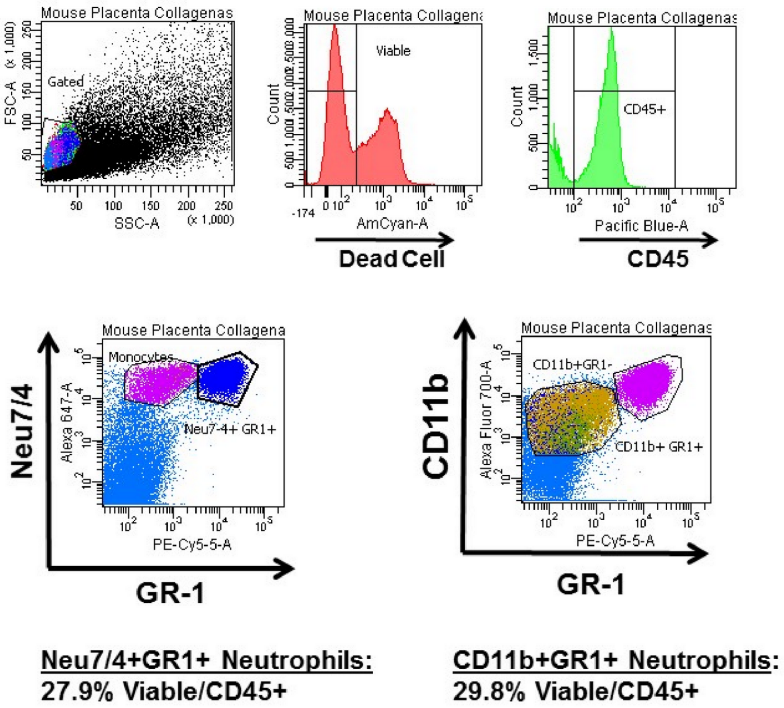

Figure V.5: Gating strategy for flow cytometry analyses of neutrophils isolated from mouse reproductive tissues. Neutrophils were stained with antibodies specific to 1A8 GR1 clone (Ly6g), CD45, and Neu7/4, and analyzed by flow cytometry using a gating strategy to quantify cells defined as Neu7/4^{high}, GR1^{high} within the viable CD45^{+} cells (27.9% of Viable CD45^{+} cells). In comparison, similar results were obtained when neutrophils were stained with antibodies specific to 1A8 GR1 clone (Ly6g), CD45, and CD11b, and analyzed by flow cytometry using a gating strategy to quantify cells defined as CD11b^{high}, GR1^{high} within the viable CD45^{+} cells (29.8% of Viable CD45^{+} cells).

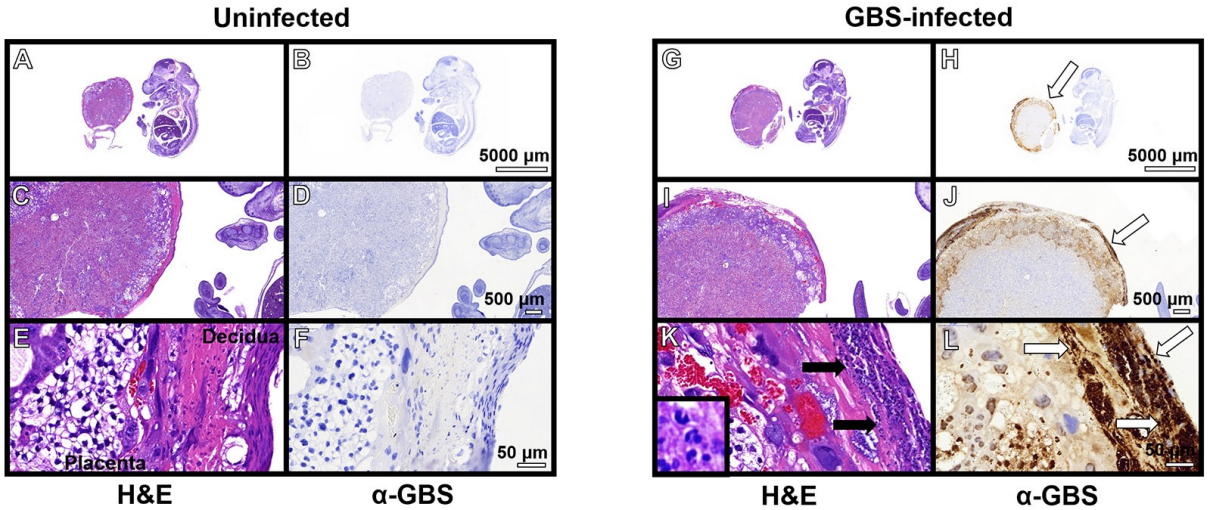

Figure V.6. Immunopathological analyses of fetal-placental units. Hematoxylin and eosin (H&E) stained samples (H&E) of uninfected (Panels A-F) and GBS-infected (Panels G-L) fetal-placental units reveal profound infiltration of polymorphonuclear cells in response to infection (Panel K, black arrows), a result that was not observed in uninfected animals (Panel E). IHC analyses using a polyclonal rabbit antibody to total GBS cell lysate (α-GBS) indicate GBS penetrates the decidua and the placenta to invade the gestational tissues (Panels H, J, and L, white arrows), a result that was not seen in uninfected animals (Panels B, D, F). GBS staining is found within tissue compartments containing polymorphonuclear cell infiltrates indicating neutrophils are present at the site of infection (representative images of N=3-5).

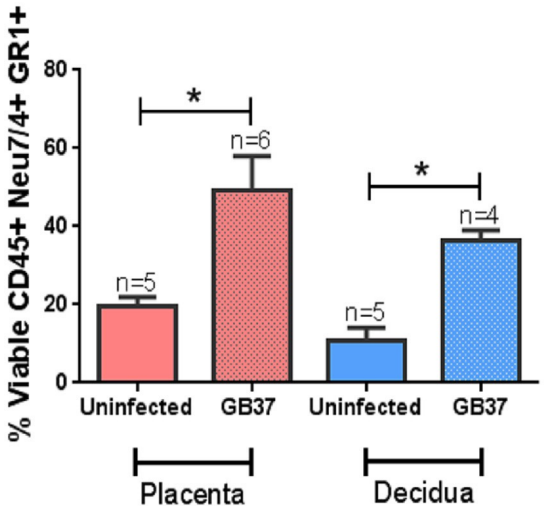

Figure V.7: Flow cytometry analyses of placenta and decidua to evaluate the relative abundance of neutrophils. Neutrophils were evaluated by CD45+ Neu7/4+ GR1+ gating strategy on cells derived from the placental or decidual compartment of uninfected or GBS-infected pregnant mice. Bars represent mean percent (viable cells CD45+ Neu7/4+ GR1+) +/- SEM. GBS-infection results in enhanced presence of neutrophils in the decidua and placenta (*P <0.05 Student's t test, N=4-6).

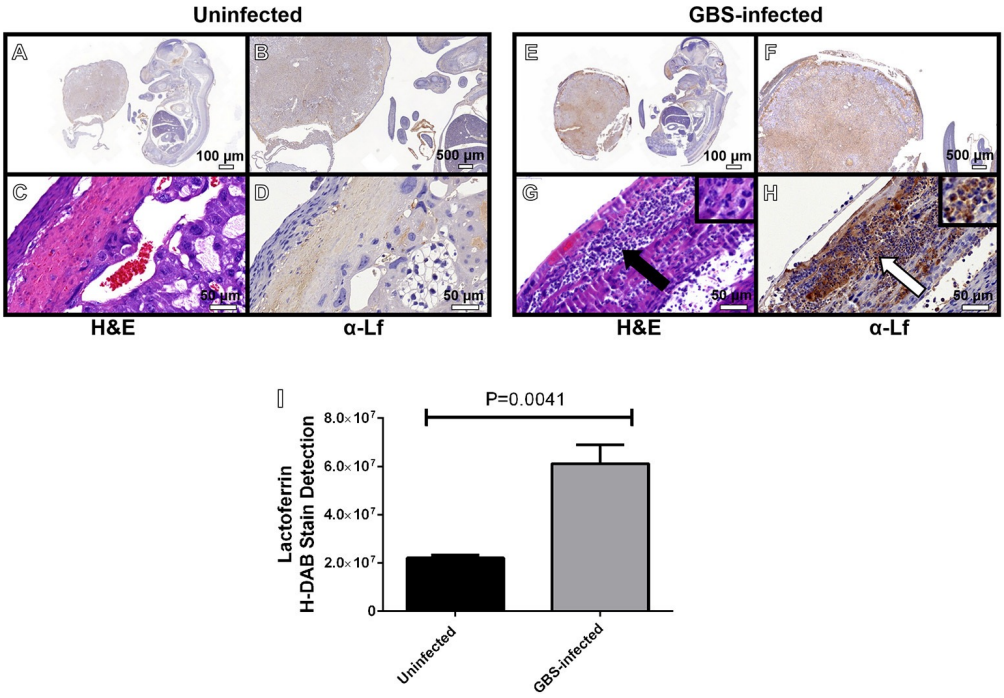

Figure V.8: Microscopic analyses of the spatial localization of lactoferrin within uninfected (Panels A-D) or GBS-infected (Panels E-H) fetal-placental tissue. Representative micrographs collected at 4X (Panels A and E), 20X (Panels B and F), and 400X (Panels C-D, and G-H). Panels A, B, D, E, F, H indicate IHC staining with a mouse monoclonal antibody to lactoferrin (α-Lf). Panels C and G indicate hematoxylin and eosin staining (H&E) staining for immunopathology. Panel I) Quantification of anti-lactoferrin HDAB stain by ImageJ IHC toolbox reveals GBS infection results in elevated lactoferrin within the fetal-placental tissue (bars indicate mean quantified HDAB stain +/- SEM, P =0.0041, Student's t test, N=3). Panels G-H demonstrate the preponderance of lactoferrin stain (white arrow) is associated with polymorphonuclear cells (black arrow).

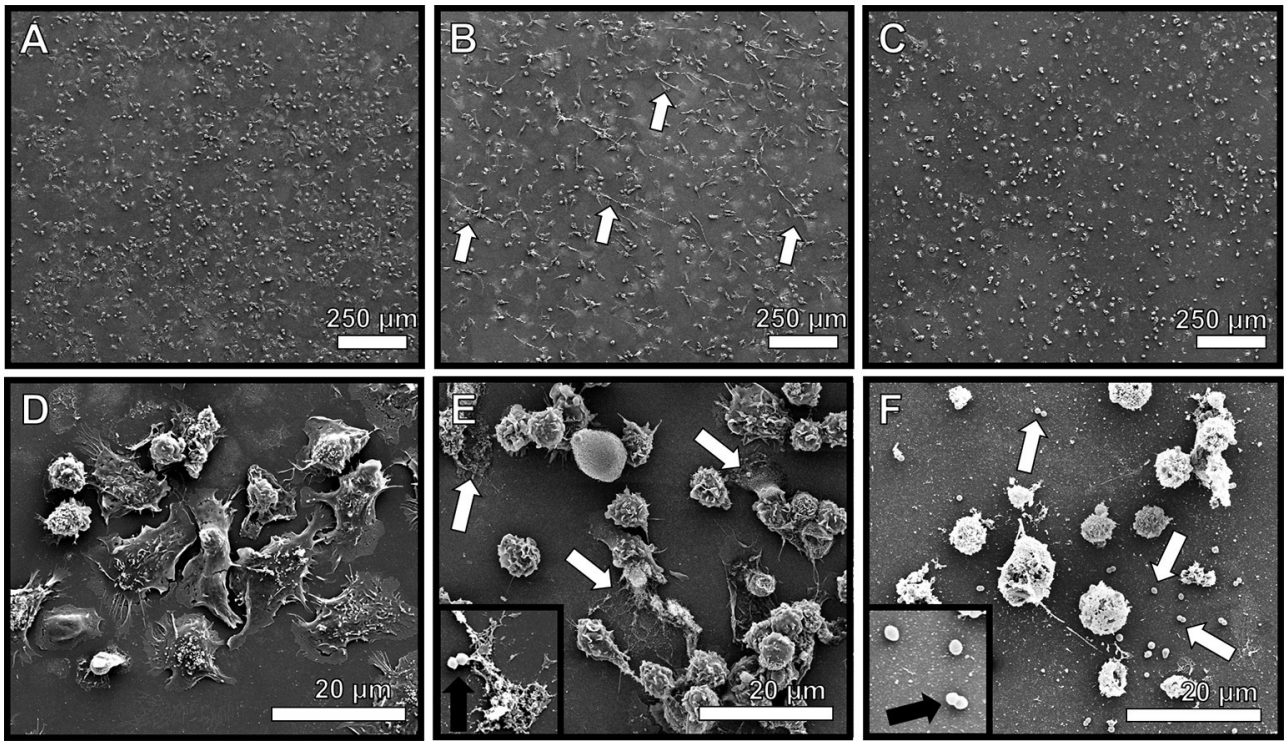

Figure V.9: **Neutrophils encountering GBS elaborate extracellular traps (NETs) comprised of extracellular DNA.** High resolution scanning electron microscopy analyses reveals murine neutrophils elaborate extracellular traps in response to GBS co-culture (Panels B and E, white arrows), a result which was not seen in uninfected mouse neutrophils (Panels A and D). Treatment with DNase I abrogates observation of extracellular traps (Panels C and F, white arrows), indicating traps are structurally comprised of DNA. Inset panels of E and F show GBS associated with NET fibers or not associated with NETs due to DNA degradation, respectively (black arrows).

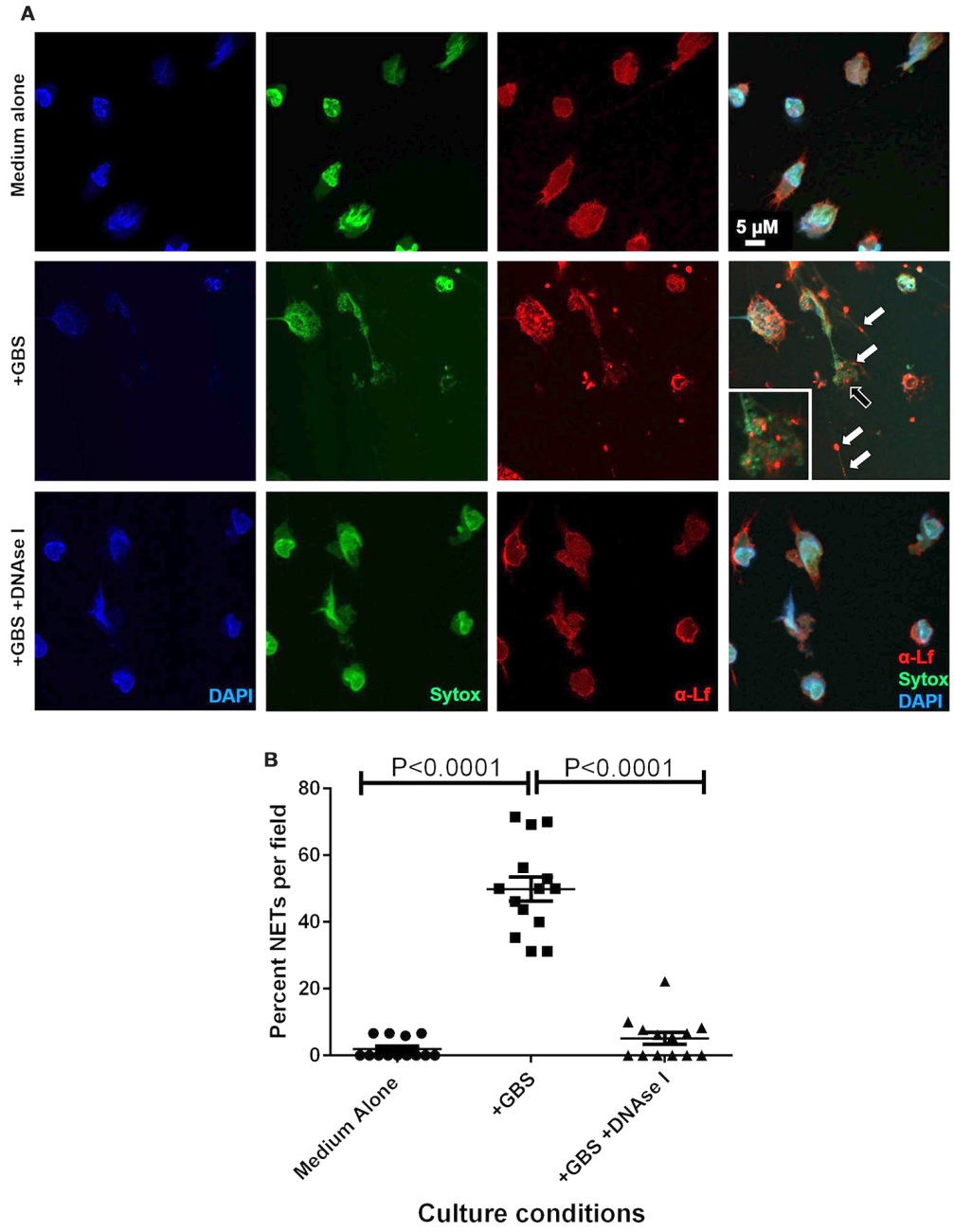

Figure V.10: Extracellular traps formed in response to GBS are decorated with lactoferrin. Panel A) Confocal laser scanning microscopy analyses of neutrophils cultured in the absence of GBS (Medium Alone), in the presence of GBS (+GBS) alone or in co-cultures supplemented with DNase I (+GBS +DNase I) were subjected to intracellular nuclear DNA stain (DAPI, blue), extracellular DNA stain (Sytox, green), or antibody to lactoferrin (α-Lf). Merge images reveal that GBS co-culture with neutrophils results in the elaboration of neutrophil extracellular traps comprised of extracellular DNA (representative images of N=3 biological replicates). These traps immobilize GBS (black arrow) and are studded with lactoferrin (white arrow) which is found in close contact with GBS, indicating lactoferrin is part of the antimicrobial repertoire secreted in the NETs in response to GBS. Enumeration of the percentage of NETs per field was performed and demonstrate that NETs are enriched in GBS-containing co-cultures but are ablated by treatment with DNase I (Bars indicate mean percent of NETs per field +/- SEM, *P* <0.0001, One Way ANOVA, N=3 biological replicates and at least 5 fields per replicate, 150+ cells total).

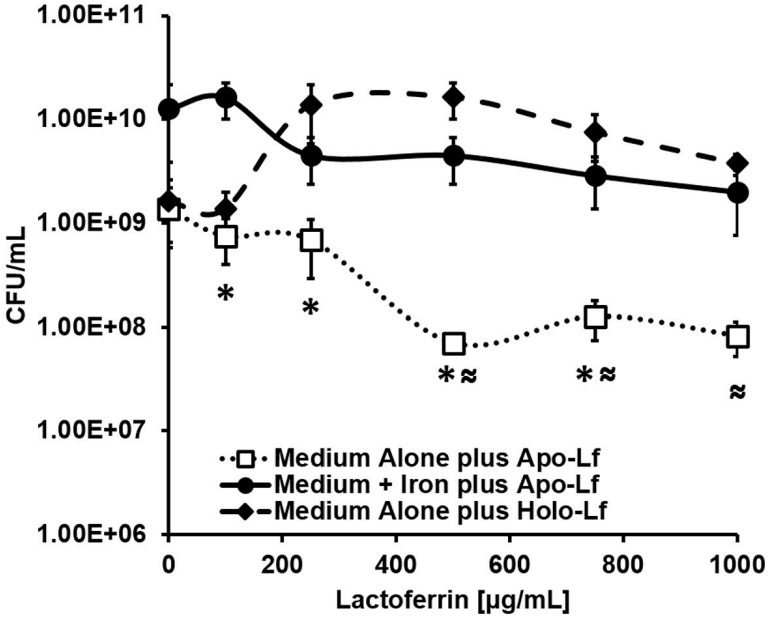

Figure V.11: Analysis of bacterial viability after 24 hours of culture. Exposure to apo-lactoferrin (Apo-Lf, open squares) results in decreased GBS growth and viability in a dose-dependent manner, a result which was reversed by the addition of a source of exogenous nutrient iron (closed circles). Conversely, exposure to increasing concentrations of holo-lactoferrin (Holo-Lf, closed diamonds) does not significantly inhibit bacterial viability. Points indicate mean CFU/mL +/- SEM per timepoint (N=3 biological replicates). **P* <0.05, compared to Medium + Iron plus Apo-Lf,≈ *P* <0.05, compared to Medium plus Holo-Lf.

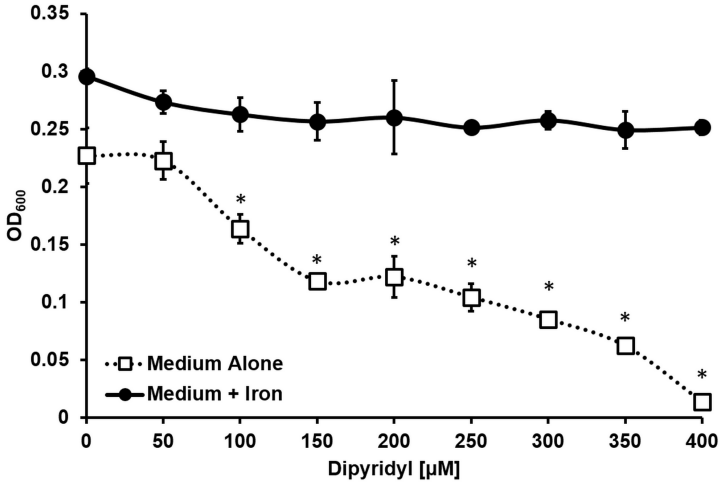

Figure V.12: Iron chelation inhibits GBS growth. Spectrophotometric analyses reveal increasing concentrations of the synthetic iron chelator 2, 2' dipyridyl (Dipyridyl) repress GBS cell density in medium alone (Medium Alone) after 24 hours of culture. Supplementation with excess exogenous nutrient iron (250 µM ferric chloride, Medium + Iron) restores bacterial growth in the presence of the synthetic chelator (*P* <0.05, Student's *t* test comparing medium alone to medium + iron), indicating iron is a critical micronutrient for GBS growth and proliferation.

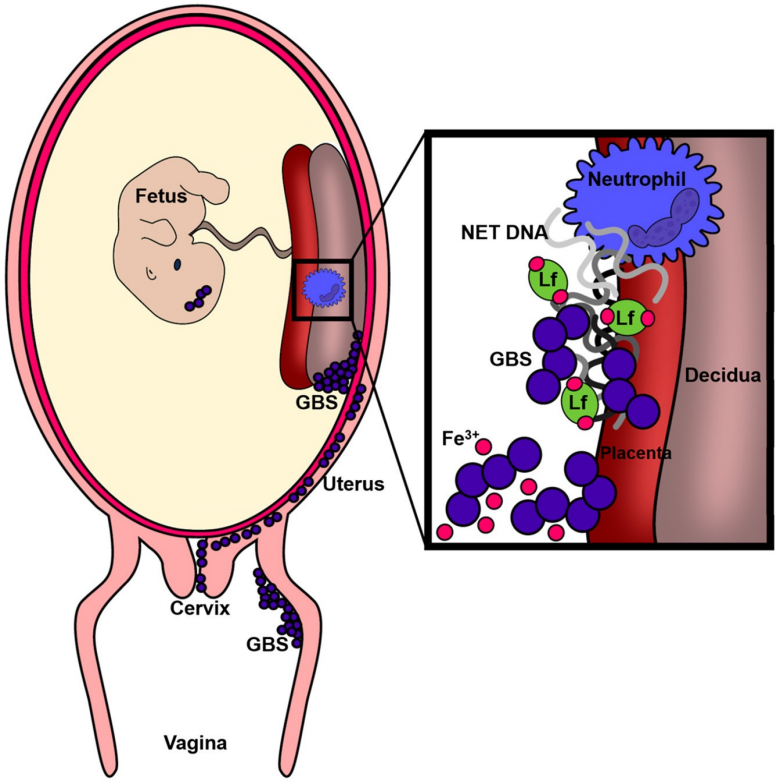

Figure V.13: Conceptual diagram of the murine model of GBS infection during pregnancy. Results derived from *in vivo* and *ex vivo* experimental reveal GBS has the capacity to cause ascending vaginal infection during pregnancy, induction of neutrophil recruitment to invaded tissues, and that GBS-neutrophil interactions promote extracellular trap formation and deposition of antimicrobial molecules (such as lactoferrin) that promote nutritional immunity.

CHAPTER VI

Macrophage extracellular traps: a scoping review

INTRODUCTION:

Macrophages comprise a diverse group of cells that are found in all tissues and demonstrate remarkably diverse functions (208-210). Tissue macrophages are derived from either circulating blood monocytes that originate in the bone marrow or embryonic precursors that establish residence within tissues and can be maintained independent of bone marrow progenitors (208, 211). Macrophage functions range from supporting development, maintenance of homeostasis, and immune surveillance and regulation to tissue remodeling and repair (208). These professional phagocytes play key roles during both initiation of inflammation and orchestrating its resolution as is seen by the spectrum of macrophage 'activation states' (210). In addition to classical macrophage functions, recent investigation has demonstrated that macrophages are capable of producing extracellular traps (ETs).

An initial description of neutrophil extracellular traps (NETs) appeared in 2004, and this discovery was quickly followed by description of a new, programmed cell death pathway termed 'ETosis' (159, 212, 213). ETosis comprises a unique series of cellular events by which nuclear contents including chromatin mix with cellular proteins and are then extruded from the cell body to form extracellular structures capable of 'trapping' and killing microorganisms (159, 212, 213). Since the original report in neutrophils, other leukocytes including mast cells, eosinophils, and basophils are now known to produce 'extracellular trap' structures (214-218). ETs have been implicated in diverse disease states ranging from conditions of aseptic inflammation such as gout to vascular disorders including preeclampsia and thrombosis (219-222). Inadequate resolution and degradation of these structures is also a topic of recent research; prolonged exposure of self-antigens comprising ETs can result in autoimmune diseases including systemic lupus erythematosus and antineutrophil cytoplasmic autoantibodies (ANCA)-associated vasculitis (223, 224).

As macrophage functions are vital to host immune defense and tissue homeostasis, we sought to understand the role of macrophage and monocyte ETs (METs) in the context of host defense and disease states. We conducted a structured, scoping review to assess the current literature regarding the diversity of macrophages known to produce ETs, identification of METs, proposed functions, and mechanisms by which macrophage ETosis (METosis) may occur. Data regarding ETs produced by neutrophils and other leukocytes have been reviewed elsewhere and were excluded from this review (225, 226).

METHODS:

We performed a scoping review based on methods described by Arksey and O'Malley (227). The central research question was "What is known from the existing literature about ETs produced by monocytes or macrophages?" To address this question, we searched for and reviewed papers with the following inclusion criteria: English language primary studies that provided some evaluation of monocytes or tissue differentiated macrophages for the ability to produce ETs. For the purposes of this review we refer to both monocyte and macrophage ETs as METs and the process of extruding these structures as 'METosis.' These studies were not limited to human cells.

Our search was conducted using PubMed with the search phrase ((monocyte OR macrophage) AND extracellular traps(s)) with the last search for new manuscripts performed on March 30th, 2017. The search is summarized in **Figure VI.1**. We identified additional studies through references of the reviewed articles. Further review to include/exclude identified articles consisted of reading article abstracts. If an article appeared relevant, but the inclusion criteria could not be established, the full article was reviewed to determine if inclusion criteria were satisfied.

RESULTS AND DISCUSSION:

Defining and identifying macrophage extracellular traps (METs): The original description of NETs included high-resolution scanning electron microscopy imaging; by this modality Brinkmann *et al.* identified fibers that were 15-17 nm in diameter and were beaded with globular domains (159). Using immunofluorescence staining, this study determined that these globular domains contained proteins from neutrophil azurophilic, secondary, and tertiary granules including elastase, myeloperoxidase, lactoferrin, and gelatinase. Interestingly, these extracellular fibers did not contain cytoskeleton components or other cytoplasmic proteins. DNA was found to be the major structural component of these fibers demonstrated by staining with DNA intercalating dyes and the destruction of these structures when treated with DNase.

The time course by which cells undergo ETosis seems to be variable. The original description of NETs demonstrated rapid release of extracellular DNA that occurred in as few as ten minutes following stimulation with phorbol myristate acetate (PMA), but later reports have suggested ETosis could take several hours (159, 212). Yousefi *et al*. described DNA release from eosinophils within five minutes of stimulation with complement component C5a or lipopolysaccharide and maximum effect, measured as fluorescence of a cell impermeable DNA-staining dye, occurred within 30 minutes (215). METosis has been described as a rapid process that can occur in less than 30 minutes (228, 229).

In order to identify METs, most studies utilize either scanning electron microscopy looking for fibers similar to those described by Brinkmann or fluorescent DNA-binding dyes such as Sytox®,

PicoGreen®, TO-PRO®-3, DAPI, or Hoechst visualized by scanning laser confocal microscopy. These dyes have also been used to construct spectrofluorometric assays as an effort to quantify MET release by measuring fluorescence staining of extracellular DNA (212, 230, 231). Typical definitions of METs, like NETs, include extracellular fibers composed of DNA that extend outside the bounds of the cell and are degraded by treatment with DNase I or micrococcal nuclease (example in **Figure VI.2**). Additional verification that proposed structures are ETs can be obtained by staining for known ET components such as histones, elastase, or myeloperoxidase. Elastase, often considered a neutrophil specific marker has been identified in METs of human peripheral blood monocytes and THP-1 macrophage-like cells (228, 232). Similarly, myeloperoxidase has been identified in METs of diverse macrophage populations including human glomerular macrophages, human peripheral blood monocytes, THP-1 macrophage-like cells, murine J774A.1 macrophage-like cells, bovine monocytes, and caprine monocytes (228, 229, 232-235) (**Table VI.1**).

Factors that influence MET release: Like NETs, diverse pathogens and chemical stimuli have been noted to induce METs (**Tables VI.2 and VI.3**). In addition to live bacterial cells, Wong *et al.* described that particular virulence factors such as the *Mycobacterium tuberculosis* secretion system, ESX-1, may specifically contribute to MET release by human peripheral blood monocyte-derived macrophages, a result that was augmented in the presence of other chemical activators including interferon-γ (236). Aulik *et al.* noted that *Mannheimia haemolytica* infection of bovine monocyte-derived macrophages led to MET release in a leukotoxin dependent manner as infection with leukotoxin deficient *M. haemolytica* cells did not result in MET release (231). Several publications have noted that proinflammatory mediators that stimulate generation of reactive oxygen species (ROS) induce METs, though this finding is not consistent across all cell types and experimental conditions (231, 237). Liu *et al.* demonstrated that treatment of mouse macrophage-like J774A.1 cells or primary mouse peritoneal macrophages with PMA, hydrogen peroxide, interferon-γ (100 U/mL), or macrophage-colony stimulating factor (25 ng/mL) did not result in MET release, whereas infection with *Candida albicans* or *Escherichia coli* was able to stimulate METosis (234). Based on this evidence, the authors suggested that MET structures extruded from these cells occurred by a ROS-independent mechanism.

Despite the great diversity of tissue macrophages, few studies currently exist regarding the different types of macrophages that respond to pathogens with MET release (**Table VI.1**). Knowledge is also limited regarding why some macrophages undergo METosis while others do not. For instance, Bonne-Année *et al.* noted that although human monocyte-derived macrophages produced METs in response to *Strongyloides stercoralis* infection, mouse peritoneal macrophages did not, despite that

both human and mouse neutrophils produced NETs during infection (238). Similarly, Schorn *et al.* reported that neutrophils, basophils, and eosinophils respond to monosodium urate crystals in gouty arthritis by producing ETs, but peripheral blood monocytes, despite phagocytosing the crystals, did not produce METs (216). Chow *et al.* made the interesting observation that treating either mouse RAW 264.7 macrophage-like cells or primary mouse peritoneal macrophages with members of the statin family of cholesterol lowering drugs resulted in enhanced MET release from these cells, whereas Halder *et al.* was not able to demonstrate similar responses with human peripheral blood monocytes (228, 237). The current evidence is insufficient to determine if the differential responses are due to experimental conditions or if some types of macrophages are inherently more prone to METosis.

Aside from interactions between macrophages and specific microorganisms, other factors including the cellular environment and polarization state may alter a macrophage's ability to undergo METosis. As in macrophages, the neutrophil literature reveals a growing appreciation of distinct neutrophil subsets that play particular roles in immunity and disease pathogenesis. These subsets, including the proinflammatory, anti-tumorigenic N1 and the tumorigenic N2, represent spectrums of cellular phenotypes that differ in morphological and functional properties (239). Type I interferons have recently been shown to promote a proinflammatory subset of neutrophils (N1, anti-tumorigenic) which display an enhanced ability for form NETs (240). Likewise, Shrestha *et al*. used retinoic acid to drive neutrophil nuclear hypersegmentation, a characteristic finding of N1 cell morphology, and found that retinoic acid treatment also resulted in augmented NETs release in response to PMA stimulation (241). In both studies, the NET-producing, N1 neutrophils also exhibited an increased capacity for cytotoxicity against cancer cells, and Shrestha *et al*. demonstrated that the addition of DNase reversed this effect, suggesting an antitumor role for NETs. Additionally, Villanueva *et al*. demonstrated a subset of 'low-density granulocytes' isolated from patients with systemic lupus erythematosus had a greater capacity to produce NETs than normal-density neutrophils from patients with lupus or control neutrophils from patients without lupus (242). By producing a higher proportion of NETs, these cells may provide increased exposure of autoantigens and have an increased capacity to kill endothelial cells, driving disease pathogenesis.

Macrophages are known to function along a spectrum of activated phenotypes, or, polarization states (210). Only one report to date specifically investigated how macrophage polarization may influence METosis. Nakazawa *et al.* made the observation that PMA differentiated THP-1 cells polarized toward an inflammatory M1 activation state (treated with 20 ng/mL IFN-γ and 1 mg/mL LPS for 6 hours) but not the anti-inflammatory/pro-healing M2 state (treated with 20 ng/mL IL-4 for 24 hours) resulted in extracellular DNA release when exposed to NET material (243). Of note, these

authors did not specifically label this extracellular DNA release as METs, but their findings suggest that this extracellular DNA extended beyond cellular boundaries and originated from the macrophages, despite that the DNA release was noted to be 'less drastic' than that seen by neutrophils undergoing ETosis. These authors found similar results with peripheral blood mononuclear cells differentiated to polarized macrophages after 7 day incubation with 10 ng/mL GM-CSF (M1) or 10 ng/mL M-CSF (M2). Interestingly, DNA release by THP-1 macrophage-like cells was specific to interaction with NETs, as macrophage extracellular DNA release was not stimulated by interactions with neutrophils undergoing other types of cell death.

Changes in the cellular environment might also alter macrophage behavior. Bryukhin and Shopova used a rat model of liver injury, which has been shown to depress immune function including monocyte migration and phagocytic activity to demonstrate that alveolar macrophages and peripheral blood monocytes taken from pups of mothers with drug-induced hepatitis were impaired in MET formation and bactericidal activity (244). This work suggests that cellular programming or environmental signals may modify the ability of macrophage to complete METosis. Vega *et al.* demonstrated that mouse J774A.1 and RAW264.7 macrophage-like cells undergoing stress response (incubation at 42°C for 1.5 hours followed by recovery at 37°C) were more prone to produce METs when exposed to *Streptococcus agalactiae* (245). In their experimental conditions, *S. agalactiae* infection resulted in decreased ROS/RNS production and elevated levels of IL-10, which are most typically associated with ET inhibition in neutrophils. The authors of this study suggested that changes in the cytoskeleton triggered by stress responses, potentially via Hsp70 and Hsp27, might lead to METosis in the absence of oxidative stress or pro-inflammatory mediators.

Together these studies demonstrate that MET release can occur in response to a diverse collection of pathogens, but data are limited regarding the responses of specific types of tissue macrophages. More work is needed to better understand how polarization states and environmental signals might alter cellular function with respect to METs and whether these changes would affect all tissue macrophages in a similar way. These future studies will be important as the functions of METs in both immunity and pathophysiology become clearer.

Functions attributed to METs: NETs have been attributed several functions including trapping diverse pathogens, suppression and destruction of bacterial toxins of trapped organisms, and bactericidal activity (159). The bactericidal activity of NETs has been attributed to a localized, high concentration of antimicrobial peptides contained on the globules of NET fibers as DNase treatment eliminates this cidal activity (159). Several studies have examined the fundamental question if METs have cidal activity for different microorganisms. In order to assess microbicidal activity, most MET

killing assays compare macrophages infected with or without the presence of DNase and compare recovered microorganisms (230, 231). In order to separate killing that results from MET-dependent and MET-independent mechanisms (mainly phagocytosis), some studies have used the actin cytoskeletal inhibitor, cytochalasin D, to inhibit macrophage phagocytosis (230, 234). There have been mixed results using this technique as some groups have noted decreased MET release in cells pretreated with cytochalasin D (231, 232). To date, there are reports of potential MET microbicidal activity against pathogens including *Staphylococcus aureus*, *S. agalactiae*, *E. coli*, and *C. albicans* (234, 244-246). Halder *et al.* isolated monocyte ETs by digesting immobilized traps with the restriction enzyme *Alu*I and then added ET material to *C. albicans* culture; ET material, but not monocyte chromosomal DNA, was able to inhibit fungal growth even at 30 hours of incubation (228). Instead of using direct counting of microorganisms, Chow *et al.* used SYTO™9 and propidium iodide staining of *S. aureus* cells trapped within METs to demonstrate decreased viability of bacterial cells (237).

Despite results stated above, several studies question any direct bactericidal activity of METs. For example, a recent study evaluated infection of PMA-differentiated THP-1 macrophage-like cells with *Mycobacteria massiliense* and noted that MET release actually enhanced bacterial growth, potentially by providing a scaffold for bacterial aggregation, which facilitates survival in this organism (232). Liu *et al.* demonstrated that mouse J774A.1 macrophage-like cells infected with *E. coli* or *C. albicans* resulted in small but significant microbial killing attributed to METs (10-20% less organisms recovered compared to cells treated with DNase and cytochalasin D), but peritoneal macrophages in similar assays did not show any significant MET microbicidal activity against either organism. Of note, in this study the extent of microbial killing attributed to METs was considerably less than that attributed to intracellular killing (234).

It has been proposed that METs may act synergistically with other components of host defense. Halder *et al.* demonstrated that human monocyte release of METs was enhanced in the presence of human serum (228). During infection with *C. albicans* in media containing serum, this study used immunofluorescent staining to establish that complement factors C3b and C5b-9 were deposited onto METs. The authors proposed that activated complement might add microbicidal activity and allow for enhanced opsonization and phagocytosis of organisms within ETs during the resolution of inflammatory responses (228). Shen *et al.* showed that the antibiotic fosphomycin may boost MET release, potentially by increasing production of ROS, and enhance total extracellular killing of *S. aureus* by mouse peritoneal macrophages producing METs (246).

One of the difficulties of these studies is successfully demonstrating that METosis and METs occur *in vivo* and are not an artifact of *ex vivo* experimental conditions. Just as NETs are now recognized in diverse tissues, METs have now been identified within tissues during disease states.

O'Sullivan *et al.* evaluated renal biopsy tissues from patients with myeloperoxidase (MPO)-ANCA-associated glomerulonephritis (233). Tissues from patients with glomerulonephritis had significantly more macrophages than control tissues. The authors used immunofluorescent probes against nuclear components and MPO to identify NETs and METs, which they differentiated by the presence of neutrophil elastase (NET marker) and CD68 positivity (MET marker). Six of ten biopsies from patients with glomerulonephritis were found to have MPO containing METs. This is particularly interesting given that MPO, a component of both NETs and METs, is considered to be a major autoantigen in the development of ANCA-associated vasculitis, suggesting that macrophage and neutrophil ETs contribute to the pathophysiology of this disease. Mohanan *et al.* examined macrophage function at 'crown-like structures' in breast adipose tissue (247). Crown-like structures are thought to be areas where macrophages clear dying adipocytes. This study evaluated mammary adipose tissue from obese mice and found that macrophages at crown-like structures stained strongly for PAD2 and citrullinated histones (anti-H4Cit3), which extended from macrophage nuclei into the extracellular space. The authors propose these macrophages were undergoing hypercitrullination via PAD2 as part of METosis. This report suggested that METosis in adipose tissue could be driven by TNF-α release from dying adipocytes. Pro-inflammatory signals may promote MET release and drive further inflammatory signals within adipose tissue, influencing macrophage infiltration and activation.

Cellular pathways implicated in MET release: Identifying mechanisms by which neutrophils undergo ETosis and subsequently release NETs continues to be an area of active research. The 'NETotic cascade' comprises several steps including cytoplasmic and nuclear swelling, vacuolization, membrane protrusion, enzyme binding to DNA, histone citrullination and chromatin decondensation, and terminating in membrane rupture and NET release (248). During this cascade cellular granule membranes also break down allowing for nuclear and granular proteins to mix and for granular proteins such as elastase to be found within NETs after release (212). Early descriptions of NETs noted that this process was dependent on the NADPH oxidase system, in which NADPH oxidase-derived ROS acted intracellularly to initiate the NET cascade through actions that include activation of elastase, which then escapes from neutrophil azurophilic granules (248, 249). Once released, elastase translocates to the nucleus where it degrades histones and thereby promotes chromatin decondensation (249). Reports have also suggested that interactions between ROS formation, cellular autophagy, and PAD4-dependent histone citrullination result in collapse of intracellular membranes allowing for chromatin decondensation and subsequent release (250).

Alternative forms of ETosis with unique pathways are now being described. Yousefi *et al.* reported that neutrophils primed with GM-CSF and stimulated with lipopolysaccharide or complement

component C5a could produce NETs from mitochondrial DNA in a pathway that depended on ROS but did not result in cellular death (251). Pilscek *et al.* described another alternative form of neutrophil ETosis in which nuclear DNA was deposited extracellularly via membrane vesicles, a process which was not inhibited by diphenylene iodonium (DPI), suggesting an NADPH-independent pathway (252).

Investigations into mechanisms of MET release have been less numerous. Reports have demonstrated that inhibitors of the NADPH-oxidase system including DPI reduce MET formation, although this has not been consistent across all studies (229, 231, 234, 235, 246). King *et al.* used a fluorescent readout of ROS production (dihydrorhodamine 123) to indicate that human alveolar macrophages producing METs had a two-fold increase in ROS fluorescence compared to cells not forming METs (253). Treating alveolar macrophages with the ROS inhibitor apocynin inhibited MET release. Aulik *et al.* established that other pathways that boost intracellular ROS including treatment with glucose oxidase or PMA enhanced MET release from bovine macrophages (231).

As with neutrophils, there are reports of alternative pathways of METosis (232, 234). Je *et al.* suggested that calcium influx into PMA-differentiated THP-1 macrophage-like cells may influence MET production by an NADPH oxidase-independent mechanism (232). Treatment of THP-1 cells with 20 μM 1,2-bis (o-aminophenoxy) ethane-N,N,N',N'-tetraacetic acid (BAPTA) or 1 μM ethylene glycol tetraacetic acid (EGTA) to chelate calcium diminished but did not eliminate MET release in this study. Interestingly, this report suggested that DNA present in these METs was composed of nuclear and mitochondrial DNA as the authors were able to identify nuclear (*ACTB*, *GAPDH*) and mitochondrial genes (*ATP6*, *NDS1*) from supernatants of infected cells by PCR. Similarly, Liu *et al.* which also proposed an ROS independent mechanism of MET release from mouse J774A.1 macrophage-like cells, was also able to identify both mitochondrial (*Atp6* and *Nds1*) and nuclear (*Actb* and *Gapdh*) genes via *in situ* hybridization and PCR amplification of supernatants from *C. albicans* stimulated macrophages (234).

Other important steps in METosis remain poorly understood. In neutrophils, both elastase and myeloperoxidase contribute to ETosis (249, 254). Elastase promotes NET release by degrading histones and promoting chromatin decondensation and myeloperoxidase synergizes with elastase chromatin decondensation in a mechanism that is independent of enzymatic activity (249). To date, four studies have evaluated if elastase and myeloperoxidase contribute to METosis. Wong *et al.* used the elastase inhibitor, N-methoxysuccinyl-Ala-Ala-Pro-Val-chloromethyl ketone (AAPV), to block monocyte-derived macrophages infected with *M. tuberculosis* or *S. aureus* from releasing METs and Shen *et al.* found similar results with AAPV treated mouse peritoneal macrophages infected with *S. aureus* (236, 246). In contrast, Je *et al.* noted AAPV treated THP-1 macrophage-like cells infected with *M. massiliense* were unaffected in regards to MET release despite that elastase was identified

within the MET structures (232). Muñoz-Caro *et al.* inhibited MET release by bovine monocytes infected with *Besnoitia besnoiti* tachyzoites using the myeloperoxidase inhibitor, 4-aminobenzoic acid hydrazide (ABAH) (229). These studies suggest an active role for elastase and myeloperoxidase in METosis, but it remains to be determined if the mechanisms by which these enzymes contribute mirror those seen in neutrophils.

Chow *et al.* used statin drugs to implicate sterol production pathways as a potentially important mediator of MET formation. They demonstrated that MET formation was enhanced in statin treated murine peritoneal macrophages. They found similar results using siRNA knockdown of HMG-CoA reductase, a finding that was reversed with treatment of the HMG-CoA reductase product mevalonate (237). The authors proposed that the effect of statins to boost MET production might be mediated by intermediates of the sterol synthetic pathways, although the exact mechanism by which these intermediates may alter METosis is not well understood.

The role of cytoskeleton rearrangement in both neutrophils and macrophage ETs remains a topic of debate. Pretreatment with the actin cytoskeletal inhibitor, cytochalasin D, often used to block phagocytosis, has demonstrated the ability to decrease MET formation in some studies (231, 232). Cytochalasin D treatment did not have a significant effect on METosis of bovine monocytes exposed to *B. besnoiti* or murine J774A.1 macrophage-like cells in response to *E. coli* or *C. albicans* (229, 234). Aulik *et al.* reported that cytochalasin D reduced bovine peripheral blood and alveolar macrophage METosis response to *M. haemolytica* and its leukotoxin, but in this same study cytochalasin D had no significant effect on MET release from THP-1 or RAW 264.7 macrophage-like cells in response to *E. coli* hemolysin (231). Contrary to this report, Je *et al.* found that THP-1 macrophage-like cells treated with cytochalasin D were impaired in regards to phagocytosis and MET release in response to *M. massiliense* (232). These findings have led some authors to speculate that phagocytosis of particular microorganisms or microbial toxins maybe an important trigger for MET formation (231, 232).

There are also conflicting reports regarding the role of cytoskeletal inhibitors in NET biology. In the original NET description, cytochalasin D effectively prevented phagocytosis of *Shigella flexneri* or *S. aureus* but not NET release (159). Other studies have also reported that cytoskeletal inhibitors had no effect on NET formation in response to *Paracoccidioides brasiliensis* or gold nanoparticles (255, 256). Neeli *et al.* reported that 10 μM treatment with either the microtubule inhibitor nocodazole or cytochalasin D diminished histone deamination and NET release in response to LPS, and similar results were documented by Jerjomiceva *et al.* using enrofloxacin treated bovine neutrophils (257, 258). The basis for the divergent results in these studies is not clear, but more research is needed to

better define the role of the cytoskeleton during the processes of ETosis in neutrophils and macrophages.

A few studies have investigated the role of protein arginine deiminases (PADs) and histone hypercitrullination as an important step in METosis. PAD4 mediated hypercitrullination has been shown to be an important pathway during neutrophil ETosis leading to chromatin decondensation; inhibition of this pathway impairs NET release (259). Nakazawa *et al.* made the observation that PAD4 expression in PMA-differentiated THP-1 cells accompanied M1 phenotype induction; treatment of these cells with PAD4 siRNA resulted in inhibition of extracellular DNA release (243). Mohanan *et al.* demonstrated that treatment with TNF-α resulted in histone hypercitrullination via PAD2 in RAW 264.7 cells prior to chromatin decondensation and MET release (247).

Overall, the limited studies that have evaluated the steps of METosis mirror findings of neutrophil ETosis, but there are discrepancies within the literature particularly with regard to the role ROS and cytoskeleton polymerization during METosis. More work is needed to further define differences in the ROS dependent and independent pathways of METosis and whether particular-signaling pathways may favor one pathway over the other.

Is METosis a cell death pathway? ETosis is considered to be a different cellular pathway than apoptosis as neutrophils undergoing ETosis do not demonstrate typical DNA fragmentation, lack phosphatidylserine localization to the outer leaflet of cellular membrane, and lack typical caspase activation that are hallmarks of cells undergoing apoptosis (212). ETosis is also notably different from cellular necrosis, as in ETosis both the nuclear and granular membranes disintegrate while the plasma membrane is intact (212). As noted above, reports of alternative forms of ETosis have been documented in neutrophils and eosinophils and suggest that not all ETosis pathways end in cell death (215, 251).

A few studies have evaluated monocyte and macrophage viability while undergoing METosis. Using a fluorescent cell staining for intracellular esterase activity and plasma membrane integrity, Chow *et al.* revealed that staining of MET producing RAW 264.7 macrophage-like cells was consistent with loss of membrane integrity, suggesting these cells were no longer viable (237). Vega *et al.* used a similar approach and noted mouse J774A.1 macrophage-like cells producing METs were dead within 3 hours (245). Nakazawa *et al.* used TUNEL staining to evaluate M1-polarized THP-1 cells releasing extracellular DNA after exposure to NETs. These cells demonstrated positive TUNEL staining, which contradicts a report in neutrophils suggesting that NET producing cells are TUNEL negative (212, 243).

One study evaluated the role of caspase-1 in METosis. Webster *et al.* illustrated that human peripheral blood monocytes infected with either *E. coli* or *Klebsiella pneumoniae* resulted in caspase-1 activation, which is considered part of some non-apoptotic cell death pathways, particularly pyroptosis (260). Inhibiting caspase-1 with the chemical z-YVAD-fmk reduced MET release. With caspase-1 activation, the authors remarked on a general loss of cell viability over the first 12 hours of infection. Caspase-1, while not previously noted to be activated in neutrophil ETosis, was found to be activated in macrophages in response to NET material and the antibacterial protein LL-37 present on NET fibers (261). It remains unclear if exposure to MET fibers could induce a similar response in surrounding macrophages, potentially driving further proinflammatory responses including METs.

The sparse data available suggest that METosis is indeed a cell death process, similar to classical pathways in neutrophils. More work is needed to define the principle triggers and pathways that move a macrophage from other immune responses to METosis. Additional studies are also needed to differentiate makers of different cellular death pathways including METosis and to clarify conflicting data.

Area of future research: As interest in METs grows, future research will likely focus on differences between macrophages and other cells that produce ETs. As opposed to other leukocytes like neutrophils or basophils, macrophage functions can vary dramatically based on differentiation, microenvironment, and polarization states. As such, it may not be surprising that the current literature in this field contains many conflicting reports. Future studies will need to find ways to delineate how subtle shifts in cellular programing such as macrophage polarization may direct macrophages to different immune responses against pathogens. Additionally, whether METosis occurs globally in all macrophages including specialized cells like Kupffer cells or microglia is yet to be explored. As the NET literature has widely expanded since the first description in 2004, it seems likely that appreciation of METs and their role in immunity and pathophysiology will continue to gain recognition and stimulate additional studies to add to our current understanding of METosis.

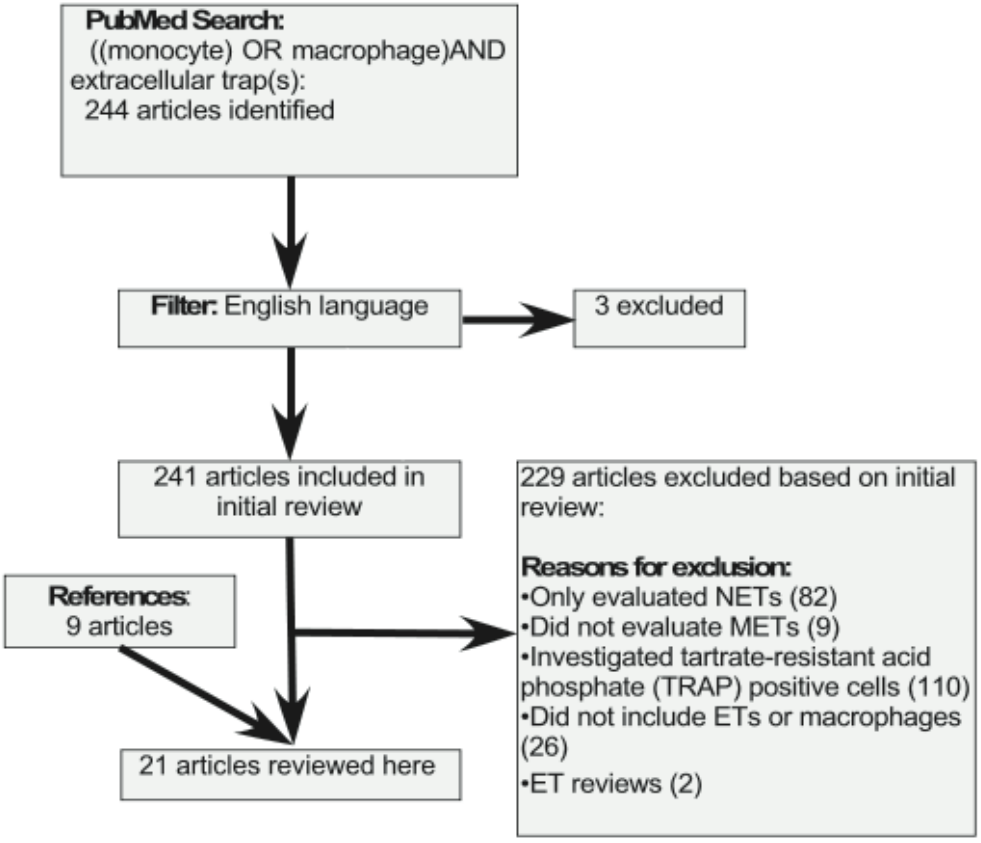

Figure VI.1: Search and review flow. 244 articles were identified by primary PubMed search. 3 were excluded based on language. 241 articles underwent initial review of abstracts and 229 were excluded. 12 primary articles were identified for inclusion in this review based on primary search and from the reference of these articles an additional 9 articles were identified. ET: extracellular traps, NETs: neutrophil extracellular traps, METs: macrophage extracellular traps.

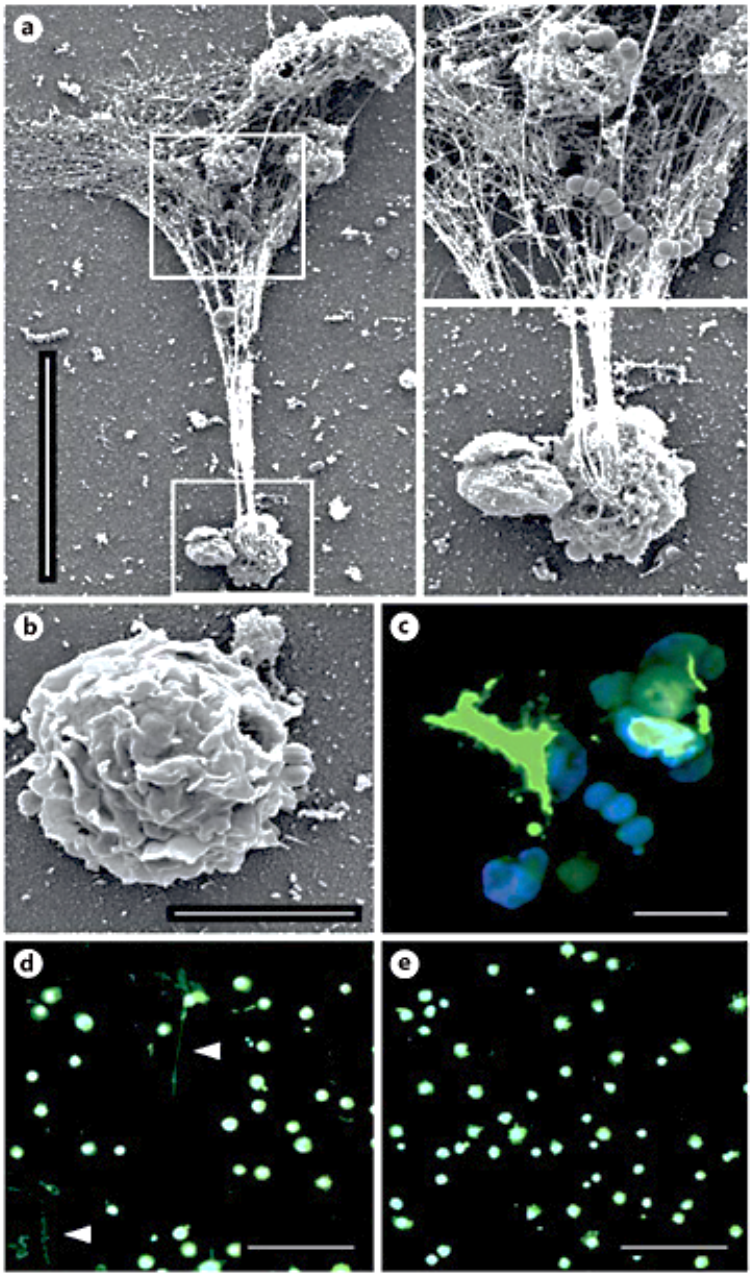

Figure VI.2: Examples of METs. A: Scanning electron micrograph image of a placental macrophage with expelled MET in response to *S. agalactiae*. Measurement bar represents 20 μm. As can be seen in magnified panels (right) these fibers originate from the macrophage cell (bottom) and bacterial cells become embedded in these fibers (top). B: Placental macrophage infected with *S. agalactiae* and treated with DNase I leaving a defect in macrophage cell surface where MET fibers exited the cell. Measurement bar represents 5 μm. C: Confocal microscopy 3D reconstruction image of a placental macrophage MET in response to *S. agalactiae*. Measurement bar represents 10 μm. Cells were stained with Sytox Green (green) for extracellular DNA and Hoechst 33342 (blue) for condensed chromatin. Extracellular DNA fibers (green) are seen extending beyond the nucleus structure (blue). Placental macrophages were obtained as published from de-identified, term, non-labored placenta provided by the Cooperative Human Tissue Network, which is funded by the National Cancer Institute (262). All tissues were collected in accordance with Vanderbilt University Institutional Review Board (approval #131607).

Table VI.1. Types of monocytes and macrophages known to produce METs and the cellular proteins identified within MET structures.

Cell Type	MET Contents	Reference
Human alveolar macrophages	Matrix metalloproteinase 12	(253)
Human glomerular macrophages	Myeloperoxidase	(233)
Human monocyte derived macrophages	Histone H4	(236, 238, 255)
Human peripheral blood monocytes	Histone H2 and H3 Neutrophil Elastase Myeloperoxidase Lactoferrin	(228, 260, 263)
THP-1 cells	Myeloperoxidase Neutrophil Elastase Histone H3 and H4	(231, 232, 236, 243, 246)
Murine peritoneal macrophages		(234, 237, 246)
RAW 264.7 cells	Histone H2 and H4	(231, 237, 245, 247)
J774A.1 cells	Histone H2 Myeloperoxidase Lysozyme	(234, 245)
Rat macrophages (peripheral blood monocytes, alveolar, peritoneal)		(244)
Bovine macrophages (peripheral blood monocytes, alveolar)		(230, 231)
Bovine monocytes	Histone H3 Myeloperoxidase	(229)
Caprine monocytes	Histone H3 Myeloperoxidase	(235)
Carp (*Cyprinus carpio*) monocyte/macrophages		(264)
Harbor seal (Phoca vitulina) monocytes		(265)

Table VI.2. Microbial organisms that elicit a macrophage extracellular trap response.

Gram negative bacteria	Gram positive bacteria	Parasites	Acid fast bacilli	Fungi
Escherichia coli[228, 234, 260]	*Staphylococcus aureus*[237, 246]	*Besnoitia besnoiti*[229]	*Mycobacterium abscessus*[263]	*Candida albicans*[228, 234]
Nontypeable *Haemophilus influenza*[253]	*Streptococcus agalactiae*[245]	*Eimeria ninakohlyakimovae*[235]	*Mycobacterium massiliense*[232]	
Histophilus somni[230]		*Strongyloides stercoalis*[238]	*Mycobacterium tuberculosis*[236]	
Klebsiella pneumoniae[260]		*Toxoplasma gondii*[265]		
Mannheimia haemolytica[231]				

Table VI.3: Chemical inducers and inhibitors of METosis.

Chemical inducers	Chemical Inhibitors
Fosfomycin[246]	4-aminobenzoic acid hydrazide (ABAH)[229]
Glucose oxidase[231]	Apocinin[253]
HMG-CoA reductase inhibitors (statins)[237]	Cytochalasin D[231, 232]
Interferon-γ[236]	Diphenylene iodonium[229, 231, 235, 246]
Neutrophil extracellular trap material[243]	GM-CSF[236]
Phorbol myristate acetate[231, 237]	N-methoxysuccinyl-Ala-Ala-Pro-Val-chloromethyl ketone[232, 236, 246]
TNF-α[247]	z-YVAD-fmk [260]
Zymosan[229, 265]	

CHAPTER VII

Streptococcus agalactiae induces placental macrophages to release extracellular traps loaded with tissue remodeling enzymes via an oxidative-burst-dependent mechanism

INTRODUCTION:

15 million cases of preterm birth, or birth before 37 weeks gestation, occur annually worldwide, including 500,000 cases in the United States, conferring an estimated cost of $26.2 billion (1, 92, 266). The World Health Organization estimates that preterm birth complications are a leading cause of death among children under five years of age, resulting in nearly 1 million deaths in 2015 (267, 268). In addition to loss of child lives, preterm birth increases risk of chronic health conditions including neurodevelopmental deficits, metabolic syndrome, cardiovascular abnormalities, chronic kidney disease, and chronic respiratory conditions (269, 270).

Streptococcus agalactiae, also known as Group B *Streptococcus* (GBS), is a common perinatal pathogen (11). Approximately 10-40% of women are colonized with GBS during late pregnancy (33, 34). Rectovaginal GBS carriage is associated with adverse pregnancy outcomes including stillbirth, preterm labor, chorioamnionitis, and neonatal sepsis (3, 35, 142). Because of the burden and severity of GBS-related adverse pregnancy outcomes, the CDC recommends GBS screening late in gestation and antibiotic prophylaxis during labor (24). This strategy has decreased the incidence of early-onset neonatal sepsis but misses mothers that deliver preterm, before screening is conducted (24). Despite screening and treatment interventions, GBS remains a leading neonatal pathogen (144).

Pregnancy represents a unique immunologic state in which the maternal immune system must dampen its responses against foreign antigens of the semiallogenic fetus while defending the gravid uterus from infection. Excessive inflammation can drive adverse pregnancy events including loss of pregnancy, preterm birth, intrauterine growth restriction, and preeclampsia (67). Multiple mechanisms exist to support maternal-fetal tolerance including production of anti-inflammatory cytokines that alter the number and function of immune cells at the maternal-fetal interface (68-70). Unfortunately, infection is a common complication of pregnancy. Bacterial infection of the fetal membranes, known as chorioamnionitis, occurs most often by ascending infection from the vagina (11, 15, 16). During infection, bacterial products are recognized by pathogen recognition receptors, which then stimulate production of proinflammatory cytokines (15, 271, 272). These inflammatory mediators initiate a cascade of events that result in neutrophil infiltration into the fetal membranes, production and

release of matrix metalloproteases (MMPs), and cervical contractions which eventually result in membrane rupture and preterm birth (273).

Macrophages represent 20-30% of the leukocytes within gestational tissues (71). In particular, fetally-derived macrophages, called Hofbauer cells or placental macrophages (PMs), play key roles in placental invasion, angiogenesis, tissue remodeling, and development (72, 73). The inflammatory state of these cells is carefully regulated throughout pregnancy. As the pregnancy progresses the M2 or anti-inflammatory and tissue remodeling phenotype predominates to supports fetal development (74-77). PMs contribute to immune tolerance by secretion of anti-inflammatory cytokines, which suppress production of proinflammatory cytokines (78-81). Disruption of appropriate macrophage polarization is associated with abnormal pregnancies including spontaneous abortions, preterm labor, and preeclampsia (74). We sought to understand how bacterial infection alters PM functions, and how these responses may contribute to pathologic pregnancies. These studies demonstrate that both PMs and a model macrophage cell line, the PMA-differentiated THP-1 macrophage-like cells, release macrophage extracellular traps (METs) in response to bacterial infection in a process that is dependent upon the generation of reactive oxygen species (ROS). METs, reminiscent of neutrophil extracellular traps (NETs), have recently been recognized as structures released by macrophages under a number of conditions including infection (274). PM METs contain histones, myeloperoxidase, and neutrophils elastase as well as several MMPs, and MET structures are found within human fetal membranes infected with GBS *ex vivo*.

METHODS:

Placental macrophage isolation and culture: Human placental macrophages (PM) and fetal membrane tissues were isolated from placental tissues from women who delivered healthy infants at full term by cesarean section (without labor). De-identified tissue samples were provided by the Cooperative Human Tissue Network, which is funded by the National Cancer Institute. All tissues were collected in accordance with Vanderbilt University Institutional Review Board (approval 131607). Macrophage isolation occurred as previously described (275); briefly, placental villous tissue was minced followed by digestion with DNase, collagenase, and hyaluronidase (all from Sigma-Aldrich, St. Louis MO). Cells were filtered, centrifuged, and CD14+ cells were isolated using the magnetic MACS Cell Separation system with CD14 microbeads (Miltenyi Biotec, Auburn CA). Cells were incubated in in RPMI 1640 media (ThermoFisher, Waltham MA) with 10% charcoal stripped fetal bovine serum (ThermoFisher) and 1% antibiotic/antimycotic solution (ThermoFisher) overnight at 37°C in 5% carbon dioxide. The following day, PMs were suspended in RPMI media without antibiotic/antimycotic and distributed into polystyrene plates. Cells were incubated for at least 1 hour prior to infection to

allow for cell adherence to plate or Poly-L-Lysine coated glass coverslips (Corning, Bedford MA) for microscopy assays.

THP-1 cell culture: THP-1 cells (ATCC, Manassas VA) were cultured in RPMI 1640 media with 10% charcoal treated FBS and 1% antibiotic/antimycotic media at 37°C in 5% carbon dioxide. 24-48 hours prior to co-culture experiments, cells were treated with 100 nM phorbol 12-myristate 13-acetate (PMA) (Sigma-Aldrich) to induce differentiation to macrophage-like cells. Prior to co-culture experiments, cells were suspended in RPMI media without antibiotic/antimycotic and distributed into polystyrene plates containing Poly-L-Lysine coated glass coverslips and allowed to rest for at least 1 hour prior to infection to promote cell adherence.

Bacterial culture: *Streptococcus agalactiae* strain GB00590 is a capsular type III, ST-17 strain isolated from a woman with asymptomatic colonization (139), and GB00037 is a capsular type V strain obtained from a case of neonatal sepsis (65, 140). *Escherichia coli* serotype 075:H5:K1 is a clinical isolate obtained from a fatal case of neonatal meningitis (149). Bacterial cells were cultured on tryptic soy agar plates supplemented with 5% sheep blood (blood agar plates) at 37°C in ambient air overnight. Bacteria were subcultured from blood agar plates into Todd-Hewitt broth or Luria-Bertani Broth and incubated under aerobic shaking conditions at 37°C in ambient air to stationary phase. Bacterial supernatant was collected and sterile filtered using a 0.1 μm filter (Millipore Sigma, Burlington MA) and incubated with THP-1 cells at a concentration of 10% volume. Bacterial cells were washed and suspended in phosphate buffered saline (PBS, pH 7.4) and bacterial density was measured spectrophotometrically at an optical density of 600 nm (OD_{600}) and bacterial numbers were determined with a coefficient of 1 OD600 = 10^9 CFU/mL.

Bacterial-macrophage co-cultures: PMs or PMA-differentiated macrophage-like cells in RPMI without antibiotics were infected with GBS or *E. coli* cells at a multiplicity of infection (MOI) of 20:1 unless otherwise noted. Co-cultured cells were incubated at 37°C in air supplemented to 5% carbon dioxide for 1 hour. As stated, some cells were pretreated with 10 μg/mL cytochalasin D (ThermoFisher), 10 nM nocodazole, 100 Units/mL DNase I, 500 nM PMA, or 10μM diphenyleneiodonium chloride (all from Sigma-Aldrich) for at least 20 minutes prior to infection. At 1 hour, supernatants were collected, and cells were fixed with 2.0% paraformaldehyde and 2.5% glutaraldehyde in 0.05 M sodium cacodylate buffer (Electron Microscopy Sciences, Hatfield PA) for at least 12 hours prior to processing for microscopy.

Field-emission gun scanning electron microscopy: Following treatment and infection as above, macrophages were incubated in 2.0% paraformaldehyde and 2.5% glutaraldehyde in 0.05 M sodium cacodylate buffer for at least 12 hours prior to sequential dehydration with increasing concentrations of ethanol. Samples were dried at the critical point, using a CO_2 drier (Tousimis, Rockville MD), mounted onto an aluminum stub, and sputter coated with 80/20 gold-palladium. A thin strip of colloidal silver was painted at the sample edge to dissipate sample charging. Samples were imaged with a FEI Quanta 250 field-emission gun scanning electron microscope. Quantification of macrophages producing extracellular traps was determined by evaluating scanning electron micrograph images at 750X magnification and counting total macrophages and those macrophages releasing extracellular traps. Extracellular traps were defined as previously described with typical appearing fibers extending from the cell body into the extracellular space (274).

Confocal laser scanning microscopy: Co-cultures were completed, and macrophages fixed as above. Coverslips were washed once with PBS prior to staining with SYTOX® Green (10 μM final concentration, ThermoFisher) for double stranded DNA (dsDNA), and Hoechst 33342 (5 μM final concentration, ThermoFisher) for condensed chromatin (nuclei). Additional staining for histones and MMPs were accomplished by blocking cells in 1% bovine serum albumin in PBS for 30 minutes at 37°C followed by a 1 hour incubation at 37°C with antibodies for histone H3 (ab5103, abcam, Cambridge, MA), neutrophil elastase (ab68672, abcam), myeloperoxidase (ab9535, abcam), matrix metalloproteinase (MMP)-1 (ab551168, abcam), MMP-7 (ab5706, abcam), MMP-8 (ab81286, abcam), MMP-9 (ab38898, abcam), or MMP-12 (ab137444, abcam). Cells were then washed 3 times with 1% BSA in PBS followed by a 30 minute incubation with an Alexa-594 conjugated goat anti-rabbit secondary antibody (ThermoFisher) and 2 additional washes with 1% BSA in PBS prior to mounting coverslips onto glass microscope slides with Aqua Poly/Mount (Polysciences Inc, Warrington PA). Macrophages were visualized with a Zeiss LSM 710 META Inverted Laser Scanning Confocal Microscope, and extracellular traps were identified by dsDNA staining that extended into the extracellular environment.

Bacterial killing by macrophages releasing extracellular traps: PMs were infected with GBS cells at a MOI of 20:1 as described above. As indicated some PMs were incubated with100 U/mL DNase I during infection to degrade extracellular trap structures as has been described previously (159). At the end of 1 hour, DNase I was added to previously untreated wells for 10 minutes to release trapped bacterial cells. Supernatants were collected, and PMs were permeabilized with 0.05% Tween-20 in sterile ice-cold water to release intracellular bacteria. Samples were vortexed vigorously, serially

diluted, and plated on blood agar plates to enumerate bacterial cells. Untreated PMs were compared to DNase I treated cells and data are expressed as the percent colony forming units (CFU) recovered compared to untreated cells. To further evaluate bacterial killing, PMs were seeded onto coverslips and infected as above. Following infection, cells were stained using the Live/Dead BacLight Bacterial Viability Kit (Invitrogen) prior to confocal laser scanning microscopy.

LDH cytotoxicity assay: Placental macrophages were incubated in RPMI media without antibiotics or serum and infected as above. Supernatants were collected and centrifuged to pellet cellular debris. Supernatants were analyzed using the Cytotoxicity Detection Kit (Sigma-Aldrich) per manufacturer instructions. Results are expressed as percent toxicity using media without cells as the low control and cells treated with 2% Triton X as a high control. Percent cytotoxicity was calculated using the following equation: cytoxicity (%) = (experimental value-low control)/(high control-low control) x 100.

Apoptosis assay: Placental macrophages were incubated in RPMI media without antibiotics and infected as above. Following infection supernatants were removed and cells were fixed with 2.0% paraformaldehyde and 2.5% glutaraldehyde in 0.05 M sodium cacodylate buffer for at least 15 minutes. Click-iT Plus TUNEL Assay with Alexa-Fluor 594 dye (ThermoFisher) was used to identify cells undergoing apoptosis and staining was conducted per manufacturer instructions with additional staining that included Hoechst 33342 to visualize nuclei prior to confocal laser scanning microscopy.

Macrophage viability assay: To determine if DNase I treatment resulted in alterations in PM viability or function, TNF-α release was used a functional measure. Cells were left untreated or treated with 100 U/mL DNase I for 60 minutes. All cells were then washed, and fresh media added prior to stimulation with 150:1 heat-killed GBS cells (incubated at 42°C for 2 hours) for 24 hours. Supernatants were collected and centrifuged to pellet cellular debris before TNF- α release was determined using a DuoSet TNF- α ELISA (R&D Systems) per manufacturer instructions.

Measurement of intracellular ROS production: Measurements of intracellular ROS production was made by staining cells with CellROX® Deep Red Reagent (ThermoFisher) which measures oxidative stress by producing fluorescence upon oxidation by ROS. PMs were isolated and treated as described above. At the time of infection, a cellular stain mixture containing CellROX Deep Red (5 μM final concentration), SYTOX GREEN, and Hoechst 33342 was added to co-cultures. After 1 hour of infection, cells were washed 3 times with PBS before a 15-minute fixation with 3.7% formaldehyde to preserve CellROX Reagent signal. Coverslips were then mounted onto glass slides and visualized

with a visualized with a Zeiss LSM 710 confocal microscope as above. Images obtained were analyzed using Fiji Version 1.0 (276). In order to quantify ROS production, a cellular ROS production index was calculated using the following equation: ((total image intensity – (mean background fluorescence x image area))/total macrophages counted) x (number of macrophages with ROS production/total macrophages counted). Images capturing only ROS staining (without other stains/channels) were measured to determine the total corrected fluorescence for the total image area. Mean background fluorescence was determined by at least 3 different measurements in areas of the image lacking cellular contents (277). Data are presented as the mean +/- SE ROS cellular production index of 10 images per sample.

Metalloproteinase ELISA: Supernatants from macrophage-GBS co-cultures were collected and centrifuged as above to remove cellular debris. Supernatants were then evaluated for the concentration of human MMP-8 and MMP-9 using DuoSet ELISA kits (R&D Systems, Minneapolis, MN) per the manufacturer's protocol and protein levels were calculated from a standard curve.

Matrix metalloproteinase activity: MMP activity of co-culture supernatants was measured using the MMP Activity Assay Kit (abcam). Supernatants were incubated with assay buffer for 30 minutes and fluorescence signal was measured with a fluorescence microplate reader at an Ex/Em = 490/525 nm. Sample values were normalized to uninfected cells from the same placental sample to calculate a percent change for each placental sample assayed.

Human fetal membrane infections: Fetal membrane tissue was obtained and cultured as previously described (119). Briefly, fetal membranes were excised from placental tissues. Fetal membrane tissue sections were suspended over a 12 mm Transwell Permeable Support without membrane (Corning) and immobilized using a ¼ inch intraoral elastic band (Ormco, Orange CA) so that the choriodecidua was oriented facing up. Both transwell chambers were incubated with Dulbecco's modified Eagle's medium (DMEM), high-glucose, HEPES, no-phenol-red cell culture medium (Gibco, Carlsbad, California) supplemented with 1% fetal bovine serum and PEN-STREP antibiotic/antimycotic mixture (Gibco). Transwells were incubated overnight at 37°C in ambient air containing 5% CO_2 before media was replaced with DMEM, high-glucose, HEPES, no-phenol-red cell culture medium (lacking the PEN-STREP antibiotic/antimycotic mixture). Bacterial cells were added to the choriodecidual surface of the gestational membranes at a multiplicity of infection of 1 × 10^6 cells per transwell. Co-cultures were incubated at 37°C in ambient air containing 5% CO_2 for 48 hours at which time membrane tissues were fixed in 10% neutral buffered formalin prior to paraffin

embedding.

Human fetal membrane immunohistochemistry staining: Tissues were cut to 5 μm sections and multiple sections were placed on each slide for analysis. For immunohistochemistry, slides were deparaffinized and heat induced antigen retrieval was performed on the Bond Max automated IHC stainer (Leica Biosystems, Buffalo Grove IL) using their Epitope Retrieval 2 solution for 5-20 minutes. Slides were incubated with a rabbit polyclonal anti-GBS antibody (abcam, ab78846), rabbit polyclonal anti-histone H3 antibody (abcam, ab8580), or a mouse monoclonal anti-CD163 antibody (MRQ-26, Cell Marque, Rocklin CA) for 1 hour. The Bond Polymer Refine detection system (Leica Biosystems) was used for visualization. Slides were the dehydrated, cleared and coverslipped before light microscopy analysis was performed.

Human fetal membrane immunofluorescence staining: For immunofluorescence evaluation of METs within fetal membrane tissue, tissues were fixed and sectioned as above. Sections were briefly incubated with xylene to deparaffinize. Tissues were blocked for greater than 1 hour with 10% bovine serum albumins (Sigma-Aldrich) before staining with 1/100 dilutions of mouse monoclonal anti-H3 antibodies conjugated with Alexa Fluor® 647 (ab205729, abcam), rabbit monoclonal anti-CD163 antibodies conjugated with Alexa Fluor® 488 (ab218293, abcam), and mouse monoclonal anti-MMP-9 antibodies conjugated with Alexa Fluor® 405 (NBP-259699AF405, Novus biological, Littleton CO) overnight at room temperature. Additional tissues staining were conducted as previously described (278). Tissues were deparaffinized and then incubated in R universal Epitope Recovery Buffer (Electron Microscopy Sciences, Hatfield PA) at 50°C for 90 minutes. Samples were then rinsed in deionized water three times followed by washing with TRIS-buffered saline (TBS, pH 7.4). Samples were permeabilized for 5 minutes with 0.5% Triton X100 in TBS at room temperature followed by 3 washes with TBS. Samples were then blocked with TBS with 10% BSA for 30 minutes prior to incubation with 1:50 dilutions of rabbit poly-clonal anti-neutrophil elastase antibodies (481001, MilliporeSigma, Burlington MA) and mouse monoclonal anti-H3 antibodies conjugated with Alexa Fluor® 647 in blocking buffer at room temperature overnight. The following day, samples were washed in TBS followed by repeat blocking with blocking buffer for 30 minutes at room temperature before incubation with 1/00 dilution of Alexa Fluor® 488 conjugated donkey anti-rabbit IgG (Invitrogen) for 4 hours at room temperature. Samples were then washed and incubated with 5 μM Hoechst 33342 for 30 minutes to stain nuclei. After final washes, slides were dried and coverslipped. Tissues were visualized with a Zeiss LSM 710 META Inverted Laser Scanning Confocal Microscope. Images shown are representative of 4 separate experiments using tissues from different placental samples.

Statistical analyses: Statistical analysis of MET quantifications was performed using one-way ANOVA with either Tukey's or Dunnet's post-hoc correction for multiple comparisons and all reported *p* values are adjusted to account for multiple comparisons. MMP activities assays and bacterial killing assay were normalized to untreated or uninfected cells and analyzed with Student's *t*-test or one-way ANOVA. *P* values ≤ 0.05 were considered significant. All data analyzed in this work were derived from at least three biological replicates (representing different placental samples). Statistical analyses were performed using GraphPad Prism 6 for MAC OS X Software (Version 6.0g, GraphPad Software Inc., La Jolla CA).

RESULTS:

Placental macrophages release METs in response to GBS: To understand PM responses to GBS at the host-pathogen interface, isolated PMs were infected *ex vivo* with GBS and cellular interactions examined using field-gun high-resolution scanning electron microscopy (SEM). At one hour following infection, fine, reticular structures were noted extending from macrophages, and these structures were less abundant in uninfected samples (**Figure VII.1A**, lower panels). These structures resembled NETs. Recent reports suggest that macrophages also release fibers composed of DNA and histones, known as METs (159, 274). To determine if these structures were METs, macrophages were evaluated by scanning laser confocal microscopy after staining with the DNA binding dye SYTOX Green, which demonstrated extracellular structures extending from PMs that were not seen when PMs were treated with DNase I (**Figure VII.1A**, top panels). Cells were then evaluated to assess the degree to which these structures contained proteins previously associated with NETs and METs, including histones, myeloperoxidase, and neutrophil elastase (159, 274). Each of these proteins co-localized to extracellular DNA structures extending from the PMs (**Figure VII.1B**). The staining for MET-associated proteins was specific as no fluorescent signal was seen when either a secondary conjugated antibody alone or an isotype control secondary conjugated antibody was used to evaluate these structures (**Figure VII.2**). Together, these data suggest that these structures are METs released by PMs. The extent of MET release was then quantified, and PMs co-cultured with GBS released significantly more METs than uninfected cells and DNase I treatment degraded these extracellular structures (**Figure VII.1C**). Additionally, MET release by PMs occurred in a dose dependent fashion (**Figure VII.3**), and MET release was not GBS strain or bacterial species specific as PMs infected with GBS strain GB00037, a capsular type V strain, *Escherichia coli*, or heat killed bacteria resulted in similar MET release (**Figure VII.4**).

One major immunologic function of extracellular traps is the ability to immobilize and kill microorganisms through the locally high concentration of cellular proteins including histones that have

antimicrobial effects (159, 279). In order to investigate the bactericidal activity of PM METs, PMs were co-cultured with GBS cells alone or in the presence of DNase I. After 1 hour of infection, significantly more bacterial colony forming units (CFU) were recovered from co-cultures treated with DNase I, suggesting that PM METs have bactericidal activity and eliminating METs with DNase treatment impaired bacterial killing (**Figure VII.1D**). To verify that DNase treatment itself did not result in significant PM cell death, thus decreasing bactericidal ability, PMs were incubated with DNase I for one hour prior to washing and stimulating PMs with heat-killed GBS for 24 hours. PM TNF-α release was used as a marker of macrophage viability and function; there was no difference in TNF-α from supernatants of cells treated with DNase compared to untreated cells (**Figure VII.3**). Additionally, live-dead bacterial staining of PMs infected with GBS demonstrated dead GBS cells adjacent to MET fibers (**Figure VII.3C**). Together, these data provide evidence that PMs release METs in response to bacteria and that these structures are capable of killing GBS cells.

Extracellular trap formation, or etosis, occurs by a cell death pathway distinct from pyroptosis and apoptosis (249). To investigate if GBS infection results in different cell death pathways, GBS infected PMs were assayed for LDH release as a marker of cellular death, TUNEL staining as a marker of apoptosis, and IL-1β release to indicate pyroptosis. At one hour of GBS infection, supernatants of PMs co-cultured with GBS demonstrated an increase in macrophage death, determined by LDH release (**Figure VII.5A**). However, GBS infected PMs did not exhibit a significant difference in IL-1β release or TUNEL positive cells compared to uninfected cells treated with vehicle controls at 1 hour (**Figure VII.5B-D**).

PMA-differentiated THP-1 macrophage-like cells release METs after direct bacterial contact: Experiments were conducted to determine if MET responses against GBS were specific to PMs or might represent a broader macrophage response. The immortalized monocyte-like cell line, THP-1 cells, was evaluated after differentiation into macrophage-like cells with phorbol 12-myristate 13-acetate (PMA) for 24 hours. THP-1 macrophage-like cells infected with GBS released significantly more METs than uninfected cells, and DNase I treatment degraded the MET structures (**Figure VII.6**). The THP-1 MET response required contact with bacterial cells, as treatment of the macrophage-like cells with sterile filtered bacterial culture supernatant did not stimulate MET release compared to uninfected cells.

Actin polymerization is required for GBS-induced MET release: Actin polymerization has been shown to be important for MET release (274). A similar role of cytoskeletal changes on GBS-induced MET release in THP-1 macrophage-like cells was examined. Treatment prior to infection with the

actin polymerization inhibitor, cytochalasin D, but not nocodazole, which inhibits microtubule polymerization, inhibited MET release compared to GBS infected, untreated cells (**Figure VII.6**). As noted below (and shown in **Figure VII.7**), cytochalasin D also inhibited MET release by human PMs infected with GBS.

Placental macrophage MET responses require ROS production: Neutrophil release of NETs occurs in a ROS-dependent manner (248). It was hypothesized that MET release from PMs may require production of ROS. Treatment of PMs prior to infection with the NADPH oxidase inhibitor diphenyleneiodonium (DPI) inhibited release of METs, whereas treatment of uninfected macrophages with PMA resulted in similar levels of MET release to GBS infected cells (**Figure VII.7 A&B**). As with the THP-1 macrophage-like cells, treatment of PMs with cytochalasin D prior to infection inhibited MET release. To further define that ROS production was associated with MET release a fluorescent ROS dye was used to evaluate PMs for intracellular ROS production. Treatment with DPI inhibited ROS production, and GBS infection as well as PMA treatment of uninfected PMs resulted in significantly more ROS production than uninfected cells (**Figure VII.7 C&D**). Interestingly, pretreatment with cytochalasin D decreased levels of intracellular ROS production similar to that of DPI, suggesting that pretreatment with the actin cytoskeletal inhibitor may actually be preventing MET release by impeding ROS production. Additionally, ROS production in these experiments mirrored the degree of MET release under similar conditions (**Figure VII.7B**), suggesting that ROS production is necessary for MET release from these macrophages.

Placental macrophage METs contain MMPs: During pregnancy, PMs support gestational tissue remodeling through release of MMPs. Because macrophage release of MMPs has been implicated in the pathogenesis of fetal membrane rupture (280), we hypothesized that these proteases may also be released in METs. Five MMPs that have been implicated in development and pathologic pregnancies were evaluated. Immunofluorescent staining of METs was significant for the co-localization of MMP-1, -7, -8, -9, and -12 with extracellular DNA structures (**Figure VII.8A**). As MMPs are present within METs and GBS infection induced MET release, metalloprotease concentrations within co-culture supernatants were examined to determine if GBS infection would result in an increase in metalloprotease release. MMP-8 and MMP-9 have been investigated as potential biomarkers for intrauterine infection (281-283), and concentrations of both were significantly elevated in supernatants of GBS infected cells compared to uninfected controls (**Figure VII.8 B&C**). Global MMP activity of co-culture supernatants was then assessed to determine if the MMPs released were active by using a MMP activity assay, which uses fluorescence resonance energy transfer peptides

that, when cleaved by MMPs, are fluorescent. Supernatants taken from placental macrophages co-cultured with GBS demonstrated significantly more MMP activity compared to uninfected controls (**Figure VII.8D**). Together these data suggest that PMs express several MMPs, and these MMPs are released during bacterial infection within METs and into the extracellular spaces, where they might contribute to breakdown of gestational tissue extracellular matrix.

MET structures are present in human fetal membrane tissues infected *ex vivo*: To determine if METs were present within gestational tissues in response to infection, fetal membrane tissues from healthy, term, non-laboring caesarian sections were obtained, excised, and organized into transwell structures, creating two chambers separated by the fetal membranes. GBS cells were added to the choriodecidual surface and infection was allowed to progress for 48 hours prior to fixing tissues for immunohistochemistry and immunofluorescence analysis. $CD163^{+}$ cells were found localized to an area of GBS microcolonies within the membranes that demonstrated histone staining extending beyond the nucleus and into the extracellular space, suggesting the release of a MET-like structure (**Figure VII.9A**). Immunofluorescence staining demonstrated $CD163^{+}$ cells associated with extracellular material that stained positive for histones and MMP-9 (**Figure VII.9B**). Additional staining of fetal membrane tissues using neutrophil elastase as was previously described for identification of extracellular traps in tissues (278), identified cells within the choriodecidua with long extensions that stained strongly for neutrophil elastase that co-localized to histone H3 and DNA staining (**Figure VII.10**). Cells releasing MET-like structures could be compared to cells with intact nuclei and neutrophil elastase staining limited to granule structures suggesting that cells releasing MET-like structures had undergone cellular changes consistent with etosis.

DISCUSSION:

In the initial description of NETs in 2004, several potential immune functions were described including the trapping and killing of microorganisms and degradation of bacterial products (159). Release of cellular DNA and proteins within extracellular traps has also been associated with autoimmune pathology in systemic lupus erythematosus and anti-neutrophil cytoplasmic autoantibodies (ANCA)-associated vasculitis, as well as and in diseases of aseptic inflammation (219, 222-225). Other leukocytes including mast cells, eosinophils, basophils and macrophages have now been shown to release extracellular trap structures (214, 215, 217, 218, 274).

In this manuscript, PMs are added to a growing list of monocytes and tissue differentiated macrophages capable of releasing METs, which includes human alveolar macrophages, glomerular macrophages, peripheral blood monocytes, and macrophages from other mammalian and non-

mammalian species (274). These data demonstrate that human PMs and PMA-differentiated THP-1 macrophage-like cells release METs in response to bacterial infection and after treatment with the protein kinase C agonist, PMA. The present data correlate with previous reports that neutrophils and murine macrophages release traps in response to GBS infection and that METs are capable of killing GBS cells (57, 245).

These data also demonstrate that PM METs contain many proteins previously identified in NETs, including histones, neutrophil elastase, and myeloperoxidase (159). These results mirror other MET investigations demonstrating that diverse macrophages produce and release proteins including neutrophil elastase within MET structures. For example, human glomerular macrophages releasing METs containing myeloperoxidase has been demonstrated in cases of ANCA-associated glomerulonephritis and human alveolar macrophages have been shown to release METs containing histones and MMP-9 (233, 284). Human blood monocytes release METs containing H3 histones, myeloperoxidase, lactoferrin, and neutrophil elastase in response to *Candida albicans* cells, and similar MET contents have been demonstrated in THP-1 macrophage-like cells infected with *Mycobacterium massiliense* (228, 232).

Similar to neutrophil etosis, these data suggest that ROS generation is necessary for PM MET release as this response was inhibited by treatment with the NADPH oxidase inhibitor, DPI. These results mirror reports that inhibition of ROS production via chemical inhibitors resulted in diminished MET release in bovine, caprine, murine, and human macrophages (229-231, 235, 253). In neutrophils, ROS act to break down intracellular membranes and activates neutrophil elastase, which translocates to the nucleus where it degrades histones and promotes chromatin decondensation (249). Myeloperoxidase is thought to contribute chromatin decondensation by a enzymatic-independent mechanism (249). It is unclear at this time if neutrophil elastase and myeloperoxidase perform similar roles in macrophages.

Our data indicate an increase in LDH release during infection, which is consistent with reports that MET release results in cell death (237). Etosis has been noted to be distinct from other cellular death pathways including pyroptosis and apoptosis. At one hour of infection when MET responses were identified, there was no significant difference in TUNEL staining or IL-1β release suggesting that PM METs occur by a distinct pathway. This is notable as previous reports have shown that the GBS toxin β-hemolysin is capable of inducing pyroptosis of macrophages, though in this study infection was allowed to progress for 4 hours, longer than that required for the PM MET response (63). Previous studies have also demonstrated that GBS is capable to inducing macrophage apoptosis, but again this occurred over longer periods of infection than the one hour that was capable of inducing MET responses (285).

Pretreatment of THP-1 macrophage-like cells and PMs with the actin cytoskeletal inhibitor, cytochalasin D, inhibited MET release, but not the microtubule inhibitor, nocodazole. Conflicting reports exist regarding the role of actin polymerization in etosis. Studies evaluating bovine macrophages and THP-1 cells demonstrated a decrease in MET release after cytochalasin treatment, but similar treatment of murine J744A.1 macrophage-like cells, RAW macrophage-like cells, and bovine blood monocytes did not have a significant effect on MET release (229, 231, 232, 234). This collection of conflicting reports mirrors the NET literature. In the original NET description, cytochalasin D prevented cell phagocytosis but not NET release (159). Others have documented NET inhibition with nocodazole or cytochalasin D in response to LPS or enrofloxacin (257, 258). Because of the differential responses, some authors have postulated that phagocytosis may be an important first step towards cell stimulation and ROS generation, and cytoskeletal inhibition may block the initial steps toward MET release. Another possibility is that the pretreatment with cytochalasin D may interrupt trafficking of the NADPH oxidase complex, thus impairing ROS production. NADPH oxidase is a complex of six components, and the cytosolic proteins $p40^{phox}$ and $p47^{phox}$ are known to interact with F-actin; treatment with cytochalasins have been shown to interrupt NADPH complex formation and lead to impaired ROS formation (286, 287). Timing of the cytochalasin treatment is important, as treatment of cells after pre-stimulation with molecules such as LPS, which stimulates NADPH oxidase assembly, may actually increase generation of ROS in these cells (288). In our study, macrophages were pretreated with cytochalasin D and were not stimulated prior to infection. It remains unclear if the conflicting literature with regards to the impact of cytoskeletal inhibition on extracellular traps may be explained by the timing of cytoskeletal inhibition and subsequent effects on ROS production.

PMs were found to produce and release several MMPs within MET structures. During chorioamnionitis, inflammatory mediators lead to the production and release of several metalloproteinases including MMP-1, MMP-7, MMP-8, and MMP-9 (289, 290). MMP-9 is considered to be the major MMP responsible for collagenase activity within the membranes, but many other MMPs are thought to contribute to the processes of membrane weakening (289, 291). This study reinforces and expands previous reports that identified placental leukocytes as being able to secrete MMPs including MMP-1, -7, and -9 (292). Several MMPs have been implicated in preterm birth and pathologic pregnancies. MMP-1 and MMP-9 were found to be elevated in placental tissues of women with preterm births compared to women delivering at full term (293). MMP-1 and neutrophil elastase have been shown to stimulate uterine contractions (294). Interestingly, proteomic comparisons of amniotic fluid from women with premature preterm rupture of membranes demonstrated increases in histones (H3, H4, H2B), myeloperoxidase, neutrophil elastase, and MMP-9 in women with histologic chorioamnionitis and proven intrauterine infection, which likely represents the influx of inflammatory

cells into these tissues and potentially release of extracellular traps (295). MMP-12, or macrophage metalloelastase, is a key mediator of the breakdown of elastase and has been shown to be important for spiral artery remodeling during parturition, but to date there are no studies demonstrating changes in MMP-12 release during cases of pathologic pregnancies (296). MMP-12 is better studied in conditions of lung pathology including emphysema, and alveolar macrophages are known to release MMP-12 in METs during infection, suggesting that protease release from leukocytes may contribute to this disease process (253). Analogous to a controlled burn, we speculate that tethering MMPs to MET structures allows the host to control the release of these potent enzymes, thereby limiting their capacity to broadly weaken membrane structure in response to infection.

MET release appears to occur within fetal membrane tissue as demonstrated by our immunohistochemistry and immunofluorescence data. This report adds to the growing relevance of these structures within cases of disease pathology. NETs have previously been identified in placenta tissues from women with pregnancies complicated by systemic lupus erythematosus and preeclampsia (221, 297). NETs were also found in fetal membrane samples of women with spontaneous preterm labor due to acute chorioamnionitis (298). Interestingly, in this report, antibody staining with histone H3 and neutrophil elastase was used to denote NET structures, but given our data, this staining pattern would not have differentiated METs from NETs. Additionally, our group and others have demonstrated that in animal models of vaginal colonization and perinatal infection with GBS, neutrophils traffic to GBS-infected gestational tissues and release NETs containing antimicrobial peptides including lactoferrin as a means to control bacterial growth and invasion (64, 120, 158).

In conclusion, we demonstrate that placental macrophages as well as PMA-differentiated THP-1 cells respond to bacterial infection by releasing METs. These MET structures contain proteins similar to NETs, including histones, myeloperoxidase, and neutrophil elastase. MET release from these macrophages can be stimulated in the absence of bacterial cells with PMA and is inhibited by pathways that impair ROS production. Placental macrophage METs contain several MMPs that have been implicated in pathologic pregnancies including premature rupture of membranes. MET structures were identified in human fetal membrane tissue infected *ex vivo*. Together these results suggest that placental macrophages, which are thought to help maintain maternal fetal tolerance and aid in extracellular matrix remodeling, are capable of responding to GBS infection in a way that may trap and kill GBS cells but may also release important mediators of fetal membrane extracellular matrix digestion that could potentially contribute to infection related pathologies including preterm rupture of membrane and preterm birth.

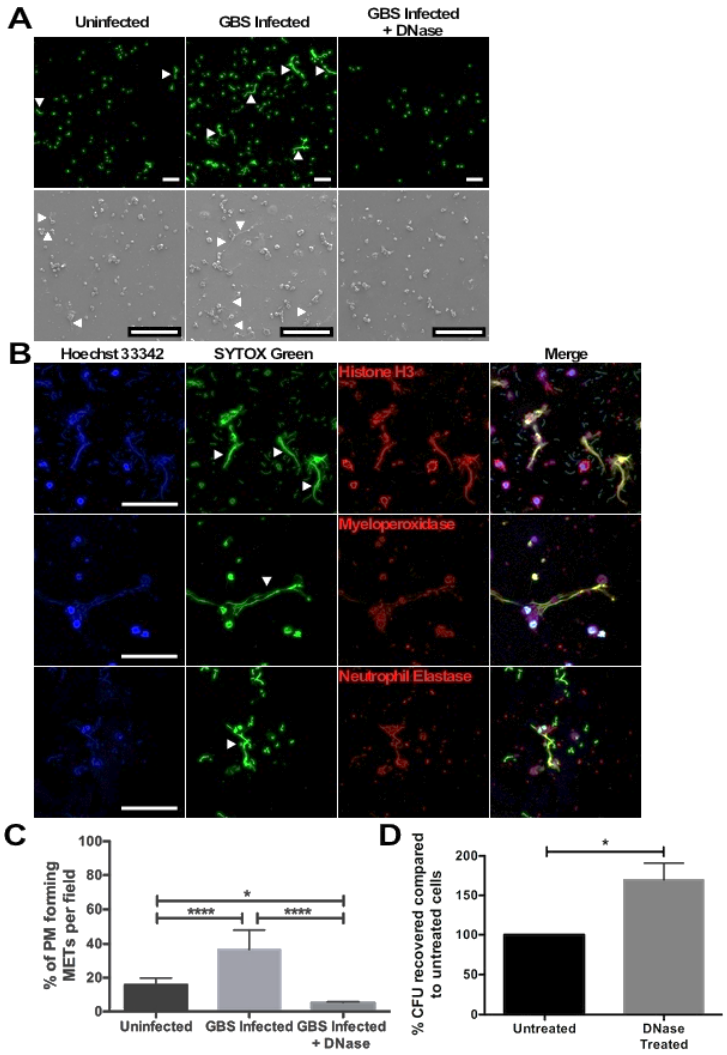

Figure VII.1: Placental macrophages infected *ex vivo* with GBS release extracellular traps capable of killing GBS cells. A: Placental macrophages were infected for 1 hour with GBS cells at a MOI of 20:1. Scanning electron micrographs (bottom row) demonstrate extracellular structures released from macrophages (white arrows), which are not seen after DNase I treatment. PMs were also stained with Sytox Green, a double stranded DNA dye, and evaluated by scanning laser confocal microscopy, which demonstrates extracellular structures composed of DNA (white arrows). Measurement bars represent 100 μm. B: Placental macrophage extracellular traps were stained with Hoechst 33342 (blue), a condensed chromatin/nuclear stain, SYTOX Green (green), and specific antibodies for either histone H3, myeloperoxidase or neutrophil elastase as listed (red). Histone, myeloperoxidase and neutrophil elastase staining co-localizes to extracellular DNA staining suggesting that MET structures contain these proteins. Measurement bars represent 100 μm. C: PMs releasing METs were quantified by counting MET producing cells seen in SEM images and expressed as the number of macrophages releasing METs per field. GBS infected PMs release significantly more METs than uninfected cells, and DNase I treatment degraded these structures. Data represent samples from 6-8 different placental samples, one-way ANOVA, $F = 32.7$, $P < 0.0001$, with post hoc Tukey's multiple comparison test. D: Placental macrophage METs kill GBS cells. PMs were infected for 1 hour at MOI 20:1 in the presence of DNase I to degrade METs or without (Untreated). Untreated wells were treated with DNase I for the last 10 minutes of infection to break up DNA complexes prior to serial dilution and plating. DNase I treatment significantly impairs bactericidal activity. Data represent the percent recovered colony forming units (CFU), normalized to untreated cells from 7 separate experiments from different placenta samples, Student's *t* test, $t = 3.224$, df = 6, $P = 0.0180$. **** represents $P \leq 0.0001$, * represents $P \leq 0.05$.

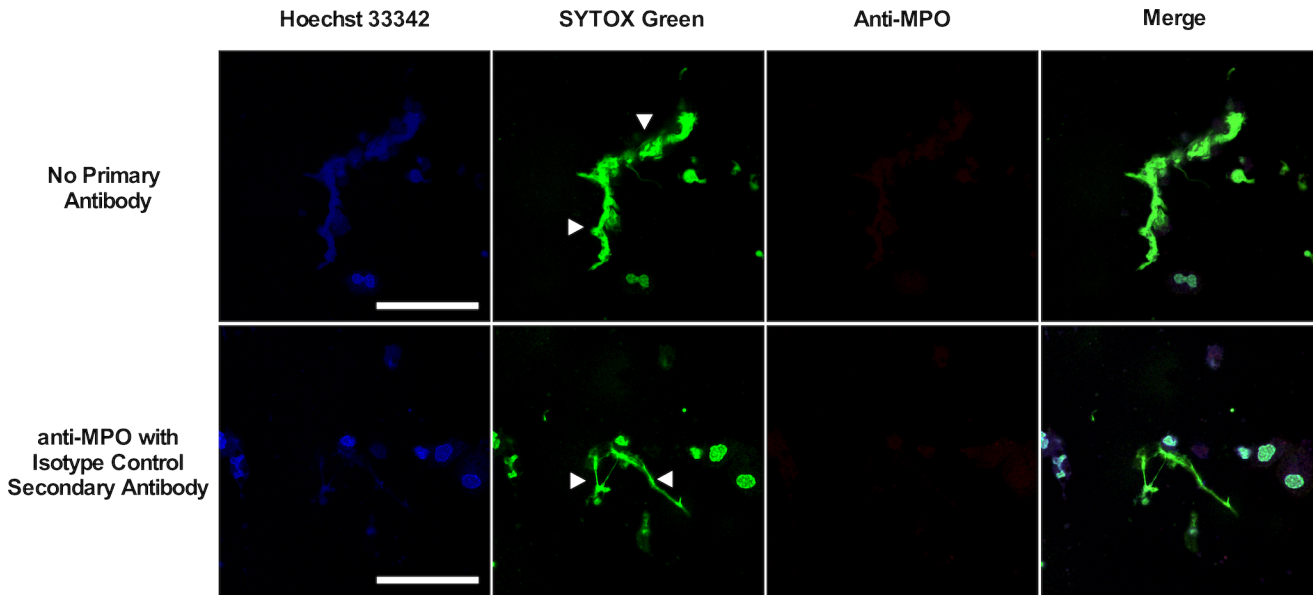

Figure VII.2: Staining controls for MET content evaluation. Placental macrophages were treated as in Figure VI.1B but were either stained without a primary antibody (top row) or with an isotype control fluorophore-conjugated secondary antibody. Negligible myeloperoxidase (MPO) staining was identified in these samples compared to Figure VI.1B (middle row) confirming the specificity of the staining protocol. Measurement bars represent 100 μm.

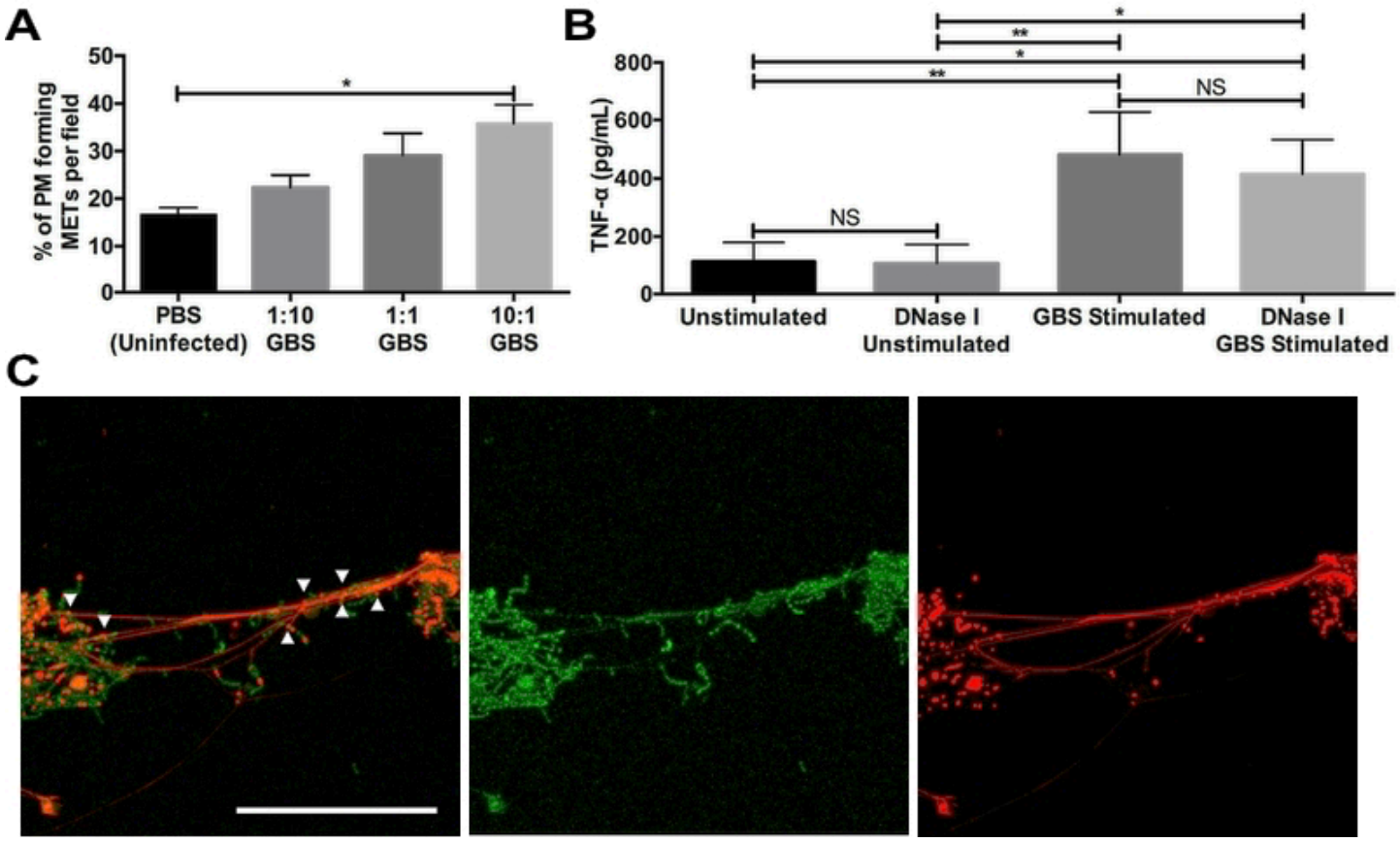

Figure VII.3: GBS infection of PMs results in release of METs capable of killing GBS. A: PMs release METs in a dose dependent response. PMs were infected for one hour at increasing MOI as indicated or treated with vehicle control (PBS) (one-way ANOVA, F = 12.3, *P* = 0.0076 with post hoc Tukey's multiple comparison test). B: DNase I treatment does not alter PM viability. PMs were either treated with DNase I or left untreated for one hour before cells were washed and stimulated with heat-killed GBS cells (MOI 150:1) or left unstimulated for 24 hours. Supernatants were assessed for TNF-α release by ELISA as a measure of viability. Treatment of PMs with DNase I did not have a significant effect on TNF-α release (one-way ANOVA, F = 7.75, *P* = 0.0016 with post hoc Tukey's multiple comparison test). C: PM METs are capable of killing GBS cells. PM co-cultures were stained with live-dead bacterial staining including Syto9 and propidium iodide. Both dyes stain DNA but propidium iodide (red) is excluded from live cells. Dead GBS cells (red) are shown in close proximity to MET fibers (white arrows). Measurement bar represents 50 μm.

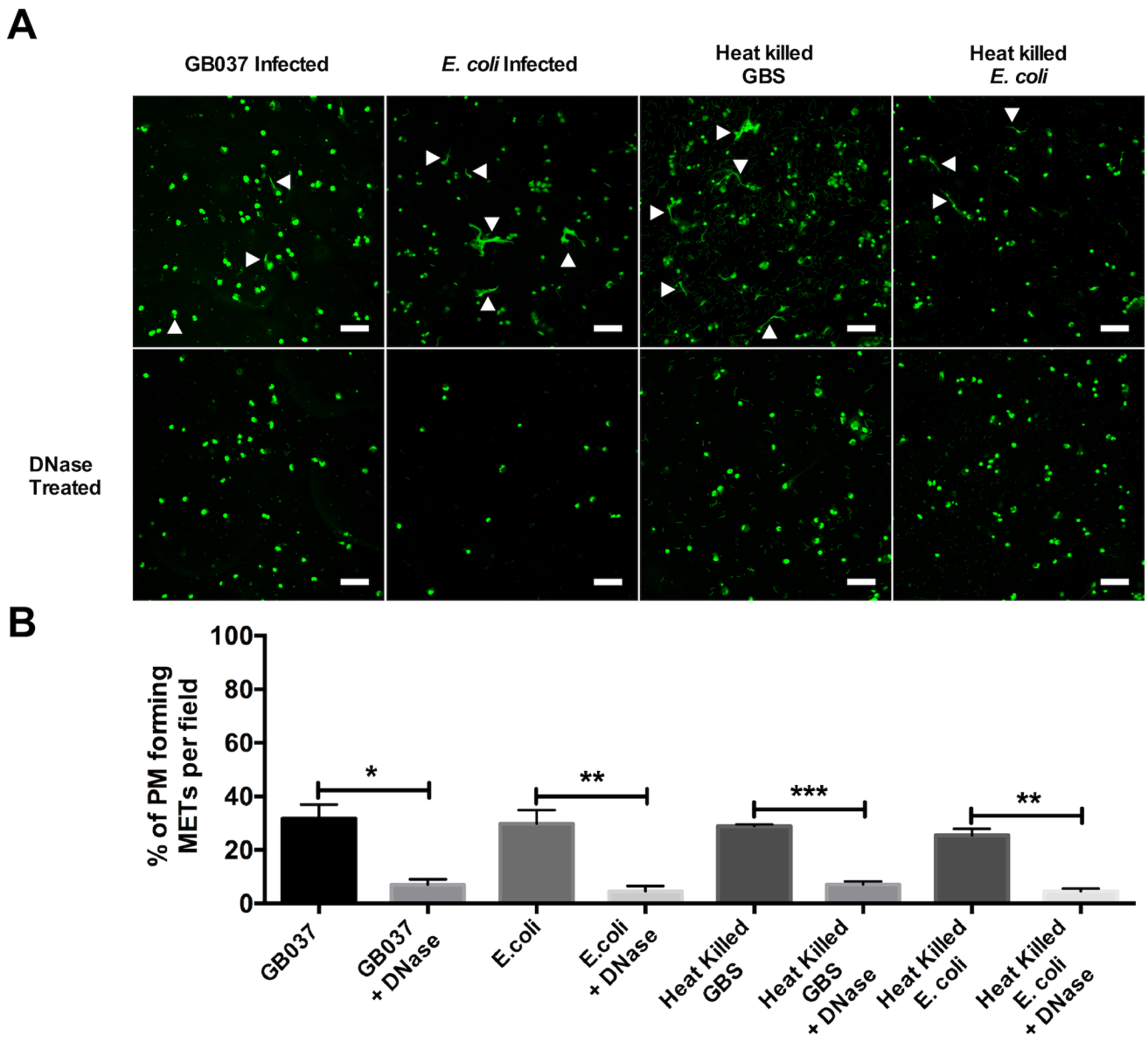

Figure VII.4: Placental macrophages release extracellular traps in response to different GBS strains as well as *E. coli* cells. A: Placental macrophages were co-cultured with live GBS strain GB00037, *E. coli* cells, or heat killed GBS or *E. coli* cells at a MOI of 20:1 for 1 hour. Cells were pretreated with DNase I as indicated. Cells were then fixed and subsequently stained with SYTOX Green and evaluated for MET release by confocal microscopy. Measurement bars represent 100 µm. B: Placental macrophages releasing METs were quantified by counting MET producing cells from SEM images (not shown) and expressed as the number of macrophages releasing METs per field. At 1 hour of infection live GB00037, heat killed GB00590 (GBS), and live or dead *E. coli* stimulated MET release as DNase I treatment significantly reduced the number of extracellular structures (unpaired *t*-test of similar treated groups of at least 3 separate experiments from separate placental samples). *** represents $P \leq 0.001$, ** represents $P \leq 0.01$, * represents $P \leq 0.05$.

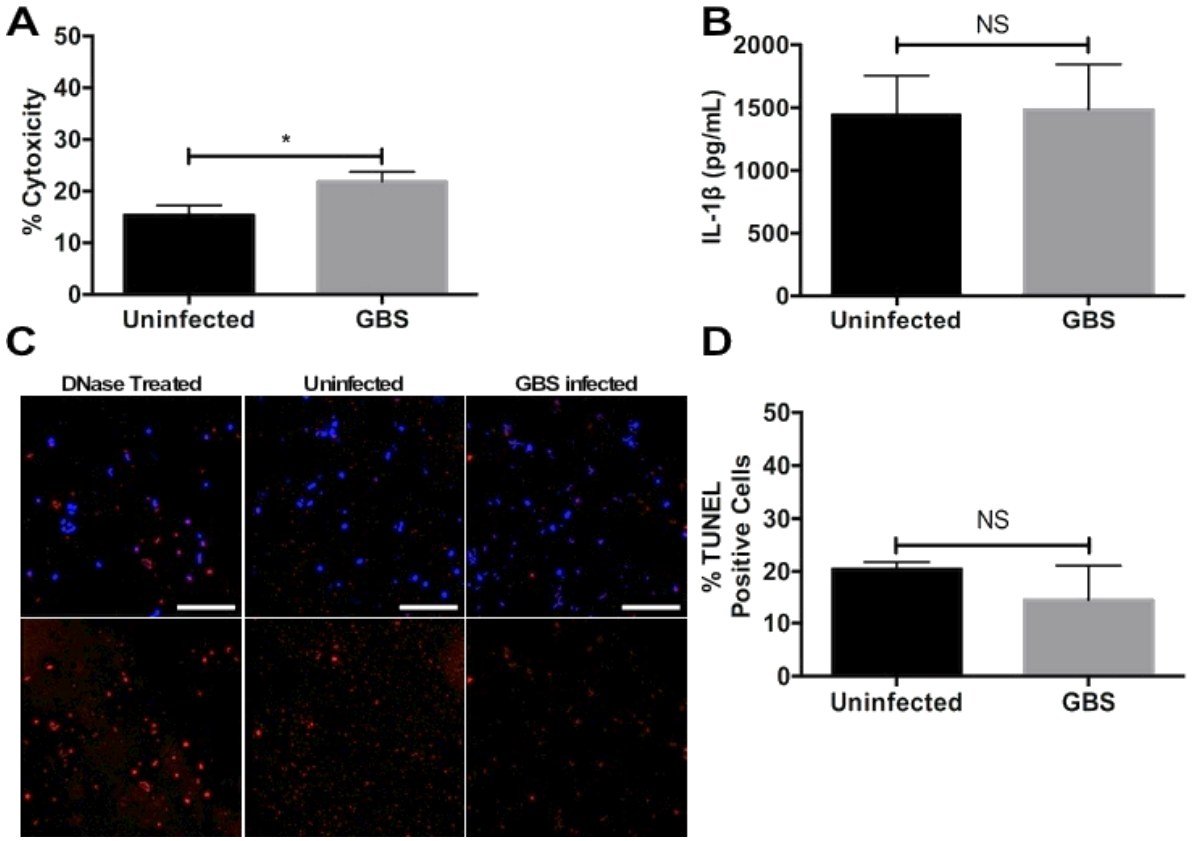

Figure VII.5: GBS infection results in PM cell death but not pyroptosis or apoptosis at 1 hour of infection. PMs were isolated and co-cultured with GBS as in Figure VI.1. A: Following 1 hour of infection, co-culture supernatants were assayed for LDH release and percent cytotoxicity was calculated. GBS infection results in a significant increase in cell death (two-tailed, paired Student's *t* test, $t = 4.13$, df = 4, $P = 0.0145$). B: GBS infection does not result in significant PM pyroptosis at 1 hour. Following infection as above, co-culture supernatants were assessed for IL-1β release by ELISA. GBS infection does not result in significant IL-1β release (two-tailed Student's *t* test, $t = 0.08945$, df = 11, $P = 0.9303$). C,D: Following infection as above, PMs underwent TUNEL staining to evaluate cells for apoptotic changes. C: Representative confocal images demonstrate nuclear staining (blue) and TUNEL positive cells (red, bottom row). Permeabilized, DNase I treated cells are shown as a positive control. D: Quantification of TUNEL positive cells. One hour of GBS infection does not result in an increase in TUNEL positive PMs (two-tailed, paired Student's *t* test, $t = 1.056$, df = 2, $P = 0.4017$).

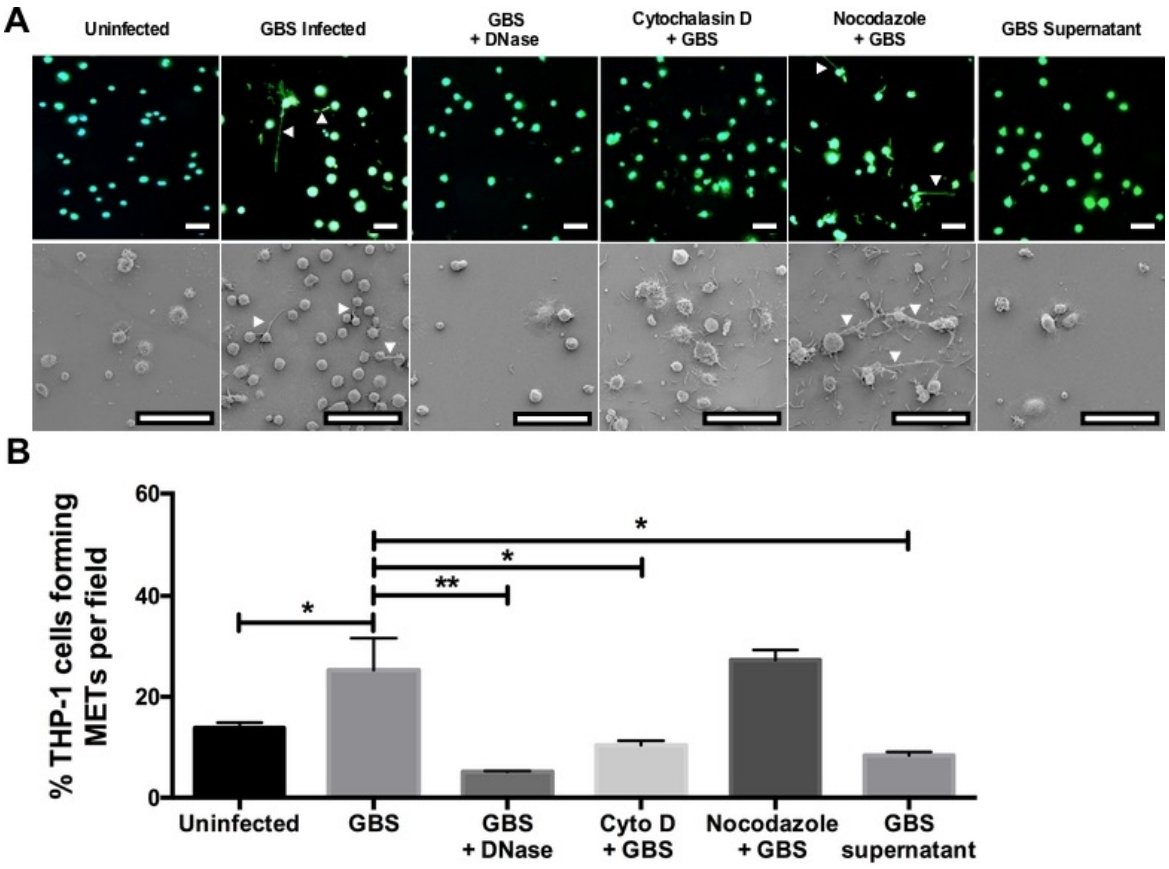

Figure VII.6: PMA activated THP-1 macrophage-like cells release METs in response to GBS. S5A: THP-1 cells were incubated with 100 nM PMA for 24 hours prior to infection to induce differentiation to macrophage-like cells. Cells were infected with GBS at a MOI of 20:1 for 1 hour. As indicated, cells were pre-incubated with DNase I, cytochalasin D, nocodazole, or exposed to 10% volume of sterile filtered bacterial supernatant from GBS cultures grown overnight to steady state. After infection, cells were fixed and evaluated by confocal microscopy after staining with SYTOX Green (top) or by SEM (bottom). White arrows denote METs. Measurement bars represent 100 μm. S5B: Macrophages releasing METs were quantified by counting MET producing cells seen in SEM images and expressed as the number of macrophages releasing METs per field. Data represent mean percent of cells releasing METs per field of 3 separate experiments, one-way ANOVA, $F = 8.08$, $P = 0.028$ with Dunnett's multiple comparison test with samples compared to GBS infected. * represents $P < 0.05$, ** represents $P < 0.01$.

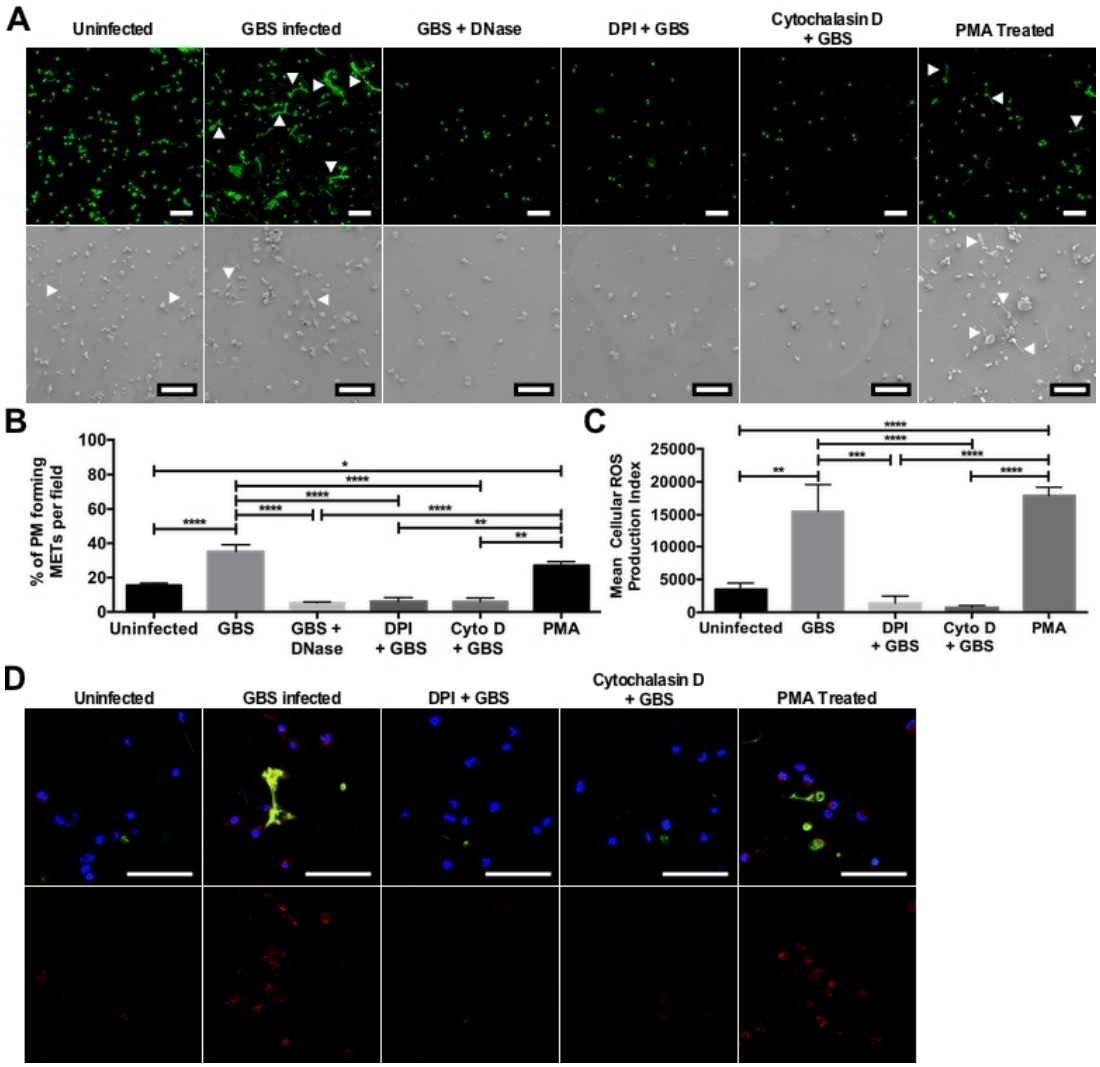

Figure VII.7: MET release from placental macrophages requires ROS generation. Placental macrophages were incubated with DNase I, DPI to inhibit ROS generation, or cytochalasin D to prevent actin polymerization and then infected with GBS at a MOI of 20:1 for 1 hour. Uninfected cells were also stimulated with 500 nM PMA to stimulate protein kinase C activation. A: Cells were then imaged to identify MET release by confocal microscopy after staining with SYTOX green (top row) or via SEM (bottom row). Measurement bars represent 100 μm. B: MET release was then quantified as in Figure 1. Treatment with DPI and cytochalasin D significantly inhibited MET release, whereas MET release from PMA stimulated uninfected cells was not different from GBS infected cells. Data represent mean ± SE percent of cells releasing METs per field of 3-9 separate experiments, one-way ANOVA, $F = 21.1$, $P < 0.0001$ with Tukey's multiple comparison test. C, D: PM cell infections were repeated with staining for intracellular ROS production using CellROX deep red reagent. This reagent becomes fluorescent when oxidized by ROS. Cells were co-cultured with GBS cells as above and stained with CellROX deep red, SYTOX green, and Hoechst (D top row). Measurement bars represent 100 μm. ROS production was quantified by measuring the total red fluorescence per image (D, bottom row) and the cellular ROS production index was calculated (C). Data are shown from a representative experiment of 3 independent experiments and are expressed as the mean cellular ROS production index ± SE of 10 images from a single placental sample. GBS infected and PMA stimulated uninfected cells generated significantly higher amounts of ROS than uninfected cells or those treated with DPI or cytochalasin D (one-way ANOVA, $F = 16.5$, $P < 0.0001$ with post hoc Tukey's multiple comparison test). **** represents $P \leq 0.0001$, *** represents $P \leq 0.001$, ** represents $P \leq 0.01$, * represents $P \leq 0.05$.

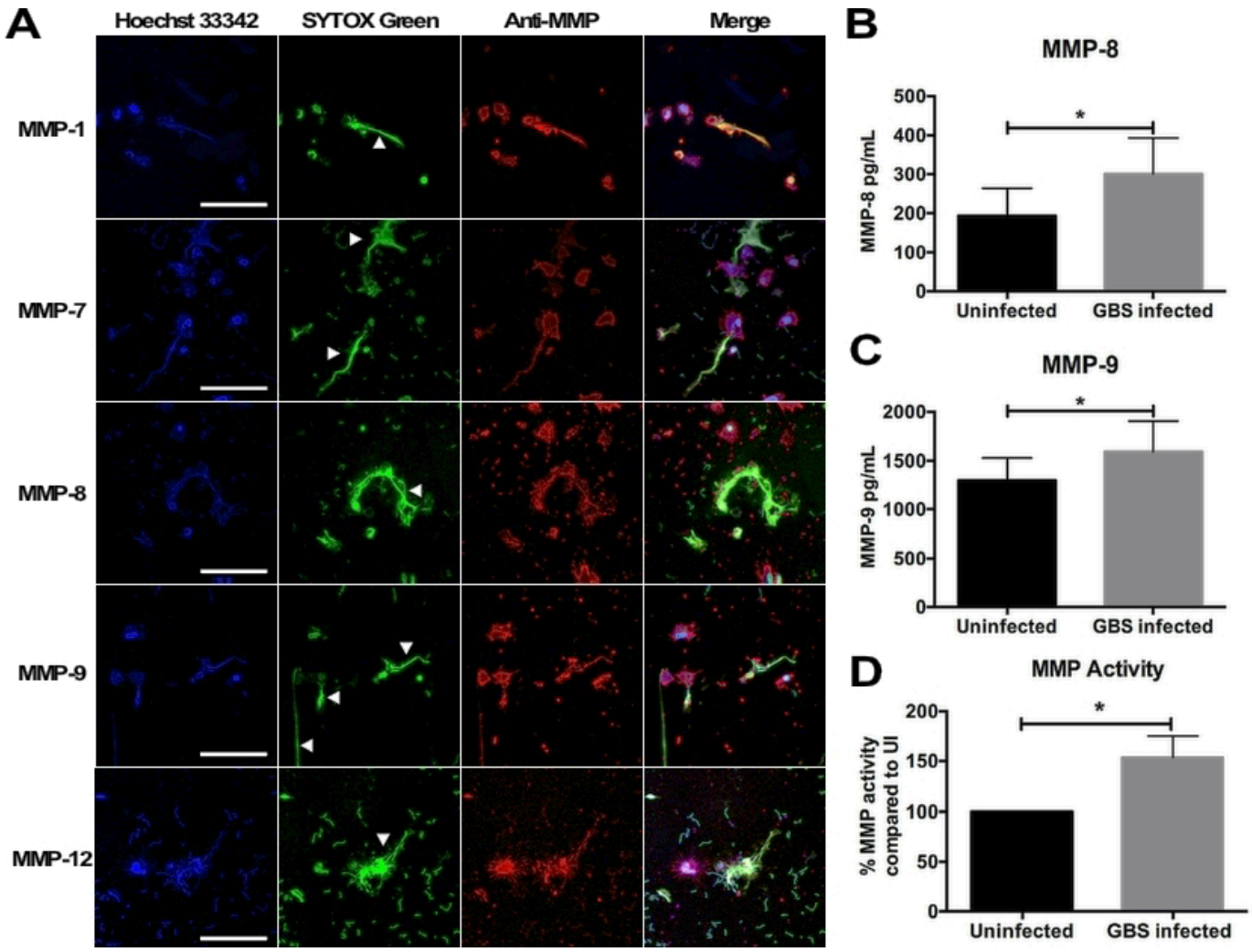

Figure VII.8: GBS infection results in release of matrix metalloproteinases (MMPs) from placental macrophages. A: PM METs contain MMP-1,- 7, -8, -9, and -12. PMs were infected as above and then fixed and stained with anti-MMP antibodies and an Alexa Fluor-conjugated secondary antibody (red), Hoechst 33342, and SYTOX green. METs (white arrows) stained strongly for MMPs. Measurement bars represent 100 μm. B, C: Supernatant from PM-GBS co-cultures were collected and evaluated for MMP-8 (B) and MMP-9 (C) concentrations by ELISA. GBS infection results in a significant increase in MMP-8 (Student's *t* test, $t = 3.599$, df = 7, $P = 0.0087$) and MMP-9 (Student's *t* test, $t = 3.160$, df = 10, $P = 0.0102$) release compared to uninfected cells. D: PMs release active MMPs in response to GBS. Supernatant from PM-GBS co-culture was evaluated for MMP activity using a MMP Activity Assay to assess global MMP activity within co-culture supernatants. Supernatant from GBS infected cells had 53% more MMP activity compared to uninfected PMs (Student's *t* test, $t = 2.439$, df = 11, $P = 0.0329$).

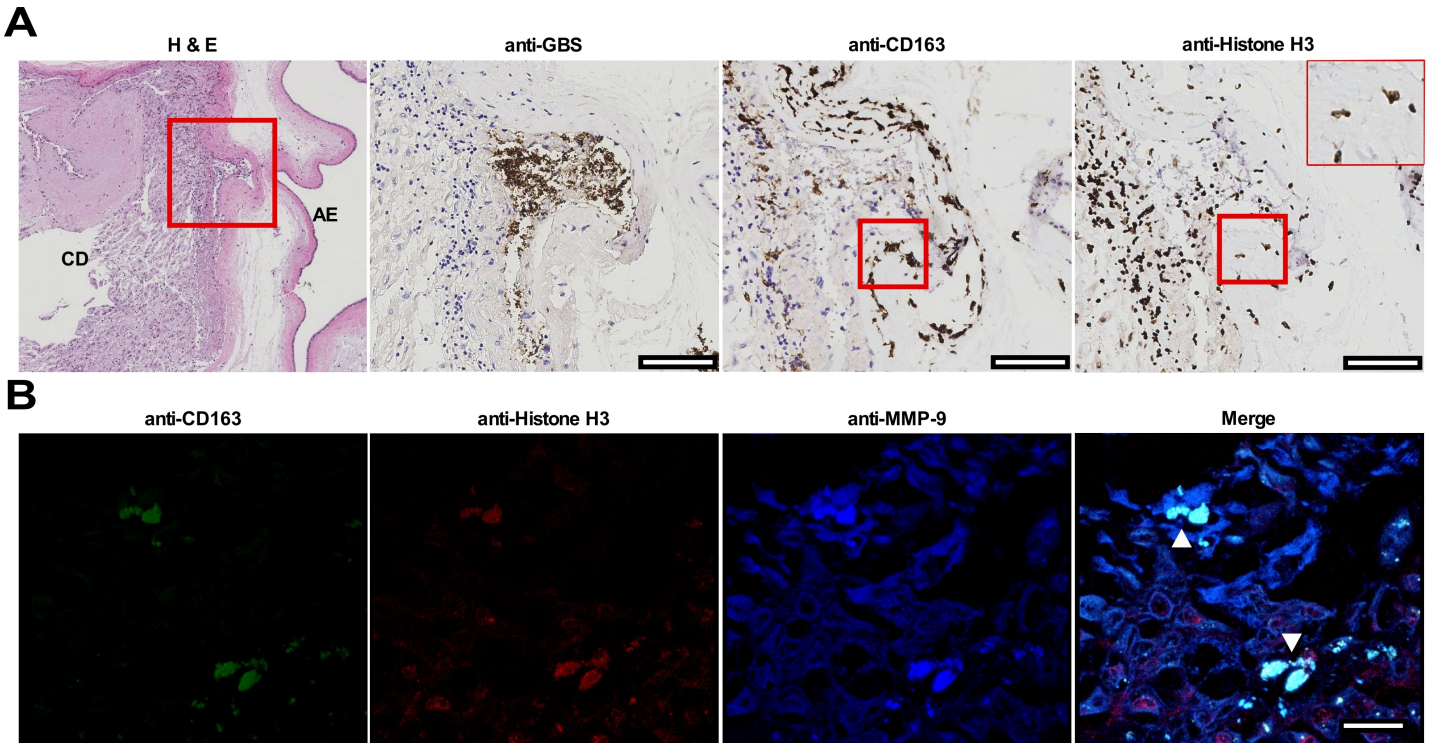

Figure VII.9: Identification of MET-like structures within human fetal membrane tissues infected with GBS *ex vivo*. Fetal membrane tissues were excised from healthy, term placental tissues from women undergoing routine cesarean section. Fetal membrane tissues were then infected with GBS on the choriodecidual surface for 48 hours prior to fixation and immunohistochemistry (A) or confocal microscopy (B). A: Fetal membrane tissues were stained with hematoxylin and eosin (far left) and representative images are shown at 4X magnification. Area within the red box is shown in sections stained with anti-GBS, anti-CD163, or anti-histone H3 antibodies and visualized by immunohistochemistry. GBS cells are able to invade from the choriodecidual surface (CD) toward the amnion epithelium (AE). Macrophages are shown in the area of GBS infection and macrophages with extracellular histone staining (far right, 40X insert) are demonstrated in an area that is also staining with the macrophage marker CD163 (red boxes). Measurement bars represent 100 μm. B: Fixed and paraffin embedded fetal membranes were stained with conjugated primary antibodies against CD163, histone H3, and MMP-9. $CD163^{+}$ cells within the membrane tissue are seen extruding contents that stain positive for histones and MMP-9 consistent with METs (white arrows). Measurement bar represents 20 μm.

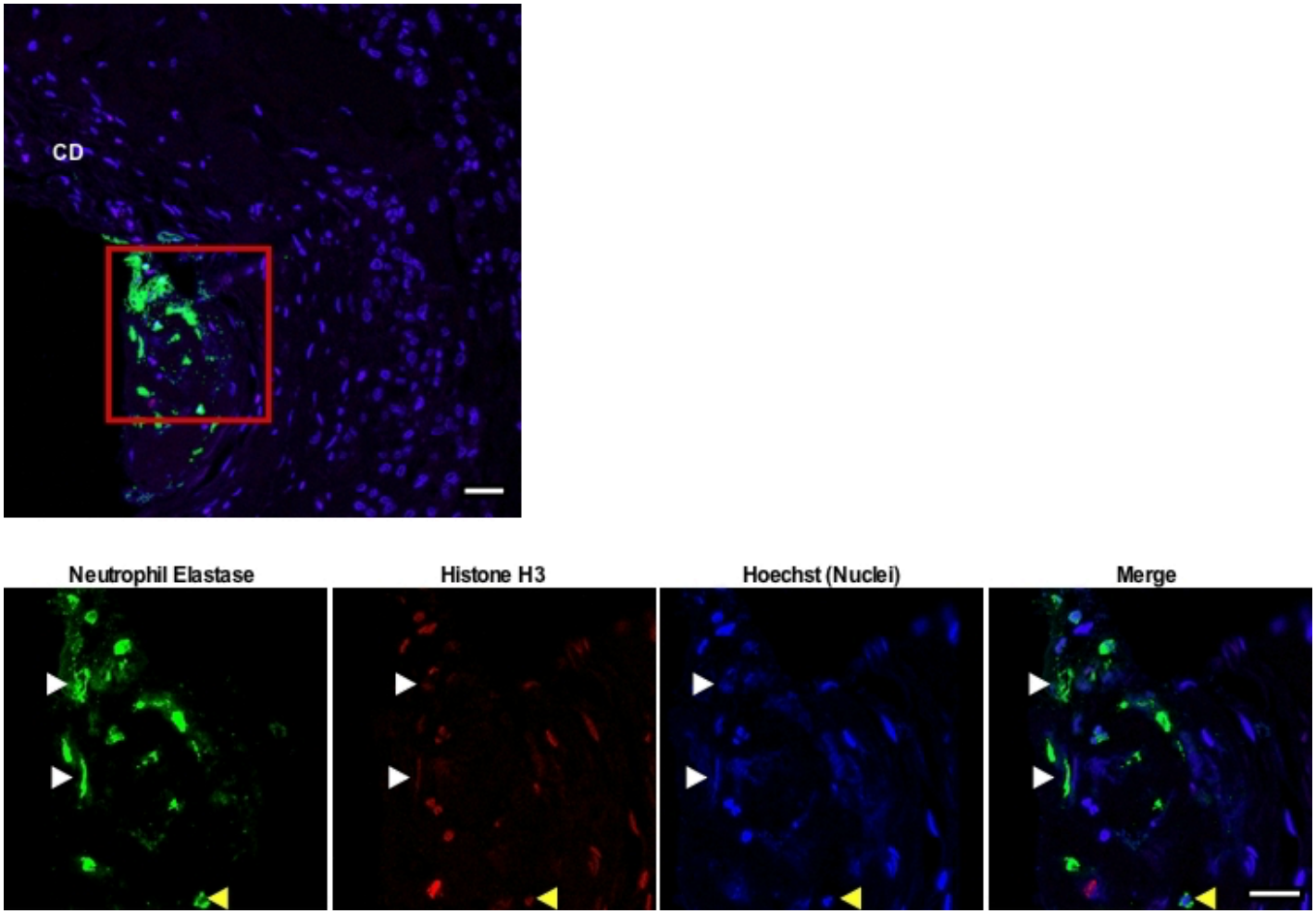

Figure VII.10: MET-like structures containing neutrophil elastase are seen in human fetal membrane tissues infected *ex vivo* with GBS. Human fetal membrane tissues were isolated and infected as in Figure 4 and then stained for neutrophil elastase (green), histones (red), or DNA/chromatin (blue). Neutrophil elastase positive cells were identified in the choriodecidua (CD) (top panel). The area in the red box was then evaluated at higher magnification and elongated structures of neutrophil elastase that co-localized with staining for histones and DNA consistent with METs were identified (white arrows). This staining pattern contrasts with staining of intact cells where neutrophil elastase staining was isolated to granule structures that did not localize to histone or DNA staining (yellow arrow). Measurement bars represent 20 μm.

CHAPTER VIII

Conclusion of these studies and future directions

CONCLUSION OF THESE STUDIES:

In these studies, I have defined that perinatal bacterial pathogens including *S. aureus*, *E.coli*, and *S. agalactiae* (GBS) are capable of infecting human fetal membrane tissues and forming biofilms on their surface (Chapters II-IV). GBS demonstrates the ability to invade membrane tissues, and bacterial infection of the fetal membranes results in proinflammatory cytokine release including IL-6 and IL-1β, which are important mediators of the chorioamnionitis cascade of proinflammatory events that result in adverse pregnancy outcomes such as preterm birth (8). GBS biofilms can be modified be environmental signals including glucose and zinc availability, which are important environmental nutrients as GBS moves from the gastrointestinal tract to the vaginal mucosa. Raman spectroscopy, an emerging microbiologic diagnostic technology, identified unique spectral features of these pathogens, that when combined with machine learning algorithms, allowed for identification of infected fetal membranes tissues compared to uninfected controls and identification of the bacterial cause of infection, suggesting that this technology could be used in the future to improve the diagnosis of chorioamnionitis (Chapter IV). GBS infection of human and mouse gestational tissues stimulates trafficking of macrophages and neutrophils to the site of infection (Chapters III&V) similar to histologic specimens from cases of human chorioamnionitis (16). These data provide evidence that our *ex vivo* and *in vivo* models can provide insight the interactions that occur during perinatal bacterial infections at the host-pathogen interface. Additionally, these data with respect of biofilm modulators may provide new avenues to modify bacterial responses and alter the continuum of perinatal infections at the stage of vaginal colonization.

I also provide a comprehensive review regarding macrophage extracellular traps (METs), extracellular structures composed of a DNA backbone and studded with proteases that are released by monocytes and tissue differentiated macrophages in response to diverse pathogens including bacteria, fungi, and parasites. I reviewed current knowledge of this innate immune response including identification of METs, factors that stimulate and inhibit this cellular response, and clinical significance of these structures (Chapter VI). Upon closer investigation into interactions between GBS and placenta resident, fetally-derived macrophages, I found that GBS infection resulted in the release of METs that are capable to ‘trapping’ and killing GBS (Chapter VII). GBS infection induced MET release by stimulating the production of reactive oxygen species. The process of MET release, or METosis, results in macrophage cell death by a mechanism independent of pyroptosis and apoptosis.

In addition to MET release, GBS infection of placental macrophages resulted in release of several matrix metalloproteinases implicated in premature rupture of membranes, and these active MMPs were found in bacterial supernatants and within MET structures. MET-like structures were found within human fetal membrane tissues infected with GBS *ex vivo*, suggesting that MET release occurs during chorioamnionitis. These data provide a new role and response of placental macrophages during perinatal infections. These responses may help protect the developing fetus by trapping and killing microorganisms but may also result in membrane degradation via the release of digestive proteases.

FUTURE DIRECTIONS:

More investigation into the basic pathogenesis of GBS perinatal infections is needed. Data regarding how GBS maintains colonization, possibly through biofilm production, and subsequently ascends to cause chorioamnionitis is still incomplete. These data demonstrate that environmental cues such as zinc and glucose availability change GBS behavior and could be harnessed to halt ascending infection at the stage of colonization, but *in vivo* studies are needed to more clearly evaluate the impact of these environmental signals.

I have shown that GBS-macrophage interactions and GBS interactions with fetal membrane tissues lead to the release of factors including cytokines and metalloproteases that are known to contribute to the chorioamnionitis cascade. Investigations of woman with perinatal infection demonstrate the potential of biomarkers like IL-6 and MMP-8 for earlier diagnosis of intrauterine infections (281, 299), but there are not yet therapies that can stall the escalating immune responses that result in infection-related adverse pregnancy outcomes including preterm birth and fetal inflammatory response syndrome. A more thorough understanding of the molecular mechanisms of GBS pathogenesis may open new opportunities for therapeutics aimed at supporting fetal tolerance while perinatal infection could be treated with antibiotics. Emerging technologies including instrumented fetal membrane on a chip platforms (300) will provide opportunities to investigate the contributions of other cells types and cell-cell interactions within membrane tissues that shape the host response to perinatal infection. These platforms will also provide a means to test novel therapies that could modify those responses that may contribute to adverse pregnancy outcomes.

This work has broadened our understanding of how macrophages within gestational tissues function during perinatal infection. Despite these advances, more work is needed to understand the consequences of macrophage responses *in vivo*. Ongoing investigation in this area includes depleting macrophages during pregnancy in mouse models of ascending bacterial infection. These studies have the potential to answer questions regarding the necessity of macrophages for

maintenance of normal pregnancy as well as further defining the role of macrophages in defense of the gravid uterus from bacterial pathogens. Additionally, macrophage extracellular trap release has recently become an area of active investigation, and reports have shown that METs contribute to clinical syndromes such as myeloperoxidase (MPO)-ANCA-associated glomerulonephritis (233). Our understanding of the impact of METs within fetal membrane and placenta tissues is still incomplete. Further investigation into the cellular events leading to MET release and the consequences of MET structures within tissues will provide opportunities to modulate macrophage responses that may be able to minimize the consequences of perinatal infections and promote healthy pregnancies.

PUBLICATIONS INCLUDED IN THIS WORK

Doster RS, Kirk LA, Tetz LM, Rogers LM, Aronoff DM, Gaddy JA. *Staphylococcus aureus* infection of human gestational membranes induces bacterial biofilm formation and host production of cytokines. *J Infect Dis*. 2017 Feb 15;215(4):653-657. doi: 10.1093/infdis/jiw300.

Ayala OD*, **Doster RS***, Manning SD, O'Brien CM, Aronoff DM, Gaddy JA, Mahadevan-Jansen A. Raman microspectroscopy identifies *Streptococcus agalactiae* on ex vivo human fetal membrane tissues. *In submission*.
*Designates co-first authors

Rogers LM, Anders AP, **Doster RS**, Gill EA, Gnecco JS, Holley JM, Randis TM, Ratner AJ, Gaddy JA, Osteen K, Aronoff DM. Decidual stromal cell-derived PGE_2 regulates macrophage responses to microbial threat. *Am J Reprod Immunol*. 2018 Aug 7:e13032. doi: 10.1111/aji.13032.

Kothary V, **Doster RS**, Rogers LM, Kirk LA, Boyd KL, Romano-Keeler J, Haley KP, Manning SD, Aronoff DM, Gaddy JA. Group B *Streptococcus* Induces Neutrophil Recruitment to Gestational Tissues and Elaboration of Extracellular Traps and Nutritional Immunity. *Front Cell Infect Microbiol*. 2017 Feb 3;7:19. doi: 10.3389/fcimb.2017.00019.

Doster RS, Rogers LM, Gaddy JA, Aronoff DM. Macrophage Extracellular Traps: A Scoping Review. *J Innate Immun*. 2018;10(1):3-13. doi: 10.1159/000480373. Epub 2017 Oct 7.

Doster RS, Sutton JA, Rogers LM, Aronoff DM, Gaddy JA. *Streptococcus agalactiae* induces placental macrophages to release extracellular traps loaded with tissue remodeling enzymes via an oxidative-burst-dependent mechanism. *mBio.* 2018; Nov 20;9(6). pii: e02084-18. doi: 10.1128/mBio.02084-18.

BIBLIOGRAPHY

1. WHO. Born Too Soon: The Global Action Report in Preterm Birth2012. Epub 5/2/2012.
2. Agrawal S, Rao SC, Bulsara MK, Patole SK. Prevalence of Autism Spectrum Disorder in Preterm Infants: A Meta-analysis. Pediatrics. 2018;142(3). Epub 2018/08/05. doi: 10.1542/peds.2018-0134. PubMed PMID: 30076190.
3. Bianchi-Jassir F, Seale AC, Kohli-Lynch M, Lawn JE, Baker CJ, Bartlett L, Cutland C, Gravett MG, Heath PT, Ip M, Le Doare K, Madhi SA, Saha SK, Schrag S, Sobanjo-Ter Meulen A, Vekemans J, Rubens CE. Preterm Birth Associated With Group B Streptococcus Maternal Colonization Worldwide: Systematic Review and Meta-analyses. Clinical infectious diseases : an official publication of the Infectious Diseases Society of America. 2017;65(suppl_2):S133-S42. doi: 10.1093/cid/cix661. PubMed PMID: 29117329.
4. Bilgin A, Mendonca M, Wolke D. Preterm Birth/Low Birth Weight and Markers Reflective of Wealth in Adulthood: A Meta-analysis. Pediatrics. 2018;142(1). Epub 2018/06/08. doi: 10.1542/peds.2017-3625. PubMed PMID: 29875181.
5. Govindaswami B, Jegatheesan P, Nudelman M, Narasimhan SR. Prevention of Prematurity: Advances and Opportunities. Clin Perinatol. 2018;45(3):579-95. Epub 2018/08/27. doi: 10.1016/j.clp.2018.05.013. PubMed PMID: 30144857.
6. Galinsky R, Polglase GR, Hooper SB, Black MJ, Moss TJ. The consequences of chorioamnionitis: preterm birth and effects on development. Journal of pregnancy. 2013;2013:412831. doi: 10.1155/2013/412831. PubMed PMID: 23533760; PMCID: 3606792.
7. Meinert M, Malmstrom A, Petersen AC, Eriksen GV, Uldbjerg N. Chorioamniontis in preterm delivery is associated with degradation of decorin and biglycan and depletion of hyaluronan in fetal membranes. Placenta. 2014;35(8):546-51. Epub 2014/06/13. doi: 10.1016/j.placenta.2014.05.004. PubMed PMID: 24920507.
8. Goldenberg RL, McClure EM, Saleem S, Reddy UM. Infection-related stillbirths. Lancet. 2010;375(9724):1482-90. Epub 2010/03/13. doi: 10.1016/S0140-6736(09)61712-8. PubMed PMID: 20223514; PMCID: PMC3893931.
9. Qazi SA, Stoll BJ. Neonatal sepsis: a major global public health challenge. The Pediatric infectious disease journal. 2009;28(1 Suppl):S1-2. Epub 2009/01/10. doi: 10.1097/INF.0b013e31819587a9. PubMed PMID: 19106756.
10. Ofman G, Vasco N, Cantey JB. Risk of Early-Onset Sepsis following Preterm, Prolonged Rupture of Membranes with or without Chorioamnionitis. Am J Perinatol. 2016;33(4):339-42. Epub 2015/10/16. doi: 10.1055/s-0035-1556758. PubMed PMID: 26469992.
11. Mendz GL, Kaakoush NO, Quinlivan JA. Bacterial aetiological agents of intra-amniotic infections and preterm birth in pregnant women. Frontiers in cellular and infection microbiology. 2013;3:58. doi: 10.3389/fcimb.2013.00058. PubMed PMID: 24137568; PMCID: 3797391.
12. Gardella C, Riley DE, Hitti J, Agnew K, Krieger JN, Eschenbach D. Identification and sequencing of bacterial rDNAs in culture-negative amniotic fluid from women in premature labor. Am J Perinatol. 2004;21(6):319-23. Epub 2004/08/18. doi: 10.1055/s-2004-831884. PubMed PMID: 15311367.
13. Burd I, Balakrishnan B, Kannan S. Models of fetal brain injury, intrauterine inflammation, and preterm birth. American journal of reproductive immunology. 2012;67(4):287-94. Epub 2012/03/03. doi: 10.1111/j.1600-0897.2012.01110.x. PubMed PMID: 22380481.
14. Ganu RS, Ma J, Aagaard KM. The role of microbial communities in parturition: is there evidence of association with preterm birth and perinatal morbidity and mortality? Am J Perinatol. 2013;30(8):613-24. Epub 2012/11/20. doi: 10.1055/s-0032-1329693. PubMed PMID: 23161352.
15. Goldenberg RL, Hauth JC, Andrews WW. Intrauterine infection and preterm delivery. The New England journal of medicine. 2000;342(20):1500-7. doi: 10.1056/NEJM200005183422007. PubMed PMID: 10816189.

16. Kim CJ, Romero R, Chaemsaithong P, Chaiyasit N, Yoon BH, Kim YM. Acute chorioamnionitis and funisitis: definition, pathologic features, and clinical significance. American journal of obstetrics and gynecology. 2015;213(4 Suppl):S29-52. doi: 10.1016/j.ajog.2015.08.040. PubMed PMID: 26428501; PMCID: PMC4774647.
17. Anders AP, Gaddy JA, Doster RS, Aronoff DM. Current concepts in maternal-fetal immunology: Recognition and response to microbial pathogens by decidual stromal cells. American journal of reproductive immunology. 2017;77(3). doi: 10.1111/aji.12623. PubMed PMID: 28044385; PMCID: PMC5321847.
18. Gotsch F, Romero R, Kusanovic JP, Mazaki-Tovi S, Pineles BL, Erez O, Espinoza J, Hassan SS. The fetal inflammatory response syndrome. Clin Obstet Gynecol. 2007;50(3):652-83. Epub 2007/09/01. doi: 10.1097/GRF.0b013e31811ebef6. PubMed PMID: 17762416.
19. Shabayek S, Spellerberg B. Group B Streptococcal Colonization, Molecular Characteristics, and Epidemiology. Front Microbiol. 2018;9:437. Epub 2018/03/30. doi: 10.3389/fmicb.2018.00437. PubMed PMID: 29593684; PMCID: PMC5861770.
20. Tudela CM, Stewart RD, Roberts SW, Wendel GD, Jr., Stafford IA, McIntire DD, Sheffield JS. Intrapartum evidence of early-onset group B streptococcus. Obstetrics and gynecology. 2012;119(3):626-9. doi: 10.1097/AOG.0b013e31824532f6. PubMed PMID: 22353962.
21. Dillon HC, Jr., Khare S, Gray BM. Group B streptococcal carriage and disease: a 6-year prospective study. J Pediatr. 1987;110(1):31-6. PubMed PMID: 3540249.
22. Schuchat A, Wenger JD. Epidemiology of group B streptococcal disease. Risk factors, prevention strategies, and vaccine development. Epidemiol Rev. 1994;16(2):374-402. PubMed PMID: 7713185.
23. Dermer P, Lee C, Eggert J, Few B. A history of neonatal group B streptococcus with its related morbidity and mortality rates in the United States. J Pediatr Nurs. 2004;19(5):357-63. Epub 2004/12/23. doi: 10.1016/j.pedn.2004.05.012. PubMed PMID: 15614260.
24. Verani JR, McGee L, Schrag SJ, Division of Bacterial Diseases NCfI, Respiratory Diseases CfDC, Prevention. Prevention of perinatal group B streptococcal disease--revised guidelines from CDC, 2010. MMWR Recommendations and reports : Morbidity and mortality weekly report Recommendations and reports / Centers for Disease Control. 2010;59(RR-10):1-36. PubMed PMID: 21088663.
25. Allen U NC, MacDonald N, Toye B, Stephens D, Marchessault V. . Relationship between antenatal group B streptococcal vaginal colonization and premature labour. Paediatr Child Health. 1999;4(7):465-9.
26. Jahromi B, Poorarian S, Poorbarfehee S. The Prevalence and Adverse Effects of Group B Streptococcal Colonization during Pregnancy. Arch Iranian Med. 2008;11(6):654-7.
27. Colicchia LC, Lauderdale DS, Du H, Adams M, Hirsch E. Recurrence of group B streptococcus colonization in successive pregnancies. Journal of perinatology : official journal of the California Perinatal Association. 2015;35:173-6. Epub 10/16/14. doi: 10.1038/jp.2014.185. PubMed PMID: 25321646.
28. Seale AC, Koech AC, Sheppard AE, Barsosio HC, Langat J, Anyango E, Mwakio S, Mwarumba S, Morpeth SC, Anampiu K, Vaughan A, Giess A, Mogeni P, Walusuna L, Mwangudzah H, Mwanzui D, Salim M, Kemp B, Jones C, Mturi N, Tsofa B, Mumbo E, Mulewa D, Bandika V, Soita M, Owiti M, Onzere N, Walker AS, Schrag SJ, Kennedy SH, Fegan G, Crook DW, Berkley JA. Maternal colonisation with Streptococcus agalactiae, and associated stillbirth and neonatal disease in coastal Kenya. Nat Microbiol. 2016;1(7). doi: 10.1038/nmicrobiol.2016.67. PubMed PMID: 27398230; PMCID: PMC4936517.
29. Kohli-Lynch M, Russell NJ, Seale AC, Dangor Z, Tann CJ, Baker CJ, Bartlett L, Cutland C, Gravett MG, Heath PT, Ip M, Le Doare K, Madhi SA, Rubens CE, Saha SK, Schrag S, Sobanjo-Ter Meulen A, Vekemans J, O'Sullivan C, Nakwa F, Ben Hamouda H, Soua H, Giorgakoudi K, Ladhani S, Lamagni T, Rattue H, Trotter C, Lawn JE. Neurodevelopmental Impairment in Children After Group B Streptococcal Disease Worldwide: Systematic Review and Meta-

analyses. Clinical infectious diseases : an official publication of the Infectious Diseases Society of America. 2017;65(suppl_2):S190-S9. Epub 2017/11/09. doi: 10.1093/cid/cix663. PubMed PMID: 29117331; PMCID: PMC5848372.
30. Russell NJ, Seale AC, O'Sullivan C, Le Doare K, Heath PT, Lawn JE, Bartlett L, Cutland C, Gravett M, Ip M, Madhi SA, Rubens CE, Saha SK, Schrag S, Sobanjo-Ter Meulen A, Vekemans J, Baker CJ. Risk of Early-Onset Neonatal Group B Streptococcal Disease With Maternal Colonization Worldwide: Systematic Review and Meta-analyses. Clinical infectious diseases : an official publication of the Infectious Diseases Society of America. 2017;65(suppl_2):S152-S9. Epub 2017/11/09. doi: 10.1093/cid/cix655. PubMed PMID: 29117325; PMCID: PMC5850448.
31. Centers for Disease Control and Prevention. Fast Facts: Group B Strep (GBS) Centers for Disease Control and Preventions2014 [updated 6/1/2014; cited 2015 1/26/2015]. Available from: http://www.cdc.gov/groupbstrep/about/fast-facts.html.
32. Phares CR, Lynfield R, Farley MM, Mohle-Boetani J, Harrison LH, Petit S, Craig AS, Schaffner W, Zansky SM, Gershman K, Stefonek KR, Albanese BA, Zell ER, Schuchat A, Schrag SJ, Active Bacterial Core surveillance/Emerging Infections Program N. Epidemiology of invasive group B streptococcal disease in the United States, 1999-2005. Jama. 2008;299(17):2056-65. doi: 10.1001/jama.299.17.2056. PubMed PMID: 18460666.
33. Kwatra G, Adrian PV, Shiri T, Buchmann EJ, Cutland CL, Madhi SA. Serotype-specific acquisition and loss of group B streptococcus recto-vaginal colonization in late pregnancy. PloS one. 2014;9(6):e98778. doi: 10.1371/journal.pone.0098778. PubMed PMID: 24979575; PMCID: PMC4076185.
34. Russell NJ, Seale AC, O'Driscoll M, O'Sullivan C, Bianchi-Jassir F, Gonzalez-Guarin J, Lawn JE, Baker CJ, Bartlett L, Cutland C, Gravett MG, Heath PT, Le Doare K, Madhi SA, Rubens CE, Schrag S, Sobanjo-Ter Meulen A, Vekemans J, Saha SK, Ip M, Group GBSMCI. Maternal Colonization With Group B Streptococcus and Serotype Distribution Worldwide: Systematic Review and Meta-analyses. Clinical infectious diseases : an official publication of the Infectious Diseases Society of America. 2017;65(suppl_2):S100-S11. doi: 10.1093/cid/cix658. PubMed PMID: 29117327; PMCID: PMC5848259.
35. Benitz WE, Gould JB, Druzin ML. Risk factors for early-onset group B streptococcal sepsis: estimation of odds ratios by critical literature review. Pediatrics. 1999;103(6):e77. PubMed PMID: 10353974.
36. Mukhopadhyay S, Puopolo KM. Risk assessment in neonatal early onset sepsis. Semin Perinatol. 2012;36(6):408-15. doi: 10.1053/j.semperi.2012.06.002. PubMed PMID: 23177799; PMCID: PMC3782302.
37. Bergal A, Loucif L, Benouareth DE, Bentorki AA, Abat C, Rolain JM. Molecular epidemiology and distribution of serotypes, genotypes, and antibiotic resistance genes of Streptococcus agalactiae clinical isolates from Guelma, Algeria and Marseille, France. Eur J Clin Microbiol Infect Dis. 2015;34(12):2339-48. doi: 10.1007/s10096-015-2487-6. PubMed PMID: 26415872.
38. Gensollen T, Iyer SS, Kasper DL, Blumberg RS. How colonization by microbiota in early life shapes the immune system. Science. 2016;352(6285):539-44. doi: 10.1126/science.aad9378. PubMed PMID: 27126036.
39. Bellais S, Six A, Fouet A, Longo M, Dmytruk N, Glaser P, Trieu-Cuot P, Poyart C. Capsular switching in group B Streptococcus CC17 hypervirulent clone: a future challenge for polysaccharide vaccine development. The Journal of infectious diseases. 2012;206(11):1745-52. doi: 10.1093/infdis/jis605. PubMed PMID: 23002446.
40. Meehan M, Cunney R, Cafferkey M. Molecular epidemiology of group B streptococci in Ireland reveals a diverse population with evidence of capsular switching. Eur J Clin Microbiol Infect Dis. 2014;33(7):1155-62. doi: 10.1007/s10096-014-2055-5. PubMed PMID: 24469423.
41. Patras KA, Nizet V. Group B Streptococcal Maternal Colonization and Neonatal Disease: Molecular Mechanisms and Preventative Approaches. Front Pediatr. 2018;6:27. Epub 2018/03/10. doi: 10.3389/fped.2018.00027. PubMed PMID: 29520354; PMCID: PMC5827363.

42. Park SE, Jiang S, Wessels MR. CsrRS and environmental pH regulate group B streptococcus adherence to human epithelial cells and extracellular matrix. Infection and immunity. 2012;80(11):3975-84. doi: 10.1128/IAI.00699-12. PubMed PMID: 22949550; PMCID: 3486057.
43. Sheen TR, Jimenez A, Wang NY, Banerjee A, van Sorge NM, Doran KS. Serine-rich repeat proteins and pili promote Streptococcus agalactiae colonization of the vaginal tract. Journal of bacteriology. 2011;193(24):6834-42. doi: 10.1128/JB.00094-11. PubMed PMID: 21984789; PMCID: PMC3232834.
44. Jiang S, Wessels MR. BsaB, a novel adherence factor of group B Streptococcus. Infection and immunity. 2014;82(3):1007-16. doi: 10.1128/IAI.01014-13. PubMed PMID: 24343649; PMCID: PMC3957996.
45. Wang NY, Patras KA, Seo HS, Cavaco CK, Rosler B, Neely MN, Sullam PM, Doran KS. Group B streptococcal serine-rich repeat proteins promote interaction with fibrinogen and vaginal colonization. The Journal of infectious diseases. 2014;210(6):982-91. Epub 2014/03/13. doi: 10.1093/infdis/jiu151. PubMed PMID: 24620021; PMCID: PMC4192050.
46. Patras KA, Derieux J, Al-Bassam MM, Adiletta N, Vrbanac A, Lapek JD, Zengler K, Gonzalez DJ, Nizet V. Group B Streptococcus Biofilm Regulatory Protein A Contributes to Bacterial Physiology and Innate Immune Resistance. The Journal of infectious diseases. 2018;218(10):1641-52. Epub 2018/06/06. doi: 10.1093/infdis/jiy341. PubMed PMID: 29868829.
47. Rosini R, Margarit I. Biofilm formation by Streptococcus agalactiae: influence of environmental conditions and implicated virulence factors. Frontiers in cellular and infection microbiology. 2015;5:6. doi: 10.3389/fcimb.2015.00006. PubMed PMID: 25699242; PMCID: PMC4316791.
48. Nie S, Lu X, Hu YW, Zheng L, Wang Q. Influence of environmental and genotypic factors on biofilm formation by clinical isolates of group B streptococci. Microbial pathogenesis. 2018;121:45-50. Epub 2018/05/16. doi: 10.1016/j.micpath.2018.05.020. PubMed PMID: 29763724.
49. D'Urzo N, Martinelli M, Pezzicoli A, De Cesare V, Pinto V, Margarit I, Telford JL, Maione D, Members of the DSG. Acidic pH strongly enhances in vitro biofilm formation by a subset of hypervirulent ST-17 Streptococcus agalactiae strains. Applied and environmental microbiology. 2014;80(7):2176-85. doi: 10.1128/AEM.03627-13. PubMed PMID: 24487536; PMCID: PMC3993151.
50. Glaser P, Rusniok C, Buchrieser C, Chevalier F, Frangeul L, Msadek T, Zouine M, Couve E, Lalioui L, Poyart C, Trieu-Cuot P, Kunst F. Genome sequence of Streptococcus agalactiae, a pathogen causing invasive neonatal disease. Molecular microbiology. 2002;45(6):1499-513. Epub 2002/10/02. PubMed PMID: 12354221.
51. Tettelin H, Masignani V, Cieslewicz MJ, Eisen JA, Peterson S, Wessels MR, Paulsen IT, Nelson KE, Margarit I, Read TD, Madoff LC, Wolf AM, Beanan MJ, Brinkac LM, Daugherty SC, DeBoy RT, Durkin AS, Kolonay JF, Madupu R, Lewis MR, Radune D, Fedorova NB, Scanlan D, Khouri H, Mulligan S, Carty HA, Cline RT, Van Aken SE, Gill J, Scarselli M, Mora M, Iacobini ET, Brettoni C, Galli G, Mariani M, Vegni F, Maione D, Rinaudo D, Rappuoli R, Telford JL, Kasper DL, Grandi G, Fraser CM. Complete genome sequence and comparative genomic analysis of an emerging human pathogen, serotype V Streptococcus agalactiae. Proceedings of the National Academy of Sciences of the United States of America. 2002;99(19):12391-6. doi: 10.1073/pnas.182380799. PubMed PMID: 12200547; PMCID: 129455.
52. Di Palo B, Rippa V, Santi I, Brettoni C, Muzzi A, Metruccio MM, Grifantini R, Telford JL, Paccani SR, Soriani M. Adaptive response of Group B streptococcus to high glucose conditions: new insights on the CovRS regulation network. PloS one. 2013;8(4):e61294. Epub 2013/04/16. doi: 10.1371/journal.pone.0061294. PubMed PMID: 23585887; PMCID: PMC3621830.
53. Whidbey C, Harrell MI, Burnside K, Ngo L, Becraft AK, Iyer LM, Aravind L, Hitti J, Waldorf KM, Rajagopal L. A hemolytic pigment of Group B Streptococcus allows bacterial penetration of human placenta. The Journal of experimental medicine. 2013;210(6):1265-81. doi: 10.1084/jem.20122753. PubMed PMID: 23712433; PMCID: 3674703.

54. Patras KA, Rosler B, Thoman ML, Doran KS. Characterization of host immunity during persistent vaginal colonization by Group B Streptococcus. Mucosal immunology. 2015. doi: 10.1038/mi.2015.23. PubMed PMID: 25850655.
55. Vornhagen J, Armistead B, Santana-Ufret V, Gendrin C, Merillat S, Coleman M, Quach P, Boldenow E, Alishetti V, Leonhard-Melief C, Ngo LY, Whidbey C, Doran KS, Curtis C, Waldorf KMA, Nance E, Rajagopal L. Group B streptococcus exploits vaginal epithelial exfoliation for ascending infection. The Journal of clinical investigation. 2018;128(5):1985-99. Epub 2018/04/10. doi: 10.1172/JCI97043. PubMed PMID: 29629904; PMCID: PMC5919824.
56. Ali SR, Fong JJ, Carlin AF, Busch TD, Linden R, Angata T, Areschoug T, Parast M, Varki N, Murray J, Nizet V, Varki A. Siglec-5 and Siglec-14 are polymorphic paired receptors that modulate neutrophil and amnion signaling responses to group B Streptococcus. The Journal of experimental medicine. 2014;211(6):1231-42. doi: 10.1084/jem.20131853. PubMed PMID: 24799499; PMCID: 4042635.
57. Carlin AF, Uchiyama S, Chang YC, Lewis AL, Nizet V, Varki A. Molecular mimicry of host sialylated glycans allows a bacterial pathogen to engage neutrophil Siglec-9 and dampen the innate immune response. Blood. 2009;113(14):3333-6. doi: 10.1182/blood-2008-11-187302. PubMed PMID: 19196661; PMCID: PMC2665898.
58. Boldenow E, Hogan KA, Chames MC, Aronoff DM, Xi C, Loch-Caruso R. Role of cytokine signaling in group B Streptococcus-stimulated expression of human beta defensin-2 in human extraplacental membranes. American journal of reproductive immunology. 2015;73(3):263-72. doi: 10.1111/aji.12325. PubMed PMID: 25263616; PMCID: 4323989.
59. Boldenow E, Jones S, Lieberman RW, Chames MC, Aronoff DM, Xi C, Loch-Caruso R. Antimicrobial peptide response to group B Streptococcus in human extraplacental membranes in culture. Placenta. 2013;34(6):480-5. Epub 2013/04/09. doi: 10.1016/j.placenta.2013.02.010. PubMed PMID: 23562109; PMCID: PMC3664555.
60. Gravett MG, Witkin SS, Haluska GJ, Edwards JL, Cook MJ, Novy MJ. An experimental model for intraamniotic infection and preterm labor in rhesus monkeys. American journal of obstetrics and gynecology. 1994;171(6):1660-7. Epub 1994/12/01. PubMed PMID: 7802084.
61. Adams Waldorf KM, Gravett MG, McAdams RM, Paolella LJ, Gough GM, Carl DJ, Bansal A, Liggitt HD, Kapur RP, Reitz FB, Rubens CE. Choriodecidual group B streptococcal inoculation induces fetal lung injury without intra-amniotic infection and preterm labor in Macaca nemestrina. PloS one. 2011;6(12):e28972. Epub 2012/01/05. doi: 10.1371/journal.pone.0028972. PubMed PMID: 22216148; PMCID: PMC3244436.
62. Randis TM, Gelber SE, Hooven TA, Abellar RG, Akabas LH, Lewis EL, Walker LB, Byland LM, Nizet V, Ratner AJ. Group B Streptococcus beta-hemolysin/cytolysin breaches maternal-fetal barriers to cause preterm birth and intrauterine fetal demise in vivo. The Journal of infectious diseases. 2014;210(2):265-73. doi: 10.1093/infdis/jiu067. PubMed PMID: 24474814; PMCID: 4092248.
63. Whidbey C, Vornhagen J, Gendrin C, Boldenow E, Samson JM, Doering K, Ngo L, Ezekwe EA, Jr., Gundlach JH, Elovitz MA, Liggitt D, Duncan JA, Adams Waldorf KM, Rajagopal L. A streptococcal lipid toxin induces membrane permeabilization and pyroptosis leading to fetal injury. EMBO molecular medicine. 2015. doi: 10.15252/emmm.201404883. PubMed PMID: 25750210.
64. Boldenow E, Gendrin C, Ngo L, Bierle C, Vornhagen J, Coleman M, Merillat S, Armistead B, Whidbey C, Alishetti V, Santana-Ufret V, Ogle J, Gough M, Srinouanprachanh S, MacDonald JW, Bammler TK, Bansal A, Liggitt HD, Rajagopal L, Waldorf KM. Group B Streptococcus circumvents neutrophils and neutrophil extracellular traps during amniotic cavity invasion and preterm labor. Sci Immunol. 2016;1(4). doi: 10.1126/sciimmunol.aah4576. PubMed PMID: 27819066; PMCID: PMC5089172.
65. Gendrin C, Vornhagen J, Armistead B, Singh P, Whidbey C, Merillat S, Knupp D, Parker R, Rogers LM, Quach P, Iyer LM, Aravind L, Manning SD, Aronoff DM, Rajagopal L. A non-

hemolytic Group B Streptococcus strain exhibits hypervirulence. The Journal of infectious diseases. 2017. doi: 10.1093/infdis/jix646. PubMed PMID: 29244079.
66. Vornhagen J, Quach P, Boldenow E, Merillat S, Whidbey C, Ngo LY, Adams Waldorf KM, Rajagopal L. Bacterial Hyaluronidase Promotes Ascending GBS Infection and Preterm Birth. mBio. 2016;7(3). doi: 10.1128/mBio.00781-16. PubMed PMID: 27353757; PMCID: PMC4937215.
67. Ghaebi M, Nouri M, Ghasemzadeh A, Farzadi L, Jadidi-Niaragh F, Ahmadi M, Yousefi M. Immune regulatory network in successful pregnancy and reproductive failures. Biomed Pharmacother. 2017;88:61-73. doi: 10.1016/j.biopha.2017.01.016. PubMed PMID: 28095355.
68. Arck PC, Hecher K. Fetomaternal immune cross-talk and its consequences for maternal and offspring's health. Nat Med. 2013;19(5):548-56. doi: 10.1038/nm.3160. PubMed PMID: 23652115.
69. Xu YY, Wang SC, Li DJ, Du MR. Co-Signaling Molecules in Maternal-Fetal Immunity. Trends Mol Med. 2017;23(1):46-58. doi: 10.1016/j.molmed.2016.11.001. PubMed PMID: 27914866.
70. Nagamatsu T, Barrier BF, Schust DJ. The regulation of T-cell cytokine production by ICOS-B7H2 interactions at the human fetomaternal interface. Immunol Cell Biol. 2011;89(3):417-25. doi: 10.1038/icb.2010.101. PubMed PMID: 20733594.
71. Houser BL. Decidual macrophages and their roles at the maternal-fetal interface. Yale J Biol Med. 2012;85(1):105-18. PubMed PMID: 22461749; PMCID: PMC3313525.
72. Reyes L, Wolfe B, Golos T. Hofbauer Cells: Placental Macrophages of Fetal Origin. Results Probl Cell Differ. 2017;62:45-60. doi: 10.1007/978-3-319-54090-0_3. PubMed PMID: 28455705.
73. Brown MB, von Chamier M, Allam AB, Reyes L. M1/M2 macrophage polarity in normal and complicated pregnancy. Frontiers in immunology. 2014;5:606. doi: 10.3389/fimmu.2014.00606. PubMed PMID: 25505471; PMCID: PMC4241843.
74. Zhang YH, He M, Wang Y, Liao AH. Modulators of the Balance between M1 and M2 Macrophages during Pregnancy. Frontiers in immunology. 2017;8:120. doi: 10.3389/fimmu.2017.00120. PubMed PMID: 28232836; PMCID: PMC5299000.
75. Mantovani A, Biswas SK, Galdiero MR, Sica A, Locati M. Macrophage plasticity and polarization in tissue repair and remodelling. J Pathol. 2013;229(2):176-85. doi: 10.1002/path.4133. PubMed PMID: 23096265.
76. Kim SY, Romero R, Tarca AL, Bhatti G, Kim CJ, Lee J, Elsey A, Than NG, Chaiworapongsa T, Hassan SS, Kang GH, Kim JS. Methylome of fetal and maternal monocytes and macrophages at the feto-maternal interface. American journal of reproductive immunology. 2012;68(1):8-27. doi: 10.1111/j.1600-0897.2012.01108.x. PubMed PMID: 22385097; PMCID: PMC3479407.
77. Gustafsson C, Mjosberg J, Matussek A, Geffers R, Matthiesen L, Berg G, Sharma S, Buer J, Ernerudh J. Gene expression profiling of human decidual macrophages: evidence for immunosuppressive phenotype. PloS one. 2008;3(4):e2078. doi: 10.1371/journal.pone.0002078. PubMed PMID: 18446208; PMCID: PMC2323105.
78. Johnson EL, Chakraborty R. Placental Hofbauer cells limit HIV-1 replication and potentially offset mother to child transmission (MTCT) by induction of immunoregulatory cytokines. Retrovirology. 2012;9:101. doi: 10.1186/1742-4690-9-101. PubMed PMID: 23217137; PMCID: PMC3524025.
79. Chen CP, Tsai PS, Huang CJ. Antiinflammation effect of human placental multipotent mesenchymal stromal cells is mediated by prostaglandin E2 via a myeloid differentiation primary response gene 88-dependent pathway. Anesthesiology. 2012;117(3):568-79. doi: 10.1097/ALN.0b013e31826150a9. PubMed PMID: 22739766.
80. Montero J, Gomez-Abellan V, Arizcun M, Mulero V, Sepulcre MP. Prostaglandin E2 promotes M2 polarization of macrophages via a cAMP/CREB signaling pathway and deactivates granulocytes in teleost fish. Fish Shellfish Immunol. 2016;55:632-41. doi: 10.1016/j.fsi.2016.06.044. PubMed PMID: 27368534.
81. Wetzka B, Clark DE, Charnock-Jones DS, Zahradnik HP, Smith SK. Isolation of macrophages (Hofbauer cells) from human term placenta and their prostaglandin E2 and thromboxane production. Hum Reprod. 1997;12(4):847-52. PubMed PMID: 9159455.

82. Talati AJ, Kim HJ, Kim YI, Yi AK, English BK. Role of bacterial DNA in macrophage activation by group B streptococci. Microbes and infection / Institut Pasteur. 2008;10(10-11):1106-13. Epub 2008/07/08. doi: 10.1016/j.micinf.2008.06.001. PubMed PMID: 18602491.
83. Henneke P, Takeuchi O, van Strijp JA, Guttormsen HK, Smith JA, Schromm AB, Espevik TA, Akira S, Nizet V, Kasper DL, Golenbock DT. Novel engagement of CD14 and multiple toll-like receptors by group B streptococci. Journal of immunology. 2001;167(12):7069-76. Epub 2001/12/12. PubMed PMID: 11739528.
84. Gupta R, Ghosh S, Monks B, DeOliveira RB, Tzeng TC, Kalantari P, Nandy A, Bhattacharjee B, Chan J, Ferreira F, Rathinam V, Sharma S, Lien E, Silverman N, Fitzgerald K, Firon A, Trieu-Cuot P, Henneke P, Golenbock DT. RNA and beta-hemolysin of group B Streptococcus induce interleukin-1beta (IL-1beta) by activating NLRP3 inflammasomes in mouse macrophages. The Journal of biological chemistry. 2014;289(20):13701-5. Epub 2014/04/03. doi: 10.1074/jbc.C114.548982. PubMed PMID: 24692555; PMCID: PMC4022842.
85. Cornacchione P, Scaringi L, Fettucciari K, Rosati E, Sabatini R, Orefici G, von Hunolstein C, Modesti A, Modica A, Minelli F, Marconi P. Group B streptococci persist inside macrophages. Immunology. 1998;93(1):86-95. Epub 1998/04/16. PubMed PMID: 9536123; PMCID: PMC1364110.
86. Marodi L, Kaposzta R, Nemes E. Survival of group B streptococcus type III in mononuclear phagocytes: differential regulation of bacterial killing in cord macrophages by human recombinant gamma interferon and granulocyte-macrophage colony-stimulating factor. Infection and immunity. 2000;68(4):2167-70. Epub 2000/03/18. PubMed PMID: 10722616; PMCID: PMC97400.
87. Teixeira CF, Azevedo NL, Carvalho TM, Fuentes J, Nagao PE. Cytochemical study of Streptococcus agalactiae and macrophage interaction. Microsc Res Tech. 2001;54(4):254-9. Epub 2001/08/22. doi: 10.1002/jemt.1137. PubMed PMID: 11514981.
88. Kwak DJ, Augustine NH, Borges WG, Joyner JL, Green WF, Hill HR. Intracellular and extracellular cytokine production by human mixed mononuclear cells in response to group B streptococci. Infection and immunity. 2000;68(1):320-7. Epub 1999/12/22. PubMed PMID: 10603404; PMCID: PMC97137.
89. Henneke P, Takeuchi O, Malley R, Lien E, Ingalls RR, Freeman MW, Mayadas T, Nizet V, Akira S, Kasper DL, Golenbock DT. Cellular activation, phagocytosis, and bactericidal activity against group B streptococcus involve parallel myeloid differentiation factor 88-dependent and independent signaling pathways. Journal of immunology. 2002;169(7):3970-7. Epub 2002/09/24. PubMed PMID: 12244198.
90. Liu GY, Doran KS, Lawrence T, Turkson N, Puliti M, Tissi L, Nizet V. Sword and shield: linked group B streptococcal beta-hemolysin/cytolysin and carotenoid pigment function to subvert host phagocyte defense. Proceedings of the National Academy of Sciences of the United States of America. 2004;101(40):14491-6. Epub 2004/09/24. doi: 10.1073/pnas.0406143101. PubMed PMID: 15381763; PMCID: PMC521972.
91. Fettucciari K, Quotadamo F, Noce R, Palumbo C, Modesti A, Rosati E, Mannucci R, Bartoli A, Marconi P. Group B Streptococcus (GBS) disrupts by calpain activation the actin and microtubule cytoskeleton of macrophages. Cellular microbiology. 2011;13(6):859-84. Epub 2011/03/19. doi: 10.1111/j.1462-5822.2011.01584.x. PubMed PMID: 21414124.
92. Blencowe H, Cousens S, Chou D, Oestergaard M, Say L, Moller AB, Kinney M, Lawn J, Born Too Soon Preterm Birth Action G. Born too soon: the global epidemiology of 15 million preterm births. Reproductive health. 2013;10 Suppl 1:S2. doi: 10.1186/1742-4755-10-S1-S2. PubMed PMID: 24625129; PMCID: 3828585.
93. Sorano S, Goto M, Matsuoka S, Tohyama A, Yamamoto H, Nakamura S, Fukami T, Matsuoka R, Tsujioka H, Eguchi F. Chorioamnionitis caused by Staphylococcus aureus with intact membranes in a term pregnancy: A case of maternal and fetal septic shock. J Infect Chemother. 2016;22(4):261-4. doi: 10.1016/j.jiac.2015.10.012. PubMed PMID: 26705749.

94. Geisler JP, Horlander KM, Hiett AK. Methicillin resistant Staphylococcus aureus as a cause of chorioamnionitis. Clin Exp Obstet Gynecol. 1998;25(4):119-20. PubMed PMID: 9987566.
95. Hoang M, Potter JA, Gysler SM, Han CS, Guller S, Norwitz ER, Abrahams VM. Human fetal membranes generate distinct cytokine profiles in response to bacterial Toll-like receptor and nod-like receptor agonists. Biol Reprod. 2014;90(2):39. doi: 10.1095/biolreprod.113.115428. PubMed PMID: 24429216; PMCID: PMC4076407.
96. Andrews WW, Schelonka R, Waites K, Stamm A, Cliver SP, Moser S. Genital tract methicillin-resistant Staphylococcus aureus: risk of vertical transmission in pregnant women. Obstetrics and gynecology. 2008;111(1):113-8. doi: 10.1097/01.AOG.0000298344.04916.11. PubMed PMID: 18165399.
97. Eleje GU, Adinma JI, Ghasi S, Ikechebelu JI, Igwegbe AO, Okonkwo JE, Okafor CI, Ezeama CO, Ezebialu IU, Ogbuagu CN. Antibiotic susceptibility pattern of genital tract bacteria in pregnant women with preterm premature rupture of membranes in a resource-limited setting. Int J Gynaecol Obstet. 2014;127(1):10-4. doi: 10.1016/j.ijgo.2014.04.016. PubMed PMID: 24994495.
98. Stoodley P, Conti SF, DeMeo PJ, Nistico L, Melton-Kreft R, Johnson S, Darabi A, Ehrlich GD, Costerton JW, Kathju S. Characterization of a mixed MRSA/MRSE biofilm in an explanted total ankle arthroplasty. FEMS Immunol Med Microbiol. 2011;62(1):66-74. doi: 10.1111/j.1574-695X.2011.00793.x. PubMed PMID: 21332826.
99. Scherr TD, Heim CE, Morrison JM, Kielian T. Hiding in Plain Sight: Interplay between Staphylococcal Biofilms and Host Immunity. Frontiers in immunology. 2014;5:37. doi: 10.3389/fimmu.2014.00037. PubMed PMID: 24550921; PMCID: PMC3913997.
100. McCarthy H, Rudkin JK, Black NS, Gallagher L, O'Neill E, O'Gara JP. Methicillin resistance and the biofilm phenotype in Staphylococcus aureus. Frontiers in cellular and infection microbiology. 2015;5:1. doi: 10.3389/fcimb.2015.00001. PubMed PMID: 25674541; PMCID: PMC4309206.
101. Anderson MJ, Lin YC, Gillman AN, Parks PJ, Schlievert PM, Peterson ML. Alpha-toxin promotes Staphylococcus aureus mucosal biofilm formation. Frontiers in cellular and infection microbiology. 2012;2:64. doi: 10.3389/fcimb.2012.00064. PubMed PMID: 22919655; PMCID: PMC3417397.
102. Watkins RL, Pallister KB, Voyich JM. The SaeR/S gene regulatory system induces a pro-inflammatory cytokine response during Staphylococcus aureus infection. PloS one. 2011;6(5):e19939. doi: 10.1371/journal.pone.0019939. PubMed PMID: 21603642; PMCID: PMC3094403.
103. Kanangat S, Postlethwaite A, Hasty K, Kang A, Smeltzer M, Appling W, Schaberg D. Induction of multiple matrix metalloproteinases in human dermal and synovial fibroblasts by Staphylococcus aureus: implications in the pathogenesis of septic arthritis and other soft tissue infections. Arthritis Res Ther. 2006;8(6):R176. doi: 10.1186/ar2086. PubMed PMID: 17129374; PMCID: PMC1794521.
104. Murtha AP, Menon R. Regulation of fetal membrane inflammation: a critical step in reducing adverse pregnancy outcome. American journal of obstetrics and gynecology. 2015;213(4):447-8. doi: 10.1016/j.ajog.2015.07.008. PubMed PMID: 26410204.
105. Cvitkovitch DG, Li YH, Ellen RP. Quorum sensing and biofilm formation in Streptococcal infections. The Journal of clinical investigation. 2003;112(11):1626-32. doi: 10.1172/JCI20430. PubMed PMID: 14660736; PMCID: 281653.
106. Moscoso M, Garcia E, Lopez R. Biofilm formation by Streptococcus pneumoniae: role of choline, extracellular DNA, and capsular polysaccharide in microbial accretion. Journal of bacteriology. 2006;188(22):7785-95. doi: 10.1128/JB.00673-06. PubMed PMID: 16936041; PMCID: 1636320.
107. Ogawa T, Terao Y, Okuni H, Ninomiya K, Sakata H, Ikebe K, Maeda Y, Kawabata S. Biofilm formation or internalization into epithelial cells enable Streptococcus pyogenes to evade antibiotic eradication in patients with pharyngitis. Microbial pathogenesis. 2011;51(1-2):58-68. doi: 10.1016/j.micpath.2011.03.009. PubMed PMID: 21443942.
108. Muzny CA, Schwebke JR. Biofilms: An Underappreciated Mechanism of Treatment Failure and Recurrence in Vaginal Infections. Clinical infectious diseases : an official publication of the

Infectious Diseases Society of America. 2015;61(4):601-6. doi: 10.1093/cid/civ353. PubMed PMID: 25935553.
109. Vandevelde NM, Tulkens PM, Van Bambeke F. Antibiotic activity against naive and induced Streptococcus pneumoniae biofilms in an in vitro pharmacodynamic model. Antimicrobial agents and chemotherapy. 2014;58(3):1348-58. doi: 10.1128/AAC.01858-13. PubMed PMID: 24342635; PMCID: 3957900.
110. Al-Ahmad A, Ameen H, Pelz K, Karygianni L, Wittmer A, Anderson AC, Spitzmuller B, Hellwig E. Antibiotic resistance and capacity for biofilm formation of different bacteria isolated from endodontic infections associated with root-filled teeth. Journal of endodontics. 2014;40(2):223-30. doi: 10.1016/j.joen.2013.07.023. PubMed PMID: 24461408.
111. Hanke ML, Heim CE, Angle A, Sanderson SD, Kielian T. Targeting macrophage activation for the prevention and treatment of Staphylococcus aureus biofilm infections. Journal of immunology. 2013;190(5):2159-68. doi: 10.4049/jimmunol.1202348. PubMed PMID: 23365077; PMCID: PMC3578052.
112. Thurlow LR, Hanke ML, Fritz T, Angle A, Aldrich A, Williams SH, Engebretsen IL, Bayles KW, Horswill AR, Kielian T. Staphylococcus aureus biofilms prevent macrophage phagocytosis and attenuate inflammation in vivo. Journal of immunology. 2011;186(11):6585-96. doi: 10.4049/jimmunol.1002794. PubMed PMID: 21525381; PMCID: PMC3110737.
113. Blanchette KA, Orihuela CJ. Future perspective on host-pathogen interactions during bacterial biofilm formation within the nasopharynx. Future microbiology. 2012;7(2):227-39. doi: 10.2217/fmb.11.160. PubMed PMID: 22324992; PMCID: PMC3286033.
114. Lewin EB, Amstey MS. Natural history of group B streptococcus colonization and its therapy during pregnancy. American journal of obstetrics and gynecology. 1981;139(5):512-5. PubMed PMID: 7008613.
115. Kwatra G, Adrian PV, Shiri T, Buchmann EJ, Cutland CL, Madhi SA. Natural acquired humoral immunity against serotype-specific group B Streptococcus rectovaginal colonization acquisition in pregnant women. Clin Microbiol Infect. 2015;21(6):568 e13-21. doi: 10.1016/j.cmi.2015.01.030. PubMed PMID: 25680313.
116. Borges S, Silva J, Teixeira P. Survival and biofilm formation by Group B streptococci in simulated vaginal fluid at different pHs. Antonie Van Leeuwenhoek. 2012;101(3):677-82. doi: 10.1007/s10482-011-9666-y. PubMed PMID: 22038130.
117. Xia FD, Mallet A, Caliot E, Gao C, Trieu-Cuot P, Dramsi S. Capsular polysaccharide of Group B Streptococcus mediates biofilm formation in the presence of human plasma. Microbes and infection / Institut Pasteur. 2015;17(1):71-6. doi: 10.1016/j.micinf.2014.10.007. PubMed PMID: 25448634.
118. Yang Q, Porter AJ, Zhang M, Harrington DJ, Black GW, Sutcliffe IC. The impact of pH and nutrient stress on the growth and survival of Streptococcus agalactiae. Antonie Van Leeuwenhoek. 2012;102(2):277-87. doi: 10.1007/s10482-012-9736-9. PubMed PMID: 22527623.
119. Doster RS, Kirk LA, Tetz LM, Rogers LM, Aronoff DM, Gaddy JA. Staphylococcus aureus Infection of Human Gestational Membranes Induces Bacterial Biofilm Formation and Host Production of Cytokines. The Journal of infectious diseases. 2017;215(4):653-7. doi: 10.1093/infdis/jiw300. PubMed PMID: 27436434.
120. Kothary V, Doster RS, Rogers LM, Kirk LA, Boyd KL, Romano-Keeler J, Haley KP, Manning SD, Aronoff DM, Gaddy JA. Group B Streptococcus Induces Neutrophil Recruitment to Gestational Tissues and Elaboration of Extracellular Traps and Nutritional Immunity. Frontiers in cellular and infection microbiology. 2017;7:19. doi: 10.3389/fcimb.2017.00019. PubMed PMID: 28217556; PMCID: PMC5289994.
121. Rogers C, Bernstein G, Nakamura R, Endahl G, Bhoopat T. Vaginal fluid zinc concentration as a marker for intercourse. J Forensic Sci. 1988;33(1):77-83. PubMed PMID: 3351473.
122. Owen DH, Katz DF. A vaginal fluid simulant. Contraception. 1999;59(2):91-5. PubMed PMID: 10361623.

123. Wu C, Labrie J, Tremblay YD, Haine D, Mourez M, Jacques M. Zinc as an agent for the prevention of biofilm formation by pathogenic bacteria. J Appl Microbiol. 2013;115(1):30-40. doi: 10.1111/jam.12197. PubMed PMID: 23509865.
124. Gaddy JA, Radin JN, Cullen TW, Chazin WJ, Skaar EP, Trent MS, Algood HM. Helicobacter pylori Resists the Antimicrobial Activity of Calprotectin via Lipid A Modification and Associated Biofilm Formation. mBio. 2015;6(6):e01349-15. doi: 10.1128/mBio.01349-15. PubMed PMID: 26646009; PMCID: PMC4669380.
125. Kim M, Jeon J, Kim J. Streptococcus mutans extracellular DNA levels depend on the number of bacteria in a biofilm. Sci Rep. 2018;8(1):13313. Epub 2018/09/08. doi: 10.1038/s41598-018-31275-y. PubMed PMID: 30190485; PMCID: PMC6127218.
126. Kristich CJ, Nguyen VT, Le T, Barnes AM, Grindle S, Dunny GM. Development and use of an efficient system for random mariner transposon mutagenesis to identify novel genetic determinants of biofilm formation in the core Enterococcus faecalis genome. Applied and environmental microbiology. 2008;74(11):3377-86. doi: 10.1128/AEM.02665-07. PubMed PMID: 18408066; PMCID: 2423031.
127. Zaga-Clavellina V, Garcia-Lopez G, Flores-Espinosa P. Evidence of in vitro differential secretion of human beta-defensins-1, -2, and -3 after selective exposure to Streptococcus agalactiae in human fetal membranes. The journal of maternal-fetal & neonatal medicine : the official journal of the European Association of Perinatal Medicine, the Federation of Asia and Oceania Perinatal Societies, the International Society of Perinatal Obstet. 2012;25(4):358-63. Epub 2011/06/03. doi: 10.3109/14767058.2011.578695. PubMed PMID: 21631237.
128. Arango Duque G, Descoteaux A. Macrophage cytokines: involvement in immunity and infectious diseases. Frontiers in immunology. 2014;5:491. Epub 2014/10/24. doi: 10.3389/fimmu.2014.00491. PubMed PMID: 25339958; PMCID: PMC4188125.
129. Rogers LM, Anders AP, Doster RS, Gill EA, Gnecco JS, Holley JM, Randis TM, Ratner AJ, Gaddy JA, Osteen K, Aronoff DM. Decidual stromal cell-derived PGE2 regulates macrophage responses to microbial threat. American journal of reproductive immunology. 2018;80(4):e13032. Epub 2018/08/08. doi: 10.1111/aji.13032. PubMed PMID: 30084522.
130. Parker RE, Laut C, Gaddy JA, Zadoks RN, Davies HD, Manning SD. Association between genotypic diversity and biofilm production in group B Streptococcus. BMC Microbiol. 2016;16:86. doi: 10.1186/s12866-016-0704-9. PubMed PMID: 27206613; PMCID: PMC4875601.
131. Rinaudo CD, Rosini R, Galeotti CL, Berti F, Necchi F, Reguzzi V, Ghezzo C, Telford JL, Grandi G, Maione D. Specific involvement of pilus type 2a in biofilm formation in group B Streptococcus. PloS one. 2010;5(2):e9216. doi: 10.1371/journal.pone.0009216. PubMed PMID: 20169161; PMCID: PMC2821406.
132. Ackerman DL, Craft KM, Doster RS, Weitkamp JH, Aronoff DM, Gaddy JA, Townsend SD. Antimicrobial and Antibiofilm Activity of Human Milk Oligosaccharides against Streptococcus agalactiae, Staphylococcus aureus, and Acinetobacter baumannii. ACS Infect Dis. 2017. doi: 10.1021/acsinfecdis.7b00183. PubMed PMID: 29198102.
133. Ackerman DL, Doster RS, Weitkamp JH, Aronoff D, Gaddy JA, Townsend SD. Human Milk Oligosaccharides Exhibit Antimicrobial and Anti-Biofilm Properties Against Group B Streptococcus. ACS Infect Dis. 2017. doi: 10.1021/acsinfecdis.7b00064. PubMed PMID: 28570820.
134. Shafeeq S, Kuipers OP, Kloosterman TG. The role of zinc in the interplay between pathogenic streptococci and their hosts. Molecular microbiology. 2013;88(6):1047-57. Epub 2013/05/09. doi: 10.1111/mmi.12256. PubMed PMID: 23650945.
135. Rose C, Parker A, Jefferson B, Cartmell E. The Characterization of Feces and Urine: A Review of the Literature to Inform Advanced Treatment Technology. Crit Rev Environ Sci Technol. 2015;45(17):1827-79. doi: 10.1080/10643389.2014.1000761. PubMed PMID: 26246784; PMCID: PMC4500995.

136. Hakansson S, Kallen K. Impact and risk factors for early-onset group B streptococcal morbidity: analysis of a national, population-based cohort in Sweden 1997-2001. BJOG. 2006;113(12):1452-8. doi: 10.1111/j.1471-0528.2006.01086.x. PubMed PMID: 17083655.
137. Keen CL, Lonnerdal B, Golub MS, Uriu-Hare JY, Olin KL, Hendrickx AG, Gershwin ME. Influence of marginal maternal zinc deficiency on pregnancy outcome and infant zinc status in rhesus monkeys. Pediatr Res. 1989;26(5):470-7. doi: 10.1203/00006450-198911000-00022. PubMed PMID: 2812899.
138. Apgar J, Everett GA. Low zinc intake affects maintenance of pregnancy in guinea pigs. J Nutr. 1991;121(2):192-200. PubMed PMID: 1847415.
139. Manning SD, Lewis MA, Springman AC, Lehotzky E, Whittam TS, Davies HD. Genotypic diversity and serotype distribution of group B streptococcus isolated from women before and after delivery. Clinical infectious diseases : an official publication of the Infectious Diseases Society of America. 2008;46(12):1829-37. doi: 10.1086/588296. PubMed PMID: 18462173.
140. Manning SD, Springman AC, Lehotzky E, Lewis MA, Whittam TS, Davies HD. Multilocus sequence types associated with neonatal group B streptococcal sepsis and meningitis in Canada. Journal of clinical microbiology. 2009;47(4):1143-8. doi: 10.1128/JCM.01424-08. PubMed PMID: 19158264; PMCID: PMC2668308.
141. Wilkinson HW. Nontypable group B streptococci isolated from human sources. Journal of clinical microbiology. 1977;6(2):183-4. PubMed PMID: 408376; PMCID: PMC274732.
142. Seale AC, Blencowe H, Bianchi-Jassir F, Embleton N, Bassat Q, Ordi J, Menendez C, Cutland C, Briner C, Berkley JA, Lawn JE, Baker CJ, Bartlett L, Gravett MG, Heath PT, Ip M, Le Doare K, Rubens CE, Saha SK, Schrag S, Meulen AS, Vekemans J, Madhi SA. Stillbirth With Group B Streptococcus Disease Worldwide: Systematic Review and Meta-analyses. Clinical infectious diseases : an official publication of the Infectious Diseases Society of America. 2017;65(suppl_2):S125-S32. doi: 10.1093/cid/cix585. PubMed PMID: 29117322.
143. Schrag SJ, Verani JR. Intrapartum antibiotic prophylaxis for the prevention of perinatal group B streptococcal disease: experience in the United States and implications for a potential group B streptococcal vaccine. Vaccine. 2013;31 Suppl 4:D20-6. doi: 10.1016/j.vaccine.2012.11.056. PubMed PMID: 23219695.
144. BJ S, NI H, PJ S, RG F, BB P, KP VM, MJ B, RN G, ID F, EC H, S S, K K, WA C, KL W, EF B, MC W, K S, AR L, AL S, SJ S, A D, RD H. Early Onset Neonatal Sepsis: The Burden of Group B Streptococcal and E. coli Disease Continues. Pediatrics. 2011;127(5):817-26; PMCID: PMC3081183.
145. Puopolo KM, Madoff LC, Eichenwald EC. Early-onset group B streptococcal disease in the era of maternal screening. Pediatrics. 2005;115(5):1240-6. doi: 10.1542/peds.2004-2275. PubMed PMID: 15867030.
146. Rabaan AA, Saunar JV, Bazzi AM, Soriano JL. Modified use of real-time PCR detection of group B Streptococcus in pregnancy. J Med Microbiol. 2017;66(10):1516-20. doi: 10.1099/jmm.0.000604. PubMed PMID: WOS:000413258800024.
147. Maquelin K, Kirschner C, Choo-Smith LP, van den Braak N, Endtz HP, Naumann D, Puppels GJ. Identification of medically relevant microorganisms by vibrational spectroscopy. J Microbiol Methods. 2002;51(3):255-71. Epub 2002/09/12. PubMed PMID: 12223286.
148. Harz M, Rosch P, Peschke KD, Ronneberger O, Burkhardt H, Popp J. Micro-Raman spectroscopic identification of bacterial cells of the genus Staphylococcus and dependence on their cultivation conditions. Analyst. 2005;130(11):1543-50. Epub 2005/10/14. doi: 10.1039/b507715j. PubMed PMID: 16222378.
149. Iqbal J, Dufendach KR, Wellons JC, Kuba MG, Nickols HH, Gomez-Duarte OG, Wynn JL. Lethal neonatal meningoencephalitis caused by multi-drug resistant, highly virulent Escherichia coli. Infect Dis (Lond). 2016;48(6):461-6. doi: 10.3109/23744235.2016.1144142. PubMed PMID: 27030919; PMCID: PMC4818964.

150. Ayala OD, Wakeman CA, Skaar EP, Mahadevan-Jansen A, editors. Identification of bacteria causing acute otitis media using Raman microspectroscopy. Proc SPIE 9704, Biomedical Vibrational Spectroscopy 2016: Advances in Research and Induustry 2016; San Francisco, California, United States.
151. Krishnapuram B, Carin L, Figueiredo MA, Hartemink AJ. Sparse multinomial logistic regression: fast algorithms and generalization bounds. IEEE Trans Pattern Anal Mach Intell. 2005;27(6):957-68. Epub 2005/06/10. doi: 10.1109/TPAMI.2005.127. PubMed PMID: 15943426.
152. Pence IJ, Patil CA, Lieber CA, Mahadevan-Jansen A. Discrimination of liver malignancies with 1064 nm dispersive Raman spectroscopy. Biomed Opt Express. 2015;6(8):2724-37. Epub 2015/08/27. doi: 10.1364/BOE.6.002724. PubMed PMID: 26309739; PMCID: PMC4541503.
153. de Siqueira e Oliveira FS, Giana HE, Silveira L, Jr. Discrimination of selected species of pathogenic bacteria using near-infrared Raman spectroscopy and principal components analysis. J Biomed Opt. 2012;17(10):107004. Epub 2012/10/12. doi: 10.1117/1.JBO.17.10.107004. PubMed PMID: 23052563.
154. Koumans EH, Rosen J, van Dyke MK, Zell E, Phares CR, Taylor A, Loft J, Schrag S, Abc, teams DR. Prevention of mother-to-child transmission of infections during pregnancy: implementation of recommended interventions, United States, 2003-2004. American journal of obstetrics and gynecology. 2012;206(2):158 e1- e11. doi: 10.1016/j.ajog.2011.08.027. PubMed PMID: 22030318.
155. McNamara MF, Wallis T, Qureshi F, Jacques SM, Gonik B. Determining the maternal and fetal cellular immunologic contributions in preterm deliveries with clinical or subclinical chorioamnionitis. Infect Dis Obstet Gynecol. 1997;5(4):273-9. Epub 1997/01/01. doi: 10.1155/S1064744997000471. PubMed PMID: 18476151; PMCID: PMC2364556.
156. Gravett MG, Novy MJ, Rosenfeld RG, Reddy AP, Jacob T, Turner M, McCormack A, Lapidus JA, Hitti J, Eschenbach DA, Roberts CT, Jr., Nagalla SR. Diagnosis of intra-amniotic infection by proteomic profiling and identification of novel biomarkers. Jama. 2004;292(4):462-9. Epub 2004/07/29. doi: 10.1001/jama.292.4.462. PubMed PMID: 15280344.
157. Goldenberg RL, Culhane JF, Iams JD, Romero R. Epidemiology and causes of preterm birth. Lancet. 2008;371(9606):75-84. doi: 10.1016/S0140-6736(08)60074-4. PubMed PMID: 18177778.
158. Carey AJ, Tan CK, Mirza S, Irving-Rodgers H, Webb RI, Lam A, Ulett GC. Infection and cellular defense dynamics in a novel 17beta-estradiol murine model of chronic human group B streptococcus genital tract colonization reveal a role for hemolysin in persistence and neutrophil accumulation. Journal of immunology. 2014;192(4):1718-31. doi: 10.4049/jimmunol.1202811. PubMed PMID: 24453257.
159. Brinkmann V, Reichard U, Goosmann C, Fauler B, Uhlemann Y, Weiss DS, Weinrauch Y, Zychlinsky A. Neutrophil extracellular traps kill bacteria. Science. 2004;303(5663):1532-5. doi: 10.1126/science.1092385. PubMed PMID: 15001782.
160. Becker KW, Skaar EP. Metal limitation and toxicity at the interface between host and pathogen. FEMS Microbiol Rev. 2014;38(6):1235-49. Epub 2014/09/12. doi: 10.1111/1574-6976.12087. PubMed PMID: 25211180; PMCID: PMC4227937.
161. Mickelson MN. Effect of lactoperoxidase and thiocyanate on the growth of Streptococcus pyogenes and Streptococcus agalactiae in a chemically defined culture medium. J Gen Microbiol. 1966;43(1):31-43. Epub 1966/04/01. doi: 10.1099/00221287-43-1-31. PubMed PMID: 5333458.
162. Willett NP, Morse GE. Long-chain fatty acid inhibition of growth of Streptococcus agalactiae in a chemically defined medium. Journal of bacteriology. 1966;91(6):2245-50. Epub 1966/06/01. PubMed PMID: 5943940; PMCID: PMC316201.
163. Davies HD, Adair C, McGeer A, Ma D, Robertson S, Mucenski M, Kowalsky L, Tyrell G, Baker CJ. Antibodies to capsular polysaccharides of group B Streptococcus in pregnant Canadian women: relationship to colonization status and infection in the neonate. The Journal of infectious diseases. 2001;184(3):285-91. doi: 10.1086/322029. PubMed PMID: 11443553.

164. Haley KP, Delgado AG, Piazuelo MB, Mortensen BL, Correa P, Damo SM, Chazin WJ, Skaar EP, Gaddy JA. The Human Antimicrobial Protein Calgranulin C Participates in Control of Helicobacter pylori Growth and Regulation of Virulence. Infection and immunity. 2015;83(7):2944-56. Epub 2015/05/13. doi: 10.1128/IAI.00544-15. PubMed PMID: 25964473; PMCID: PMC4468547.
165. Shynlova O, Nedd-Roderique T, Li Y, Dorogin A, Nguyen T, Lye SJ. Infiltration of myeloid cells into decidua is a critical early event in the labour cascade and post-partum uterine remodelling. J Cell Mol Med. 2013;17(2):311-24. Epub 2013/02/06. doi: 10.1111/jcmm.12012. PubMed PMID: 23379349; PMCID: PMC3822594.
166. Swamydas M, Luo Y, Dorf ME, Lionakis MS. Isolation of Mouse Neutrophils. Current protocols in immunology / edited by John E Coligan [et al]. 2015;110:3 20 1-3 15. Epub 2015/08/04. doi: 10.1002/0471142735.im0320s110. PubMed PMID: 26237011; PMCID: PMC4574512.
167. Brinkmann V, Laube B, Abu Abed U, Goosmann C, Zychlinsky A. Neutrophil extracellular traps: how to generate and visualize them. J Vis Exp. 2010(36). Epub 2010/02/26. doi: 10.3791/1724. PubMed PMID: 20182410; PMCID: PMC3125121.
168. Mascetti G, Carrara S, Vergani L. Relationship between chromatin compactness and dye uptake for in situ chromatin stained with DAPI. Cytometry. 2001;44(2):113-9. Epub 2001/05/30. PubMed PMID: 11378861.
169. Senkovich O, Ceaser S, McGee DJ, Testerman TL. Unique host iron utilization mechanisms of Helicobacter pylori revealed with iron-deficient chemically defined media. Infection and immunity. 2010;78(5):1841-9. Epub 2010/02/24. doi: 10.1128/IAI.01258-09. PubMed PMID: 20176792; PMCID: PMC2863533.
170. Masson PL, Heremans JF, Schonne E. Lactoferrin, an iron-binding protein in neutrophilic leukocytes. The Journal of experimental medicine. 1969;130(3):643-58. Epub 1969/09/01. PubMed PMID: 4979954; PMCID: PMC2138704.
171. Guillen C, McInnes IB, Kruger H, Brock JH. Iron, lactoferrin and iron regulatory protein activity in the synovium; relative importance of iron loading and the inflammatory response. Ann Rheum Dis. 1998;57(5):309-14. Epub 1998/09/19. PubMed PMID: 9741316; PMCID: PMC1752600.
172. Simard JC, Simon MM, Tessier PA, Girard D. Damage-associated molecular pattern S100A9 increases bactericidal activity of human neutrophils by enhancing phagocytosis. Journal of immunology. 2011;186(6):3622-31. Epub 2011/02/18. doi: 10.4049/jimmunol.1002956. PubMed PMID: 21325622.
173. Marzano AV, Cugno M, Trevisan V, Fanoni D, Venegoni L, Berti E, Crosti C. Role of inflammatory cells, cytokines and matrix metalloproteinases in neutrophil-mediated skin diseases. Clin Exp Immunol. 2010;162(1):100-7. Epub 2010/07/20. doi: 10.1111/j.1365-2249.2010.04201.x. PubMed PMID: 20636397; PMCID: PMC2990935.
174. PrabhuDas M, Bonney E, Caron K, Dey S, Erlebacher A, Fazleabas A, Fisher S, Golos T, Matzuk M, McCune JM, Mor G, Schulz L, Soares M, Spencer T, Strominger J, Way SS, Yoshinaga K. Immune mechanisms at the maternal-fetal interface: perspectives and challenges. Nat Immunol. 2015;16(4):328-34. Epub 2015/03/20. doi: 10.1038/ni.3131. PubMed PMID: 25789673; PMCID: PMC5070970.
175. Tsatsaronis JA, Ly D, Pupovac A, Goldmann O, Rohde M, Taylor JM, Walker MJ, Medina E, Sanderson-Smith ML. Group A Streptococcus Modulates Host Inflammation by Manipulating Polymorphonuclear Leukocyte Cell Death Responses. J Innate Immun. 2015;7(6):612-22. Epub 2015/05/23. doi: 10.1159/000430498. PubMed PMID: 25997401.
176. Kobayashi SD, DeLeo FR. Role of neutrophils in innate immunity: a systems biology-level approach. Wiley Interdiscip Rev Syst Biol Med. 2009;1(3):309-33. Epub 2010/09/14. doi: 10.1002/wsbm.32. PubMed PMID: 20836000; PMCID: PMC3501127.
177. Urban CF, Reichard U, Brinkmann V, Zychlinsky A. Neutrophil extracellular traps capture and kill Candida albicans yeast and hyphal forms. Cellular microbiology. 2006;8(4):668-76. Epub 2006/03/22. doi: 10.1111/j.1462-5822.2005.00659.x. PubMed PMID: 16548892.

178. Derre-Bobillot A, Cortes-Perez NG, Yamamoto Y, Kharrat P, Couve E, Da Cunha V, Decker P, Boissier MC, Escartin F, Cesselin B, Langella P, Bermudez-Humaran LG, Gaudu P. Nuclease A (Gbs0661), an extracellular nuclease of Streptococcus agalactiae, attacks the neutrophil extracellular traps and is needed for full virulence. Molecular microbiology. 2013;89(3):518-31. doi: 10.1111/mmi.12295. PubMed PMID: 23772975.
179. Yan J, Ralston MM, Meng X, Bongiovanni KD, Jones AL, Benndorf R, Nelin LD, Joshua Frazier W, Rogers LK, Smith CV, Liu Y. Glutathione reductase is essential for host defense against bacterial infection. Free Radic Biol Med. 2013;61:320-32. Epub 2013/04/30. doi: 10.1016/j.freeradbiomed.2013.04.015. PubMed PMID: 23623936; PMCID: PMC3749296.
180. Moon AF, Gaudu P, Pedersen LC. Structural characterization of the virulence factor nuclease A from Streptococcus agalactiae. Acta crystallographica Section D, Biological crystallography. 2014;70(Pt 11):2937-49. doi: 10.1107/S1399004714019725. PubMed PMID: 25372684; PMCID: 4220975.
181. Okumura CY, Nizet V. Subterfuge and sabotage: evasion of host innate defenses by invasive gram-positive bacterial pathogens. Annu Rev Microbiol. 2014;68:439-58. doi: 10.1146/annurev-micro-092412-155711. PubMed PMID: 25002085; PMCID: 4343215.
182. Xu D, Olson J, Cole JN, van Wijk XM, Brinkmann V, Zychlinsky A, Nizet V, Esko JD, Chang YC. Heparan Sulfate Modulates Neutrophil and Endothelial Function in Antibacterial Innate Immunity. Infection and immunity. 2015;83(9):3648-56. Epub 2015/07/08. doi: 10.1128/IAI.00545-15. PubMed PMID: 26150541; PMCID: PMC4534644.
183. Jean S, Juneau RA, Criss AK, Cornelissen CN. Neisseria gonorrhoeae Evades Calprotectin-Mediated Nutritional Immunity and Survives Neutrophil Extracellular Traps by Production of TdfH. Infection and immunity. 2016;84(10):2982-94. Epub 2016/08/03. doi: 10.1128/IAI.00319-16. PubMed PMID: 27481245; PMCID: PMC5038063.
184. Bennike TB, Carlsen TG, Ellingsen T, Bonderup OK, Glerup H, Bogsted M, Christiansen G, Birkelund S, Stensballe A, Andersen V. Neutrophil Extracellular Traps in Ulcerative Colitis: A Proteome Analysis of Intestinal Biopsies. Inflamm Bowel Dis. 2015;21(9):2052-67. Epub 2015/05/23. doi: 10.1097/MIB.0000000000000460. PubMed PMID: 25993694; PMCID: PMC4603666.
185. Gaddy JA, Radin JN, Loh JT, Piazuelo MB, Kehl-Fie TE, Delgado AG, Ilca FT, Peek RM, Cover TL, Chazin WJ, Skaar EP, Scott Algood HM. The host protein calprotectin modulates the Helicobacter pylori cag type IV secretion system via zinc sequestration. PLoS pathogens. 2014;10(10):e1004450. Epub 2014/10/21. doi: 10.1371/journal.ppat.1004450. PubMed PMID: 25330071; PMCID: PMC4199781.
186. Gutteberg TJ, Dalaker K, Osterud B, Vorland LH. Early response in septicemia in newborns and their mothers. Effect of Escherichia coli, Streptococcus agalactiae and tumor necrosis factor on lactoferrin release and the generation of tissue thromboplastin. APMIS. 1991;99(7):602-8. Epub 1991/07/01. PubMed PMID: 2069802.
187. Gutteberg TJ, Dalaker K, Vorland LH. Early response in neonatal septicemia. The effect of Escherichia coli, Streptococcus agalactiae and tumor necrosis factor on the generation of lactoferrin. APMIS. 1990;98(11):1027-32. Epub 1990/11/01. PubMed PMID: 2248767.
188. Arciola CR. Host defense against implant infection: the ambivalent role of phagocytosis. Int J Artif Organs. 2010;33(9):565-7. Epub 2010/10/22. PubMed PMID: 20963722.
189. Savchenko AS, Inoue A, Ohashi R, Jiang S, Hasegawa G, Tanaka T, Hamakubo T, Kodama T, Aoyagi Y, Ushiki T, Naito M. Long pentraxin 3 (PTX3) expression and release by neutrophils in vitro and in ulcerative colitis. Pathol Int. 2011;61(5):290-7. Epub 2011/04/20. doi: 10.1111/j.1440-1827.2011.02651.x. PubMed PMID: 21501295.
190. Svobodova E, Staib P, Losse J, Hennicke F, Barz D, Jozsi M. Differential interaction of the two related fungal species Candida albicans and Candida dubliniensis with human neutrophils. Journal of immunology. 2012;189(5):2502-11. Epub 2012/08/02. doi: 10.4049/jimmunol.1200185. PubMed PMID: 22851712.

191. Scapinello S, Brooks AS, MacInnes JI, Hammermueller J, Clark ME, Caswell JL. Bactericidal activity of porcine neutrophil secretions. Vet Immunol Immunopathol. 2011;139(2-4):113-8. Epub 2010/10/12. doi: 10.1016/j.vetimm.2010.09.004. PubMed PMID: 20932586.
192. Barrientos L, Marin-Esteban V, de Chaisemartin L, Le-Moal VL, Sandre C, Bianchini E, Nicolas V, Pallardy M, Chollet-Martin S. An improved strategy to recover large fragments of functional human neutrophil extracellular traps. Frontiers in immunology. 2013;4:166. Epub 2013/06/28. doi: 10.3389/fimmu.2013.00166. PubMed PMID: 23805143; PMCID: PMC3690357.
193. Bjornsdottir H, Welin A, Dahlgren C, Karlsson A, Bylund J. Quantification of heterotypic granule fusion in human neutrophils by imaging flow cytometry. Data Brief. 2016;6:386-93. Epub 2016/02/11. doi: 10.1016/j.dib.2015.12.003. PubMed PMID: 26862586; PMCID: PMC4707292.
194. Carretta MD, Hidalgo AI, Burgos J, Opazo L, Castro L, Hidalgo MA, Figueroa CD, Taubert A, Hermosilla C, Burgos RA. Butyric acid stimulates bovine neutrophil functions and potentiates the effect of platelet activating factor. Vet Immunol Immunopathol. 2016;176:18-27. Epub 2016/06/12. doi: 10.1016/j.vetimm.2016.05.002. PubMed PMID: 27288853.
195. Feintuch CM, Saidi A, Seydel K, Chen G, Goldman-Yassen A, Mita-Mendoza NK, Kim RS, Frenette PS, Taylor T, Daily JP. Activated Neutrophils Are Associated with Pediatric Cerebral Malaria Vasculopathy in Malawian Children. mBio. 2016;7(1):e01300-15. Epub 2016/02/18. doi: 10.1128/mBio.01300-15. PubMed PMID: 26884431; PMCID: PMC4791846.
196. Okubo K, Kamiya M, Urano Y, Nishi H, Herter JM, Mayadas T, Hirohama D, Suzuki K, Kawakami H, Tanaka M, Kurosawa M, Kagaya S, Hishikawa K, Nangaku M, Fujita T, Hayashi M, Hirahashi J. Lactoferrin Suppresses Neutrophil Extracellular Traps Release in Inflammation. EBioMedicine. 2016;10:204-15. Epub 2016/07/28. doi: 10.1016/j.ebiom.2016.07.012. PubMed PMID: 27453322; PMCID: PMC5006695.
197. van der Spek AH, Bloise FF, Tigchelaar W, Dentice M, Salvatore D, van der Wel NN, Fliers E, Boelen A. The Thyroid Hormone Inactivating Enzyme Type 3 Deiodinase is Present in Bactericidal Granules and the Cytoplasm of Human Neutrophils. Endocrinology. 2016;157(8):3293-305. Epub 2016/06/30. doi: 10.1210/en.2016-1103. PubMed PMID: 27355490.
198. Ellison RT, 3rd. The effects of lactoferrin on gram-negative bacteria. Adv Exp Med Biol. 1994;357:71-90. Epub 1994/01/01. PubMed PMID: 7762448.
199. Bezkorovainy A. Antimicrobial properties of iron-binding proteins. Adv Exp Med Biol. 1981;135:139-54. Epub 1981/01/01. PubMed PMID: 6452038.
200. Weinberg ED. Nutritional immunity. Host's attempt to withold iron from microbial invaders. Jama. 1975;231(1):39-41. Epub 1975/01/06. PubMed PMID: 1243565.
201. Weinberg ED. Infection and iron metabolism. Am J Clin Nutr. 1977;30(9):1485-90. Epub 1977/09/01. doi: 10.1093/ajcn/30.9.1485. PubMed PMID: 409273.
202. Rainard P. Bacteriostatic activity of bovine milk lactoferrin against mastitic bacteria. Vet Microbiol. 1986;11(4):387-92. Epub 1986/04/01. PubMed PMID: 3523963.
203. Rainard P. Activation of the classical pathway of complement by binding of bovine lactoferrin to unencapsulated Streptococcus agalactiae. Immunology. 1993;79(4):648-52. Epub 1993/08/01. PubMed PMID: 8406591; PMCID: PMC1421935.
204. Berlutti F, Ajello M, Bosso P, Morea C, Petrucca A, Antonini G, Valenti P. Both lactoferrin and iron influence aggregation and biofilm formation in Streptococcus mutans. Biometals. 2004;17(3):271-8. Epub 2004/06/30. PubMed PMID: 15222477.
205. Andre GO, Politano WR, Mirza S, Converso TR, Ferraz LF, Leite LC, Darrieux M. Combined effects of lactoferrin and lysozyme on Streptococcus pneumoniae killing. Microbial pathogenesis. 2015;89:7-17. Epub 2015/08/25. doi: 10.1016/j.micpath.2015.08.008. PubMed PMID: 26298002.
206. Otsuki K, Tokunaka M, Oba T, Nakamura M, Shirato N, Okai T. Administration of oral and vaginal prebiotic lactoferrin for a woman with a refractory vaginitis recurring preterm delivery: appearance of lactobacillus in vaginal flora followed by term delivery. J Obstet Gynaecol Res. 2014;40(2):583-5. Epub 2013/10/15. doi: 10.1111/jog.12171. PubMed PMID: 24118573.

207. Trend S, Strunk T, Hibbert J, Kok CH, Zhang G, Doherty DA, Richmond P, Burgner D, Simmer K, Davidson DJ, Currie AJ. Antimicrobial protein and Peptide concentrations and activity in human breast milk consumed by preterm infants at risk of late-onset neonatal sepsis. PloS one. 2015;10(2):e0117038. Epub 2015/02/03. doi: 10.1371/journal.pone.0117038. PubMed PMID: 25643281; PMCID: PMC4314069.
208. Wynn TA, Chawla A, Pollard JW. Macrophage biology in development, homeostasis and disease. Nature. 2013;496(7446):445-55. doi: 10.1038/nature12034. PubMed PMID: 23619691; PMCID: PMC3725458.
209. Gautier EL, Shay T, Miller J, Greter M, Jakubzick C, Ivanov S, Helft J, Chow A, Elpek KG, Gordonov S, Mazloom AR, Ma'ayan A, Chua WJ, Hansen TH, Turley SJ, Merad M, Randolph GJ, Immunological Genome C. Gene-expression profiles and transcriptional regulatory pathways that underlie the identity and diversity of mouse tissue macrophages. Nat Immunol. 2012;13(11):1118-28. doi: 10.1038/ni.2419. PubMed PMID: 23023392; PMCID: PMC3558276.
210. Murray PJ, Wynn TA. Protective and pathogenic functions of macrophage subsets. Nature reviews Immunology. 2011;11(11):723-37. doi: 10.1038/nri3073. PubMed PMID: 21997792; PMCID: PMC3422549.
211. Ginhoux F, Guilliams M. Tissue-Resident Macrophage Ontogeny and Homeostasis. Immunity. 2016;44(3):439-49. doi: 10.1016/j.immuni.2016.02.024. PubMed PMID: 26982352.
212. Fuchs TA, Abed U, Goosmann C, Hurwitz R, Schulze I, Wahn V, Weinrauch Y, Brinkmann V, Zychlinsky A. Novel cell death program leads to neutrophil extracellular traps. J Cell Biol. 2007;176(2):231-41. doi: 10.1083/jcb.200606027. PubMed PMID: 17210947; PMCID: PMC2063942.
213. Wartha F, Henriques-Normark B. ETosis: a novel cell death pathway. Sci Signal. 2008;1(21):pe25. doi: 10.1126/stke.121pe25. PubMed PMID: 18506034.
214. Mollerherm H, von Kockritz-Blickwede M, Branitzki-Heinemann K. Antimicrobial Activity of Mast Cells: Role and Relevance of Extracellular DNA Traps. Frontiers in immunology. 2016;7:265. doi: 10.3389/fimmu.2016.00265. PubMed PMID: 27486458; PMCID: PMC4947581.
215. Yousefi S, Gold JA, Andina N, Lee JJ, Kelly AM, Kozlowski E, Schmid I, Straumann A, Reichenbach J, Gleich GJ, Simon HU. Catapult-like release of mitochondrial DNA by eosinophils contributes to antibacterial defense. Nat Med. 2008;14(9):949-53. doi: 10.1038/nm.1855. PubMed PMID: 18690244.
216. Schorn C, Janko C, Latzko M, Chaurio R, Schett G, Herrmann M. Monosodium urate crystals induce extracellular DNA traps in neutrophils, eosinophils, and basophils but not in mononuclear cells. Frontiers in immunology. 2012;3:277. doi: 10.3389/fimmu.2012.00277. PubMed PMID: 22969769; PMCID: PMC3432456.
217. Morshed M, Hlushchuk R, Simon D, Walls AF, Obata-Ninomiya K, Karasuyama H, Djonov V, Eggel A, Kaufmann T, Simon HU, Yousefi S. NADPH oxidase-independent formation of extracellular DNA traps by basophils. Journal of immunology. 2014;192(11):5314-23. doi: 10.4049/jimmunol.1303418. PubMed PMID: 24771850.
218. von Kockritz-Blickwede M, Goldmann O, Thulin P, Heinemann K, Norrby-Teglund A, Rohde M, Medina E. Phagocytosis-independent antimicrobial activity of mast cells by means of extracellular trap formation. Blood. 2008;111(6):3070-80. doi: 10.1182/blood-2007-07-104018. PubMed PMID: 18182576.
219. Schorn C, Janko C, Krenn V, Zhao Y, Munoz LE, Schett G, Herrmann M. Bonding the foe - NETting neutrophils immobilize the pro-inflammatory monosodium urate crystals. Frontiers in immunology. 2012;3:376. doi: 10.3389/fimmu.2012.00376. PubMed PMID: 23233855; PMCID: PMC3517988.
220. Pang L, Hayes CP, Buac K, Yoo DG, Rada B. Pseudogout-associated inflammatory calcium pyrophosphate dihydrate microcrystals induce formation of neutrophil extracellular traps. Journal of immunology. 2013;190(12):6488-500. doi: 10.4049/jimmunol.1203215. PubMed PMID: 23677474.

221. Gupta AK, Hasler P, Holzgreve W, Gebhardt S, Hahn S. Induction of neutrophil extracellular DNA lattices by placental microparticles and IL-8 and their presence in preeclampsia. Hum Immunol. 2005;66(11):1146-54. doi: 10.1016/j.humimm.2005.11.003. PubMed PMID: 16571415.
222. Fuchs TA, Brill A, Duerschmied D, Schatzberg D, Monestier M, Myers DD, Jr., Wrobleski SK, Wakefield TW, Hartwig JH, Wagner DD. Extracellular DNA traps promote thrombosis. Proceedings of the National Academy of Sciences of the United States of America. 2010;107(36):15880-5. doi: 10.1073/pnas.1005743107. PubMed PMID: 20798043; PMCID: PMC2936604.
223. Simon D, Simon HU, Yousefi S. Extracellular DNA traps in allergic, infectious, and autoimmune diseases. Allergy. 2013;68(4):409-16. doi: 10.1111/all.12111. PubMed PMID: 23409745.
224. Soderberg D, Segelmark M. Neutrophil Extracellular Traps in ANCA-Associated Vasculitis. Frontiers in immunology. 2016;7:256. doi: 10.3389/fimmu.2016.00256. PubMed PMID: 27446086; PMCID: PMC4928371.
225. Delgado-Rizo V, Martinez-Guzman MA, Iniguez-Gutierrez L, Garcia-Orozco A, Alvarado-Navarro A, Fafutis-Morris M. Neutrophil Extracellular Traps and Its Implications in Inflammation: An Overview. Frontiers in immunology. 2017;8:81. doi: 10.3389/fimmu.2017.00081. PubMed PMID: 28220120; PMCID: PMC5292617.
226. Goldmann O, Medina E. The expanding world of extracellular traps: not only neutrophils but much more. Frontiers in immunology. 2012;3:420. doi: 10.3389/fimmu.2012.00420. PubMed PMID: 23335924; PMCID: 3542634.
227. Arksey H, O'Malley L. Scoping studies: towards a methodological framework. International Journal of Social Research Methodology. 2005;8(1):19-32. doi: 10.1080/1364557032000119616.
228. Halder LD, Abdelfatah MA, Jo EA, Jacobsen ID, Westermann M, Beyersdorf N, Lorkowski S, Zipfel PF, Skerka C. Factor H Binds to Extracellular DNA Traps Released from Human Blood Monocytes in Response to Candida albicans. Frontiers in immunology. 2016;7:671. doi: 10.3389/fimmu.2016.00671. PubMed PMID: 28133459; PMCID: PMC5233719.
229. Munoz-Caro T, Silva LM, Ritter C, Taubert A, Hermosilla C. Besnoitia besnoiti tachyzoites induce monocyte extracellular trap formation. Parasitol Res. 2014;113(11):4189-97. doi: 10.1007/s00436-014-4094-3. PubMed PMID: 25193048.
230. Hellenbrand KM, Forsythe KM, Rivera-Rivas JJ, Czuprynski CJ, Aulik NA. Histophilus somni causes extracellular trap formation by bovine neutrophils and macrophages. Microbial pathogenesis. 2013;54:67-75. doi: 10.1016/j.micpath.2012.09.007. PubMed PMID: 23022668.
231. Aulik NA, Hellenbrand KM, Czuprynski CJ. Mannheimia haemolytica and its leukotoxin cause macrophage extracellular trap formation by bovine macrophages. Infection and immunity. 2012;80(5):1923-33. doi: 10.1128/IAI.06120-11. PubMed PMID: 22354029; PMCID: PMC3347434.
232. Je S, Quan H, Yoon Y, Na Y, Kim BJ, Seok SH. Mycobacterium massiliense Induces Macrophage Extracellular Traps with Facilitating Bacterial Growth. PloS one. 2016;11(5):e0155685. doi: 10.1371/journal.pone.0155685. PubMed PMID: 27191593; PMCID: PMC4871462.
233. O'Sullivan KM, Lo CY, Summers SA, Elgass KD, McMillan PJ, Longano A, Ford SL, Gan PY, Kerr PG, Kitching AR, Holdsworth SR. Renal participation of myeloperoxidase in antineutrophil cytoplasmic antibody (ANCA)-associated glomerulonephritis. Kidney Int. 2015;88(5):1030-46. doi: 10.1038/ki.2015.202. PubMed PMID: 26176828.
234. Liu P, Wu X, Liao C, Liu X, Du J, Shi H, Wang X, Bai X, Peng P, Yu L, Wang F, Zhao Y, Liu M. Escherichia coli and Candida albicans induced macrophage extracellular trap-like structures with limited microbicidal activity. PloS one. 2014;9(2):e90042. doi: 10.1371/journal.pone.0090042. PubMed PMID: 24587206; PMCID: 3934966.
235. Perez D, Munoz MC, Molina JM, Munoz-Caro T, Silva LM, Taubert A, Hermosilla C, Ruiz A. Eimeria ninakohlyakimovae induces NADPH oxidase-dependent monocyte extracellular trap

formation and upregulates IL-12 and TNF-alpha, IL-6 and CCL2 gene transcription. Vet Parasitol. 2016;227:143-50. doi: 10.1016/j.vetpar.2016.07.028. PubMed PMID: 27523951.
236. Wong KW, Jacobs WR, Jr. Mycobacterium tuberculosis exploits human interferon gamma to stimulate macrophage extracellular trap formation and necrosis. The Journal of infectious diseases. 2013;208(1):109-19. doi: 10.1093/infdis/jit097. PubMed PMID: 23475311; PMCID: 3666134.
237. Chow OA, von Kockritz-Blickwede M, Bright AT, Hensler ME, Zinkernagel AS, Cogen AL, Gallo RL, Monestier M, Wang Y, Glass CK, Nizet V. Statins enhance formation of phagocyte extracellular traps. Cell Host Microbe. 2010;8(5):445-54. doi: 10.1016/j.chom.2010.10.005. PubMed PMID: 21075355; PMCID: PMC3008410.
238. Bonne-Annee S, Kerepesi LA, Hess JA, Wesolowski J, Paumet F, Lok JB, Nolan TJ, Abraham D. Extracellular traps are associated with human and mouse neutrophil and macrophage mediated killing of larval Strongyloides stercoralis. Microbes and infection / Institut Pasteur. 2014;16(6):502-11. doi: 10.1016/j.micinf.2014.02.012. PubMed PMID: 24642003; PMCID: 4076910.
239. Yang F, Feng C, Zhang X, Lu J, Zhao Y. The Diverse Biological Functions of Neutrophils, Beyond the Defense Against Infections. Inflammation. 2017;40(1):311-23. doi: 10.1007/s10753-016-0458-4. PubMed PMID: 27817110.
240. Andzinski L, Kasnitz N, Stahnke S, Wu CF, Gereke M, von Kockritz-Blickwede M, Schilling B, Brandau S, Weiss S, Jablonska J. Type I IFNs induce anti-tumor polarization of tumor associated neutrophils in mice and human. Int J Cancer. 2016;138(8):1982-93. doi: 10.1002/ijc.29945. PubMed PMID: 26619320.
241. Shrestha S, Kim SY, Yun YJ, Kim JK, Lee JM, Shin M, Song DK, Hong CW. Retinoic acid induces hypersegmentation and enhances cytotoxicity of neutrophils against cancer cells. Immunol Lett. 2017;182:24-9. doi: 10.1016/j.imlet.2017.01.001. PubMed PMID: 28065603.
242. Villanueva E, Yalavarthi S, Berthier CC, Hodgin JB, Khandpur R, Lin AM, Rubin CJ, Zhao W, Olsen SH, Klinker M, Shealy D, Denny MF, Plumas J, Chaperot L, Kretzler M, Bruce AT, Kaplan MJ. Netting neutrophils induce endothelial damage, infiltrate tissues, and expose immunostimulatory molecules in systemic lupus erythematosus. Journal of immunology. 2011;187(1):538-52. doi: 10.4049/jimmunol.1100450. PubMed PMID: 21613614; PMCID: PMC3119769.
243. Nakazawa D, Shida H, Kusunoki Y, Miyoshi A, Nishio S, Tomaru U, Atsumi T, Ishizu A. The responses of macrophages in interaction with neutrophils that undergo NETosis. J Autoimmun. 2016;67:19-28. doi: 10.1016/j.jaut.2015.08.018. PubMed PMID: 26347075.
244. Bryukhin GV, Shopova AV. Characteristics of Mononuclear Extracellular Traps in the Offspring of Female Rats with Drug-Induced Hepatitis. Bull Exp Biol Med. 2015;159(4):435-7. doi: 10.1007/s10517-015-2984-8. PubMed PMID: 26388577.
245. Vega VL, Crotty Alexander LE, Charles W, Hwang JH, Nizet V, De Maio A. Activation of the stress response in macrophages alters the M1/M2 balance by enhancing bacterial killing and IL-10 expression. J Mol Med (Berl). 2014;92(12):1305-17. doi: 10.1007/s00109-014-1201-y. PubMed PMID: 25163764.
246. Shen F, Tang X, Cheng W, Wang Y, Wang C, Shi X, An Y, Zhang Q, Liu M, Liu B, Yu L. Fosfomycin enhances phagocyte-mediated killing of Staphylococcus aureus by extracellular traps and reactive oxygen species. Sci Rep. 2016;6:19262. doi: 10.1038/srep19262. PubMed PMID: 26778774; PMCID: PMC4726045.
247. Mohanan S, Horibata S, McElwee JL, Dannenberg AJ, Coonrod SA. Identification of macrophage extracellular trap-like structures in mammary gland adipose tissue: a preliminary study. Frontiers in immunology. 2013;4:67. Epub 2013/03/20. doi: 10.3389/fimmu.2013.00067. PubMed PMID: 23508122; PMCID: PMC3600535.
248. Stoiber W, Obermayer A, Steinbacher P, Krautgartner WD. The Role of Reactive Oxygen Species (ROS) in the Formation of Extracellular Traps (ETs) in Humans. Biomolecules. 2015;5(2):702-23. doi: 10.3390/biom5020702. PubMed PMID: 25946076; PMCID: PMC4496692.

249. Papayannopoulos V, Metzler KD, Hakkim A, Zychlinsky A. Neutrophil elastase and myeloperoxidase regulate the formation of neutrophil extracellular traps. J Cell Biol. 2010;191(3):677-91. Epub 2010/10/27. doi: 10.1083/jcb.201006052. PubMed PMID: 20974816; PMCID: PMC3003309.
250. Remijsen Q, Kuijpers TW, Wirawan E, Lippens S, Vandenabeele P, Vanden Berghe T. Dying for a cause: NETosis, mechanisms behind an antimicrobial cell death modality. Cell Death Differ. 2011;18(4):581-8. doi: 10.1038/cdd.2011.1. PubMed PMID: 21293492; PMCID: PMC3131909.
251. Yousefi S, Mihalache C, Kozlowski E, Schmid I, Simon HU. Viable neutrophils release mitochondrial DNA to form neutrophil extracellular traps. Cell Death Differ. 2009;16(11):1438-44. doi: 10.1038/cdd.2009.96. PubMed PMID: 19609275.
252. Pilsczek FH, Salina D, Poon KK, Fahey C, Yipp BG, Sibley CD, Robbins SM, Green FH, Surette MG, Sugai M, Bowden MG, Hussain M, Zhang K, Kubes P. A novel mechanism of rapid nuclear neutrophil extracellular trap formation in response to Staphylococcus aureus. Journal of immunology. 2010;185(12):7413-25. doi: 10.4049/jimmunol.1000675. PubMed PMID: 21098229.
253. King PT, Sharma R, O'Sullivan K, Selemidis S, Lim S, Radhakrishna N, Lo C, Prasad J, Callaghan J, McLaughlin P, Farmer M, Steinfort D, Jennings B, Ngui J, Broughton BR, Thomas B, Essilfie AT, Hickey M, Holmes PW, Hansbro P, Bardin PG, Holdsworth SR. Nontypeable Haemophilus influenzae induces sustained lung oxidative stress and protease expression. PloS one. 2015;10(3):e0120371. doi: 10.1371/journal.pone.0120371. PubMed PMID: 25793977; PMCID: PMC4368769.
254. Metzler KD, Fuchs TA, Nauseef WM, Reumaux D, Roesler J, Schulze I, Wahn V, Papayannopoulos V, Zychlinsky A. Myeloperoxidase is required for neutrophil extracellular trap formation: implications for innate immunity. Blood. 2011;117(3):953-9. doi: 10.1182/blood-2010-06-290171. PubMed PMID: 20974672; PMCID: PMC3035083.
255. Bartneck M, Keul HA, Zwadlo-Klarwasser G, Groll J. Phagocytosis independent extracellular nanoparticle clearance by human immune cells. Nano Lett. 2010;10(1):59-63. doi: 10.1021/nl902830x. PubMed PMID: 19994869.
256. Mejia SP, Cano LE, Lopez JA, Hernandez O, Gonzalez A. Human neutrophils produce extracellular traps against Paracoccidioides brasiliensis. Microbiology. 2015;161(Pt 5):1008-17. doi: 10.1099/mic.0.000059. PubMed PMID: 25701733.
257. Neeli I, Dwivedi N, Khan S, Radic M. Regulation of extracellular chromatin release from neutrophils. J Innate Immun. 2009;1(3):194-201. doi: 10.1159/000206974. PubMed PMID: 20375577.
258. Jerjomiceva N, Seri H, Vollger L, Wang Y, Zeitouni N, Naim HY, von Kockritz-Blickwede M. Enrofloxacin enhances the formation of neutrophil extracellular traps in bovine granulocytes. J Innate Immun. 2014;6(5):706-12. doi: 10.1159/000358881. PubMed PMID: 24642685; PMCID: PMC4140967.
259. Wang Y, Li M, Stadler S, Correll S, Li P, Wang D, Hayama R, Leonelli L, Han H, Grigoryev SA, Allis CD, Coonrod SA. Histone hypercitrullination mediates chromatin decondensation and neutrophil extracellular trap formation. J Cell Biol. 2009;184(2):205-13. doi: 10.1083/jcb.200806072. PubMed PMID: 19153223; PMCID: PMC2654299.
260. Webster SJ, Daigneault M, Bewley MA, Preston JA, Marriott HM, Walmsley SR, Read RC, Whyte MK, Dockrell DH. Distinct cell death programs in monocytes regulate innate responses following challenge with common causes of invasive bacterial disease. Journal of immunology. 2010;185(5):2968-79. doi: 10.4049/jimmunol.1000805. PubMed PMID: 20656927; PMCID: PMC2929480.
261. Kahlenberg JM, Carmona-Rivera C, Smith CK, Kaplan MJ. Neutrophil extracellular trap-associated protein activation of the NLRP3 inflammasome is enhanced in lupus macrophages. Journal of immunology. 2013;190(3):1217-26. doi: 10.4049/jimmunol.1202388. PubMed PMID: 23267025; PMCID: PMC3552129.

262. Korir ML, Laut C, Rogers LM, Plemmons JA, Aronoff DM, Manning SD. Differing mechanisms of surviving phagosomal stress among group B Streptococcus strains of varying genotypes. Virulence. 2017;8(6):924-37. Epub 2016/10/30. doi: 10.1080/21505594.2016.1252016. PubMed PMID: 27791478; PMCID: PMC5626345.
263. Jonsson BE, Bylund J, Johansson BR, Telemo E, Wold AE. Cord-forming mycobacteria induce DNA meshwork formation by human peripheral blood mononuclear cells. Pathog Dis. 2013;67(1):54-66. doi: 10.1111/2049-632X.12007. PubMed PMID: 23620120.
264. Pijanowski L, Scheer M, Verburg-van Kemenade BM, Chadzinska M. Production of inflammatory mediators and extracellular traps by carp macrophages and neutrophils in response to lipopolysaccharide and/or interferon-gamma2. Fish Shellfish Immunol. 2015;42(2):473-82. doi: 10.1016/j.fsi.2014.11.019. PubMed PMID: 25453727.
265. Reichel M, Munoz-Caro T, Sanchez Contreras G, Rubio Garcia A, Magdowski G, Gartner U, Taubert A, Hermosilla C. Harbour seal (Phoca vitulina) PMN and monocytes release extracellular traps to capture the apicomplexan parasite Toxoplasma gondii. Dev Comp Immunol. 2015;50(2):106-15. doi: 10.1016/j.dci.2015.02.002. PubMed PMID: 25681075.
266. March of Dimes. Permaturity Campaign: March of Dimes; 2013 [updated 10/2013; cited 2015 1/21/2015]. Available from: http://www.marchofdimes.org/mission/the-economic-and-societal-costs.aspx.
267. Organization WH. Preterm Birth: Fact Sheet: WHO 2017; 2016 [updated November 2016; cited 2017 9/26/2017]. Available from: http://www.who.int/mediacentre/factsheets/fs363/en/.
268. Liu L, Oza S, Hogan D, Chu Y, Perin J, Zhu J, Lawn JE, Cousens S, Mathers C, Black RE. Global, regional, and national causes of under-5 mortality in 2000-15: an updated systematic analysis with implications for the Sustainable Development Goals. Lancet. 2016;388(10063):3027-35. doi: 10.1016/S0140-6736(16)31593-8. PubMed PMID: 27839855; PMCID: PMC5161777.
269. Luu TM, Rehman Mian MO, Nuyt AM. Long-Term Impact of Preterm Birth: Neurodevelopmental and Physical Health Outcomes. Clin Perinatol. 2017;44(2):305-14. doi: 10.1016/j.clp.2017.01.003. PubMed PMID: 28477662.
270. Doyle LW. Cardiopulmonary outcomes of extreme prematurity. Semin Perinatol. 2008;32(1):28-34. doi: 10.1053/j.semperi.2007.12.005. PubMed PMID: 18249237.
271. Anders AP, Gaddy JA, Doster RS, Aronoff DM. Current concepts in maternal-fetal immunology: Recognition and response to microbial pathogens by decidual stromal cells. American journal of reproductive immunology. 2017. doi: 10.1111/aji.12623. PubMed PMID: 28044385.
272. Stallmach T, Hebisch G, Joller H, Kolditz P, Engelmann M. Expression pattern of cytokines in the different compartments of the feto-maternal unit under various conditions. Reprod Fertil Dev. 1995;7(6):1573-80. PubMed PMID: 8743167.
273. Agrawal V, Hirsch E. Intrauterine infection and preterm labor. Semin Fetal Neonatal Med. 2012;17(1):12-9. doi: 10.1016/j.siny.2011.09.001. PubMed PMID: 21944863; PMCID: PMC3242863.
274. Doster RS, Rogers LM, Gaddy JA, Aronoff DM. Macrophage Extracellular Traps: A Scoping Review. J Innate Immun. 2018;10(1):3-13. doi: 10.1159/000480373. PubMed PMID: 28988241.
275. Korir ML, Laut C, Rogers LM, Plemmons JA, Aronoff DM, Manning SD. Differing mechanisms of surviving phagosomal stress among group B Streptococcus strains of varying genotypes. Virulence. 2016:1-14. doi: 10.1080/21505594.2016.1252016. PubMed PMID: 27791478.
276. Schindelin J, Arganda-Carreras I, Frise E, Kaynig V, Longair M, Pietzsch T, Preibisch S, Rueden C, Saalfeld S, Schmid B, Tinevez JY, White DJ, Hartenstein V, Eliceiri K, Tomancak P, Cardona A. Fiji: an open-source platform for biological-image analysis. Nat Methods. 2012;9(7):676-82. doi: 10.1038/nmeth.2019. PubMed PMID: 22743772; PMCID: PMC3855844.
277. McCloy RA, Rogers S, Caldon CE, Lorca T, Castro A, Burgess A. Partial inhibition of Cdk1 in G 2 phase overrides the SAC and decouples mitotic events. Cell Cycle. 2014;13(9):1400-12. doi: 10.4161/cc.28401. PubMed PMID: 24626186; PMCID: PMC4050138.

278. Brinkmann V, Abu Abed U, Goosmann C, Zychlinsky A. Immunodetection of NETs in Paraffin-Embedded Tissue. Frontiers in immunology. 2016;7:513. doi: 10.3389/fimmu.2016.00513. PubMed PMID: 27920776; PMCID: PMC5118445.
279. Hirsch JG. Bactericidal action of histone. The Journal of experimental medicine. 1958;108(6):925-44. PubMed PMID: 13598820; PMCID: PMC2136925.
280. Gomez-Lopez N, StLouis D, Lehr MA, Sanchez-Rodriguez EN, Arenas-Hernandez M. Immune cells in term and preterm labor. Cellular & molecular immunology. 2014;11(6):571-81. doi: 10.1038/cmi.2014.46. PubMed PMID: 24954221; PMCID: 4220837.
281. Chaemsaithong P, Romero R, Docheva N, Chaiyasit N, Bhatti G, Pacora P, Hassan SS, Yeo L, Erez O. Comparison of rapid MMP-8 and interleukin-6 point-of-care tests to identify intra-amniotic inflammation/infection and impending preterm delivery in patients with preterm labor and intact membranes(). The journal of maternal-fetal & neonatal medicine : the official journal of the European Association of Perinatal Medicine, the Federation of Asia and Oceania Perinatal Societies, the International Society of Perinatal Obstet. 2018;31(2):228-44. doi: 10.1080/14767058.2017.1281904. PubMed PMID: 28081646.
282. Kim KW, Romero R, Park HS, Park CW, Shim SS, Jun JK, Yoon BH. A rapid matrix metalloproteinase-8 bedside test for the detection of intraamniotic inflammation in women with preterm premature rupture of membranes. American journal of obstetrics and gynecology. 2007;197(3):292 e1-5. doi: 10.1016/j.ajog.2007.06.040. PubMed PMID: 17826425.
283. Angus SR, Segel SY, Hsu CD, Locksmith GJ, Clark P, Sammel MD, Macones GA, Strauss JF, 3rd, Parry S. Amniotic fluid matrix metalloproteinase-8 indicates intra-amniotic infection. American journal of obstetrics and gynecology. 2001;185(5):1232-8. doi: 10.1067/mob.2001.118654. PubMed PMID: 11717662.
284. Sharma R, O'Sullivan KM, Holdsworth SR, Bardin PG, King PT. Visualizing Macrophage Extracellular Traps Using Confocal Microscopy. J Vis Exp. 2017(128). doi: 10.3791/56459. PubMed PMID: 29155721.
285. Fettucciari K, Rosati E, Scaringi L, Cornacchione P, Migliorati G, Sabatini R, Fetriconi I, Rossi R, Marconi P. Group B Streptococcus induces apoptosis in macrophages. Journal of immunology. 2000;165(7):3923-33. PubMed PMID: 11034400.
286. Touyz RM, Yao G, Quinn MT, Pagano PJ, Schiffrin EL. p47phox associates with the cytoskeleton through cortactin in human vascular smooth muscle cells: role in NAD(P)H oxidase regulation by angiotensin II. Arterioscler Thromb Vasc Biol. 2005;25(3):512-8. doi: 10.1161/01.ATV.0000154141.66879.98. PubMed PMID: 15618548.
287. Shao D, Segal AW, Dekker LV. Subcellular localisation of the p40phox component of NADPH oxidase involves direct interactions between the Phox homology domain and F-actin. Int J Biochem Cell Biol. 2010;42(10):1736-43. doi: 10.1016/j.biocel.2010.07.009. PubMed PMID: 20637895; PMCID: PMC2938475.
288. Voloshina EV, Prasol EA, Grachev SV, Prokhorenko IR. Effect of cytochalasin D on the respiratory burst of primed neutrophils activated with a secondary stimulus. Dokl Biochem Biophys. 2009;424:13-5. PubMed PMID: 19341098.
289. Weiss A, Goldman S, Shalev E. The matrix metalloproteinases (MMPS) in the decidua and fetal membranes. Front Biosci. 2007;12:649-59. PubMed PMID: 17127325.
290. Nishihara S, Someya A, Yonemoto H, Ota A, Itoh S, Nagaoka I, Takeda S. Evaluation of the expression and enzyme activity of matrix metalloproteinase-7 in fetal membranes during premature rupture of membranes at term in humans. Reprod Sci. 2008;15(2):156-65. doi: 10.1177/1933719107310308. PubMed PMID: 18276951.
291. Kumar D, Moore RM, Mercer BM, Mansour JM, Redline RW, Moore JJ. The physiology of fetal membrane weakening and rupture: Insights gained from the determination of physical properties revisited. Placenta. 2016;42:59-73. doi: 10.1016/j.placenta.2016.03.015. PubMed PMID: 27238715.

292. Flores-Pliego A, Espejel-Nunez A, Castillo-Castrejon M, Meraz-Cruz N, Beltran-Montoya J, Zaga-Clavellina V, Nava-Salazar S, Sanchez-Martinez M, Vadillo-Ortega F, Estrada-Gutierrez G. Matrix Metalloproteinase-3 (MMP-3) Is an Endogenous Activator of the MMP-9 Secreted by Placental Leukocytes: Implication in Human Labor. PloS one. 2015;10(12):e0145366. doi: 10.1371/journal.pone.0145366. PubMed PMID: 26713439; PMCID: PMC4699849.
293. Sundrani DP, Chavan-Gautam PM, Pisal HR, Mehendale SS, Joshi SR. Matrix metalloproteinase-1 and -9 in human placenta during spontaneous vaginal delivery and caesarean sectioning in preterm pregnancy. PloS one. 2012;7(1):e29855. doi: 10.1371/journal.pone.0029855. PubMed PMID: 22253805; PMCID: PMC3257231.
294. Walsh SW, Nugent WH, Solotskaya AV, Anderson CD, Grider JR, Strauss JF, 3rd. Matrix Metalloprotease-1 and Elastase Are Novel Uterotonic Agents Acting Through Protease-Activated Receptor 1. Reprod Sci. 2017:1933719117732162. doi: 10.1177/1933719117732162. PubMed PMID: 28954603.
295. Tambor V, Kacerovsky M, Lenco J, Bhat G, Menon R. Proteomics and bioinformatics analysis reveal underlying pathways of infection associated histologic chorioamnionitis in pPROM. Placenta. 2013;34(2):155-61. doi: 10.1016/j.placenta.2012.11.028. PubMed PMID: 23246098.
296. Harris LK, Smith SD, Keogh RJ, Jones RL, Baker PN, Knofler M, Cartwright JE, Whitley GS, Aplin JD. Trophoblast- and vascular smooth muscle cell-derived MMP-12 mediates elastolysis during uterine spiral artery remodeling. The American journal of pathology. 2010;177(4):2103-15. doi: 10.2353/ajpath.2010.100182. PubMed PMID: 20802175; PMCID: PMC2947303.
297. Marder W, Knight JS, Kaplan MJ, Somers EC, Zhang X, O'Dell AA, Padmanabhan V, Lieberman RW. Placental histology and neutrophil extracellular traps in lupus and pre-eclampsia pregnancies. Lupus Sci Med. 2016;3(1):e000134. doi: 10.1136/lupus-2015-000134. PubMed PMID: 27158525; PMCID: PMC4854113.
298. Gomez-Lopez N, Romero R, Leng Y, Garcia-Flores V, Xu Y, Miller D, Hassan SS. Neutrophil extracellular traps in acute chorioamnionitis: A mechanism of host defense. American journal of reproductive immunology. 2017;77(3). doi: 10.1111/aji.12617. PubMed PMID: 28045214; PMCID: PMC5370569.
299. Gulati S, Bhatnagar S, Raghunandan C, Bhattacharjee J. Interleukin-6 as a predictor of subclinical chorioamnionitis in preterm premature rupture of membranes. American journal of reproductive immunology. 2012;67(3):235-40. doi: 10.1111/j.1600-0897.2011.01084.x. PubMed PMID: 22023383.
300. Gnecco JS, Anders AP, Cliffel D, Pensabene V, Rogers LM, Osteen K, Aronoff DM. Instrumenting a Fetal Membrane on a Chip as Emerging Technology for Preterm Birth Research. Curr Pharm Des. 2017;23(40):6115-24. doi: 10.2174/1381612823666170825142649. PubMed PMID: 28847303.